



University of Kentucky
UKnowledge

University of Kentucky Master's Theses

Graduate School

2005

ROLE OF WEAK ZONE GEOMETRY AND RHEOLOGY IN THE GENERATION OF INTRAPLATE SEISMICITY

Abhishek Joshi
University of Kentucky

[Right click to open a feedback form in a new tab to let us know how this document benefits you.](#)

Recommended Citation

Joshi, Abhishek, "ROLE OF WEAK ZONE GEOMETRY AND RHEOLOGY IN THE GENERATION OF INTRAPLATE SEISMICITY" (2005). *University of Kentucky Master's Theses*. 346.
https://uknowledge.uky.edu/gradschool_theses/346

This Thesis is brought to you for free and open access by the Graduate School at UKnowledge. It has been accepted for inclusion in University of Kentucky Master's Theses by an authorized administrator of UKnowledge. For more information, please contact UKnowledge@lsv.uky.edu.

ABSTRACT OF THESIS

ROLE OF WEAK ZONE GEOMETRY AND RHEOLOGY IN THE GENERATION OF INTRAPLATE SEISMICITY

In intraplate seismic zones (e.g. the New Madrid Seismic Zone, NMSZ, in the south-central United States), the source of stress that drives earthquake is very complex. Data from the NMSZ indicate 3 earthquake of magnitude $M \sim 7$, occurring at an approximate interval of 500 years during the last 2000 years. One hypothesis that satisfies these conditions proposes that short-lived bursts of earthquakes may result from perturbations in the local or regional stress field. This causes relaxation of a lower crustal weak zone which drive repeated earthquakes. The number of earthquakes is dependent on the geometry and rheology of the weak zone. Using finite element techniques which employ contact surfaces to model discrete faulting events and a maximum shear stress criteria evaluated at each node. We investigate the relevant parameter space, as it affects the concentration of stress at the base of the seismogenic fault and the number of earthquakes generated over a given time interval. Parameters that can be varied include earthquake stress drop, background tectonic stress, and maximum shear stress at failure. Results show that solutions are non-unique. With the addition of existing observational evidence, however, we can place bounds on the range of parameters which satisfy above observations.

KEYWORDS: Finite Element Methods, Friction Subroutine, Intraplate Seismic Zone, Rheological and Geometrical Parameters, New Madrid Seismic Zone.

Abhishek Joshi

April 25th, 2005

Date

**ROLE OF WEAK ZONE GEOMETRY
AND RHEOLOGY IN THE GENERATION OF INTRAPLATE SEISMICITY**

By

Abhishek Joshi

Dr Keith Rouch

Director of Thesis

Dr George Huang

Director of Graduate Study

April 25th, 2005

Date

**ROLE OF WEAK ZONE GEOMETRY
AND RHEOLOGY IN THE GENERATION OF INTRAPLATE SEISMICITY**

By

Abhishek Joshi

Dr Shelley J Kenner

Co-Director of Thesis

Dr George Huang

Director of Graduate Study

April 25th, 2005

Date

RULES FOR THE USE OF THESES

Unpublished theses submitted for the Master's degree and deposited in the University of Kentucky Library are as a rule open for inspection, but are to be used only with due regard to the rights of the authors. Bibliographical references may be noted, but quotations or summaries of parts may be published only with the permission of the author, and with the usual scholarly acknowledgments.

Extensive copying or publication of the thesis in whole or in part also requires the consent of the Dean of the Graduate School of the University of Kentucky.

THESIS

Abhishek Joshi

The Graduate School
University of Kentucky

2005

**ROLE OF WEAK ZONE GEOMETRY
AND RHEOLOGY IN THE GENERATION OF INTRAPLATE SEISMICITY**

THESIS

A thesis submitted in partial fulfillment of the requirements
for the degree of Master of Science in Mechanical Engineering in the
College of Engineering at the
University of Kentucky

By

Abhishek Joshi

Lexington, Kentucky

Director: Dr. Keith Rouch, Professor of Mechanical Engineering

Lexington, Kentucky

2005

**ROLE OF WEAK ZONE GEOMETRY
AND RHEOLOGY IN THE GENERATION OF INTRAPLATE SEISMICITY**

THESIS

A thesis submitted in partial fulfillment of the requirements
for the degree of Master of Science in Mechanical Engineering in the
College of Engineering at the
University of Kentucky

By

Abhishek Joshi

Lexington, Kentucky

Co-director Dr. Shelley J Kenner, Assistant Professor of Geological
Sciences

Lexington, Kentucky

2005

Dedicated to

LORD:

SHRI GEBI HANUMAAN (GEBI SAAHAB)

PARENTS:

SUSHMA JOSHI

ANIL KUMAR JOSHI

ACKNOWLEDGEMENTS

I would like to thank my advisors Dr. Shelly J. Kenner and Dr. Keith Rouch for their gracious guidance extended to me during my time in University of Kentucky. I thank Dr. Kenner for her support and encouragement during all the time when I was working on this research project. Dr. Kenner has always been source of inspiration for me especially during the critical moment when the best of my efforts were not aiming goals. She has given me inside to understand the project and guided me to analyze loosely connected results. The brain-storming assignments from her helped me to develop my aptitude for geo-sciences. I have had hours of enlightening discussions with her. Without these discussions with her and encouragement from her it would have been nearly impossible for me to pursue this project in the field of geo-physics.

I feel total loss of words when it comes to thank Dr. Rouch. Impact of his positive attitude will help me in all the spheres of my life. His guidance in the field of mechanical engineering has carved a more efficient and self sustainable engineer inside me.

Unconditional love and emotional support of my parent, Sushma and Anil Joshi, is the backbone of my life. They provide me strength to stand on the ground where I belong now. Without their insight and confidence invoked in me, I might not have taken single step in my career. My younger brother Chinmay, my alter ego, has always re-energized me to work harder. Finally I would like to thank friends in UK for always supporting me, especially Soumya Singhi, Faisal A Mev, Amit Sehgal, Tanmay Singhal and Akhil Deshpande for always motivating me and understanding me. They have been like my family in last couple of years.

Table of Contents

Acknowledgement.....	iii
Table of Contents.....	iv
List of Tables.....	vii
List of Figures.....	viii

Chapter 1 Introduction

Abstract	1
1.1 Background.....	1
1.2 Intraplate Earthquakes and NMSZ.....	2
1.3 Modeling Philosophy.....	6
1.4 Overview of Thesis.....	7

Chapter 2 Progressive Model Development

2.1 Introduction and Significance.....	8
2.2 Geography of NMSZ.....	8
2.3 Rheological Properties of NMSZ.....	13
2.4 Some Suggested Fact Derived from Observations in NMSZ.....	15
2.5 Weakening Mechanism.....	15
2.6 Previous Models of Tectonism/Seismicity.....	16
2.7 Conclusions.....	18

Chapter 3 Rheology and Geometry of the New Madrid Region

Abstract.....	20
3.1 Foundation of Rheological Parameter Space.....	20
3.2 Linear Viscoelasticity.....	21
3.3 Basic Rheological Models.....	22
3.4 Viscoelastic Materials Used and Their Implementation in ABAQUS	23
3.5 ABAQUS Numerical Implementation of SLS.....	25
3.6 Geometrical Parameters.....	28
3.7 Generation of Anti-plane Model.....	28
3.8 Model Pre-stressing.....	29
3.9 Geologically Appropriate Boundary Conditions.....	30
3.10 The Model.....	32
3.11 Conclusion.....	33

Chapter 4 Fault friction behavior

Abstract.....	35
4.1 Discrete Faults Using Contact Surfaces.....	35
4.2 Surface Behaviors.....	36
4.3 Maximum Shear Stress Criteria Friction Subroutine.....	37
4.4 Input Parameters.....	40
4.5 Logic.....	41
4.6 Flow-Chart Representation of the Subroutines.....	42

Chapter 5 2D Model Results and Discussions

5.1 Introduction.....	48
5.2 Viscosity Variation for 3 km Wide Weak Zone	51
5.3 Power-law Variation for 3 km Wide Weak Zone.....	52
5.4 Viscosity Variation for 6 km Wide Weak Zone	53
5.5 Power law Variation for 6 km Wide Weak Zone	55
5.6 Viscosity Variation for 12 km Wide Weak Zone	57
5.7 Power law Variation for 12 km Wide Weak Zone	58
5.8 Geometric Variation with 3, 6, 12 km Wide Weak Zones.....	60
5.9 2D Models with Constant Stress-drop.....	63
5.10 Conclusions.....	65

Chapter 6 3D Model Results and Discussions

6.1 Introduction.....	66
6.2 Viscosity Variation for 24 km Wide Weak Zone	67
6.3 Power law Variation for 24 km Wide Weak Zone	69
6.4 Viscosity Variation for 54 km Wide Weak Zone	70
6.5 Power law Variation for 54 km Wide Weak Zone	72
6.6 Viscosity Variation for 75 km Wide Weak Zone	73
6.7 Geometric Variation with 24, 54 and 75 km Wide Weak Zone	74
6.8 Conclusions.....	75

Chapter 7 Discussion.....77

Chapter 8 Limitations79

Chapter 9 Conclusions.....80

Appendix A Comparison of *VISCOELASTIC & *CREEP Keywords.....	81
Appendix B Analytical Models of Viscoelastic Behavior	
B.1 Introduction.....	87
B.2 Maxwell Model.....	87
B.2.1 Governing Equation.....	88
B.2.2 Creep for Maxwell Model.....	88
B.2.3 Stress Relaxation	88
B.2.4. Strain Recovery	89
B.3 Kelvin/Voigt Model	89
B.3.1 Governing Equation	90
B.3.2 Creep for Kelvin or Voigt Model.....	90
B.3.3 Stress Relaxation	90
B.3.4 Strain Recovery	90
B.4 General Equations	91
Appendix C Geologic Time Scale.....	92
References.....	93
Appendix D Glossary.....	95
References and Other Influential Papers.....	99
Vita	105

List of Tables

Table 1.1 Displacement history and slip-rate in the NMSZ,.....	6
Table 5.1 Range of Parameter Space Searched.....	49
Table 5.2 2D models run for 10000 years with Maximum Average Shear Stress criteria on whole fault.....	63
Table 6.1 These 3D models were run for 10000 years with Maximum Shear Stress criteria on each node with 30 % drop in stress on fault.....	74

List of Figures

Figure 1.1 Probabilistic Seismic Hazard Maps of USA by USGS.....	3
Figure 1.2 Areas affected by earthquake 1811-1812 (NMSZ) and 1906 (San Francisco).....	4
Figure 1.3 Index map of Reelfoot rift in the NMSZ.....	5
Figure 2.1 Schematic map of the NMSZ shows major tectonic features [1].....	9
Figure 2.2 Schematic map of the NMSZ shows major tectonic features [2].....	11
Figure 2.3 Bauguer Gravity profile and inferred crustal cross section normal to the Reelfoot rift in the NMSZ.....	12
Figure 2.4 Regional setting and seismicity within the NMSZ.....	13
Figure 3.1 Standard Linear Solid.....	25
Figure 4.1 Logic for the friction subroutine used in the 2D models (plane-strain or anti-plane).....	43
Figure 4.2 Logic for the friction subroutine used for 3D/anti-plane models.....	45
Figure 4.3 Figurative representation of the failure criteria.....	47
Figure 5.1 2D models in ABAQUS.....	48
Figure 5.2.1 Width 3 km, Power-law exponent 1.5, Viscosity variation.....	50
Figure 5.2.2 Width 3km, Power-law exponent 2.0, Viscosity variation.....	50
Figure 5.2.3 Width 3 km, Power-law exponent 3.0, Viscosity variation.....	51
Figure 5.3.1 Width 3km, Viscosity 10e21 Pa-s, Power-law exponent variation.....	52
Figure 5.3.2 Width 3 km, Viscosity 10e22 Pa-s, Power-law exponent variation.....	52
Figure 5.4.1 Width 6 km Power-law exponent 1.5 , Viscosity variation.....	53
Figure 5.4.2 Width 6km, Power-law exponent 2.0, Viscosity variation.....	54
Figure 5.4.3 Width 6 km, Power-law exponent 3.0, Viscosity variation.....	54
Figure 5.5.1 Width 6km, Viscosity 10e21 Pa-s, Power-law exponent variation.....	55
Figure 5.5.2 Width 6km, Viscosity 10e22 Pa-s, Power-law exponent variation.....	56
Figure 5.6.1 Width 12 km, Power-law exponent 1.5, Viscosity variation.....	57
Figure 5.6.2 Width 12 km, Power-law exponent 2.0 , Viscosity variation.....	57
Figure 5.7.1 Width 12 km, Viscosity 10e20 Pa-s, Power-law exponent variation....	58
Figure 5.7.2 Width 12 km, Viscosity 10e21 Pa-s, Power-law exponent variation....	59
Figure 5.8.1 Power-law exponent 1.5, Viscosity 10e20 Pa-s, Width variation.....	60
Figure 5.8.2 Power-law exponent 1.5, Viscosity 10e21 Pa-s, Width variation.....	60
Figure 5.9.1 Variation of stress profile along the depth on the fault section with time. Failure criteria is average shear stress on the fault, constant stress drop on the fault at every earthquake.....	64
Figure 6.1 3D models in ABAQUS. A symmetry plane is imposed perpendicular to the fault at it's midpoint. Brick elements are employed.....	66

Figure 6.2.1	Width 24 km Power-law exponent 1.5, Viscosity variation.....	67
Figure 6.2.2	Width 24 km Power-law exponent 2.0, Viscosity variation.....	68
Figure 6.3.1	Width 24 km, Viscosity 10e21 Pa-s, Power-law exponent variation....	69
Figure 6.3.2	Width 24 km, Viscosity 10e21 Pa-s, Power-law exponent variation....	69
Figure 6.4.1	Width 54 km, Power-law exponent 1.5, Viscosity variation.....	69
Figure 6.4.2	Width 54 km, Power-law exponent 2.0, Viscosity variation.....	71
Figure 6.5.1	Width 54 km, Viscosity 10e21 Pa-s, Power-law exponent variation.....	72
Figure 6.5.2	Width 54 km, Viscosity 10e22 Pa-s, Power-law exponent variation.....	72
Figure 6.6.1	Width 75 km, Power-law exponent 1.5, Viscosity variation.....	73
Figure 6.7.1	Power-law exponent 1.5, Viscosity 10e22 Pa-s, Width variation.....	74
Figure 6.7.2	Power-law exponent 1.5, Viscosity 10e21 Pa-s, Width Variation.....	74
Figure A.1	Displacement at top surface at Time t = 0.000 Years.....	82
Figure A.2	Displacement at top surface at Time t = 0.236 Years.....	83
Figure A.3	Displacement at top surface at Time t = 0.540 Years.....	83
Figure A.4	Displacement at top surface at Time t = 0.800 Years.....	83
Figure A.5	Displacement at top surface at Time t = 1.080 Years.....	84
Figure A.6	Displacement at top surface at Time t = 1.720 Years.....	84
Figure A.7	Displacement at top surface at Time t = 2.700 Years.....	84
Figure A.8	Displacement at top surface at Time t = 5.600 Years.....	85
Figure A.9	Displacement at top surface at Time t = 10.600 Years.....	85
Figure A.10	Displacement at top surface at Time t = 20.000 Years.....	85
Figure A.11	Displacement at top surface at Time t = 40.000 Years.....	86
Figure A.12	Displacement at top surface at Time t = 80.000 Years.....	86
Figure B.1	Maxwell Model.....	87
Figure B.2	Kelvin or Voigt Model.....	89
Figure C.1	geological time scale.....	91

Introduction

Abstract

There are two objective of this thesis; engineering and scientific. Each involve pushing the limits of the current state of the limits of current state of knowledge to a higher level and developing methods to solve one of the most complex existing problems in the science of the Earth *i.e.* intraplate earthquakes. This topic is relatively less understood and quite untouched in the geologic community. The aim here is to develop a time dependent Finite Element (FM) Model to simulate the New Madrid Seismic Zone (NMSZ), which is capable of generating major earthquake in the region with a frequency of 500 to 1000 years. The objective of this thesis will be to expand the geometrical and rheological parameter space to place bounds on possible geometries and rheologies.

1.1 Background

The earth is subjected to complex ongoing phenomena of creation, operation and destruction, made up of known and unknown factors, all of which are affecting human life. The tendency of the human mind has always been to find out these things, understand and master them. The basic approach has always been to divide the system into individual components or elements, whose behavior is readily understood, and then rebuild the original system from such component to study the behavior of system as a whole, through the incremental understanding of the effect of one element on the another and on the whole system. This is the way in which the scientific investigation proceeds.

Finite element procedures are prevalent in the engineering analysis. The application domain of the finite element has drastically increased in the past decade with continuous improvement in the existing methods. This growth is supposed to accelerate in the coming time. Currently this procedure is employed extensively in he field of analysis of solid, structures, heat transfer, fluids and virtually all fields of the practical engineering analysis. Given the wide applicability of finite element and successful results, the scope of Finite Element Method (FEM) has been extended to the unexplained realm of

problems of science. Investigations in this thesis concerns the application and development of finite element procedures to solve geological science problems with concentration on the intraplate earthquake mechanism.

In the efforts to ascertain the character of continuous system, we mathematically divide a system into infinitesimally small components. This leads to differential equations, which imply an infinite number of degree of freedom. This technique has evolved into FEM by keeping element size small but finite. With the current computational capability of digital computers these discrete problems can be solved. Hence the continuous problem can be approximated with reasonable accuracy depending upon the number of the finite elements the problem can be divided into. To overcome the intractability of the continuum problem, various methods of discretization have been proposed, both by engineers and mathematicians. Continuous development in the methods of discretization (mesh generation) and increasing computational capacity are pushing the limits. All tend to involve an approximation which hopefully approaches to the limit of the true continuum solution.

1.2 Intraplate Earthquake and NMSZ.

Intraplate earthquake are a geophysical phenomenon. Geophysics is the science of the earth. In order to understand the character of such phenomenon of science, experiments are essential and geophysics is no different. Experiments are required in this case as well to understand the associated backdrop. But the need for very large scale of space and time leads to practical impossibility. These leaves geologists with no solutions, other then to study the earth as it exists and draw conclusion about the processes that shaped it's currents state. Development of computation models in support of proposed hypothesis is needed.

Seismic hazards map of the USA (Figure 1.1), clearly indicates the zones, having potential danger from the earthquake that exist in the central-eastern United States, *i.e.* the NMSZ. At some probability level, the NMSZ has potential of producing earthquakes of equivalent magnitude as those that have been witnessed in California. The NMSZ is situated in the mid-continent. This area has thicker, colder, older rock, hence seismic

wave travel longer distances. This affects a larger area than affected by an equivalent magnitude earthquake in the western US (Figure 1.2). Also eastern United States on average is more densely populated as compared to the western US, which increases the overall hazards potential of NMSZ.

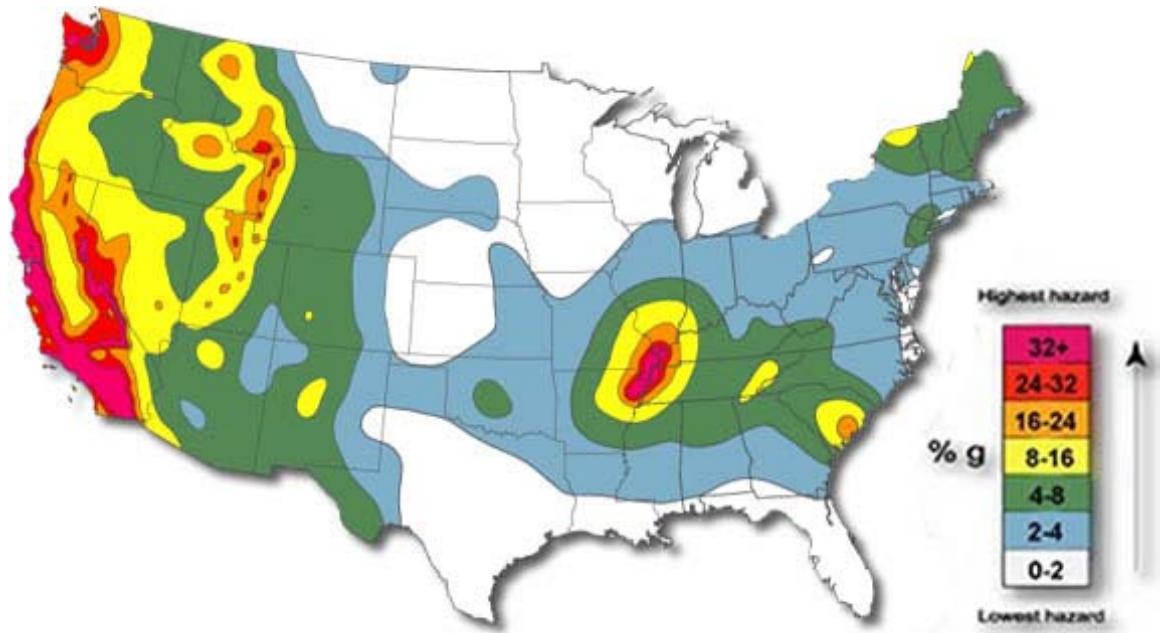


Figure 1.1 Probabilistic seismic hazards maps of USA.

[<http://eqhazmaps.usgs.gov/html/us2002.html>]

Earthquakes have been known to exist at plate boundaries where plates move against each other with intermittent slips giving birth to earthquakes. The NMSZ involves a different mechanism that gives rise to recurrent earthquakes far from the plate boundaries. The hazards in the NMSZ are many ways more challenging than in the western US and the uncertainties are much greater. In western US careful, study has led to relative consensus on the issues most critical to seismic hazards assessment.

This is not the case for the NMSZ. The low hazards model proposed by the Newman *et. al.* [1999] contradict model by Stuart *et. al.* [1997] and Kenner & Segall [2000]. For the reason explained previously, the three major earthquakes of 1811-1812 in NMSZ affected an area much larger than even the famous 1906 California M 7.8 earthquake

(Figure 1.2). The paleoliquefaction evidence from the NMSZ shows that earthquake with effects comparable to those of 1811-1812 have occurred at least three times. However, earthquakes of moderate size seem to be missing in the geologic, historic, and instrumental records of the NMSZ. There is less certainty of exact magnitude (which is $M > 7.0$ at least) of the earthquakes differing by half unit of magnitude. Various estimates for the magnitude earthquake lie between 8.5-7.3. This lack of preciseness may not be as important if we take note of historical observations of the effects of the earthquakes. Occurrence of such event may cause severe landslide hindering river traffic and potential failure of the bridges across the Mississippi river.

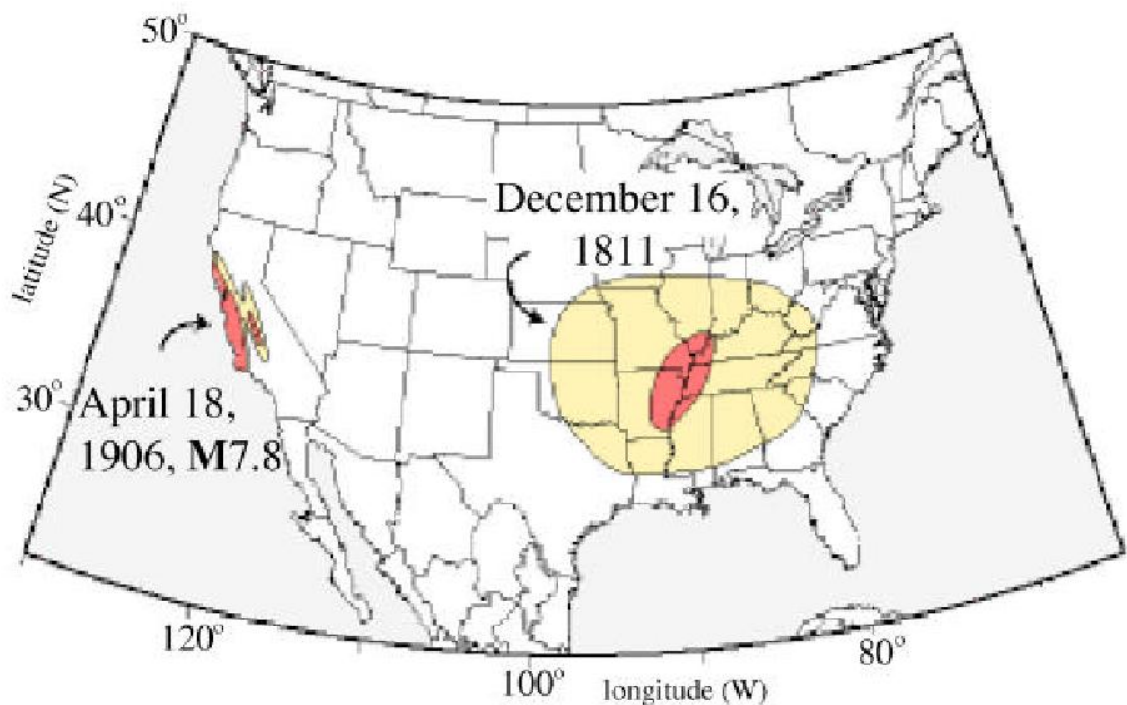
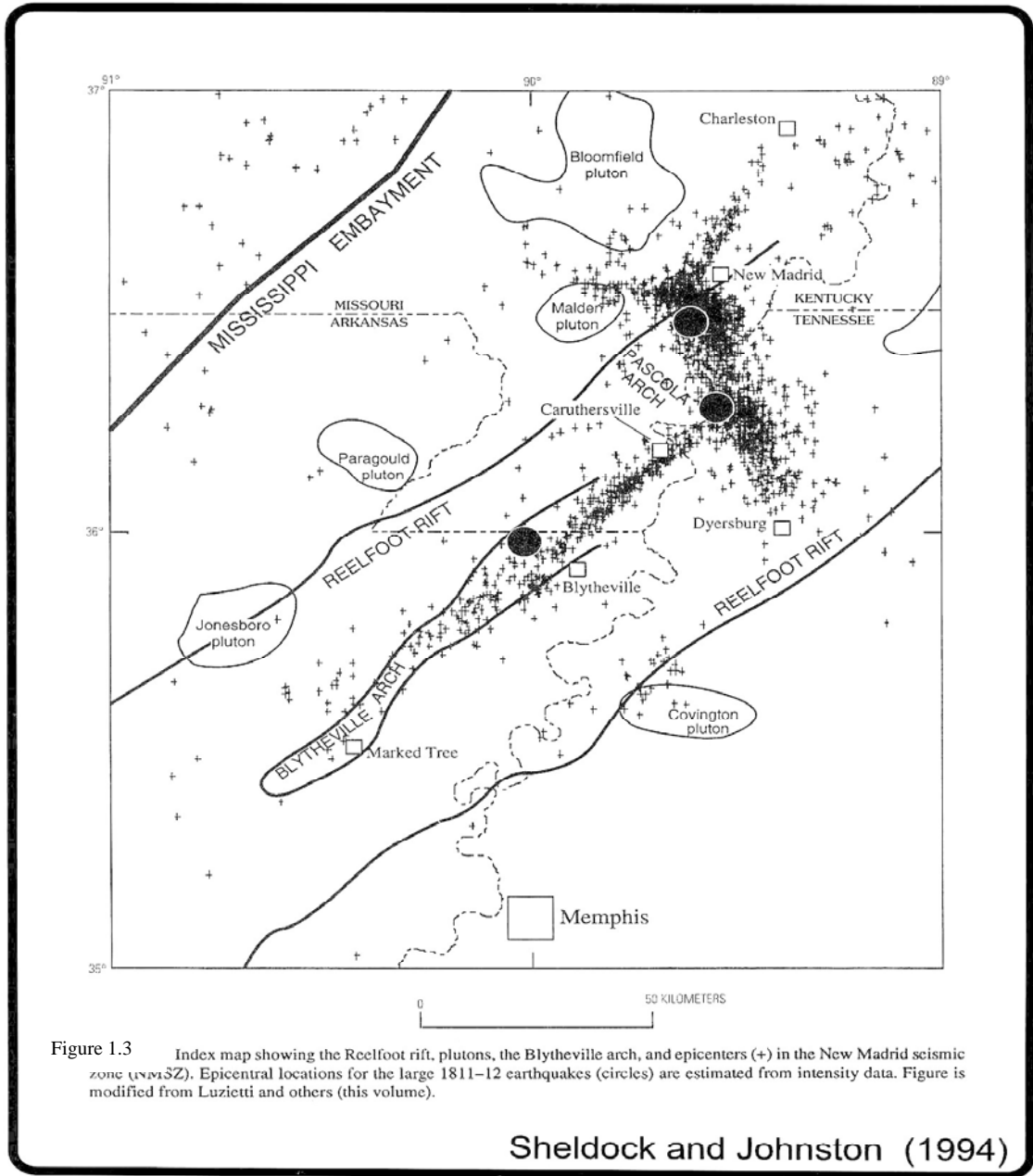


Figure 1.2 Areas affected by earthquake of similar magnitude 1811-1812 NMSZ and 1906 California. Darker shading indicates minor to major damage to buildings and their contents. Outer lighter shading indicates that shaking was felt but objects receive little or no damage.

[http://www.eas.slu.edu/Earthquake_Center/EQInfo/Flyers/CUS/NM_06_Intensities.html]

One of the factors making study of NMSZ so challenging is erosion due to the Mississippi river which buries most evidence of surface faulting and has deposited up to 1 km of unconsolidated sediments since the Cretaceous (*i.e.* 65 million years ago). This

masks deeper evidence of faulting. It is very difficult to state something firmly in absence of topographic relief in the NMSZ. Current subsurface data can give only estimates about very recent geologic time. It is a scientific mystery of, how and why such rates of stress transformation can occur in NMSZ so as to generate seismic activity of such frequency and magnitude.



1.3 Modeling Philosophy

A tectonic model of the NMSZ should satisfy at least the following criteria: events comparable to those in 1811-1812 recur about every ~500 years; the active fault system is probably not longer than ~200 km and geodetic observation show a notable lack of relative motion across the fault. There is no far field motion. These observations clearly indicate the inapplicability of physical/ computational models which work well in plate boundary conditions. A number of appropriate hypothesis have been proposed to explain the seismicity in NMSZ and computational models have been developed and analyzed for NMSZ. One of the strongest hypotheses was proposed by Kenner and Segall [2000]. This thesis is based in Kenner and Segall [2000] model, which is a unique model in the sense that it produces repeated earthquake in the NMSZ region, along with satisfying other boundary conditions like zero far-field velocities and small cumulative slip on the fault. This potentially explains how significant intraplate earthquake can occur recurrently.

The model chosen to interpret geodetic measurements, directly affects estimated fault slip rates. Such model should also be consistent with all available information like applied boundary conditions. Present day strain-rates are low but prior to Holocene (*i.e.* last 10,000 years) deformations rates were even orders of magnitude lower than that of today. A high rate of seismicity is also proposed during Holocene, which is attributed to weakening of the sub-crustal zone [R Van Arsdale, 2000]. Table 1.1 gives details of the displacement history of the NMSZ.

Table 1.1 Displacement history and slip-rate in the NMSZ [R Van Arsdale, 2000]

Geologic Time	Years (million years -my)	Slip (meter-m)	Slip Rate (mm-year⁻¹)
Late Cretaceous-Present	80 my	73	0.0009
Late Cretaceous	80-65 my	10	0.0007
Paleocene	65-54 my	21	0.002
Late Paleocene-Eocene	54-45 my	11	0.001
Late Eocene-Holocene	45 my- 9000 y	15	0.0003
Holocene	9000 y – Present	16	1.8
Late Holocene	AD 900- 1812	5.4	6.2

1.4 Overview of Thesis

The second chapter deals with the background of the NMSZ, which summarize geological structure, throws light on the recent research in the NMSZ and gives a brief description of previous FE modeling endeavors and a summary of their outcomes. A weak viscoelastic zone underlying the lithosphere is developed as the cause of induced seismicity. Strain emanating from the relaxing weak zone then gets dissipated along the critical fault with in the NMSZ.

The third chapter details the development of the different rheologies used in this analysis. It also discusses the geometric parameter space which will be studied. Finally chapter three addresses the FE technologies and initial condition which are necessary to properly precondition the model.

The fourth chapter deals with the fault friction criterion, putting up logic behind the implementation of the friction subroutines used in ABAQUS. Faulting is one of the complex phenomenon when it comes to numerical modeling of contact surfaces. Logic developed involves use of book-keeping parameters for the status of fault after every equilibrium state/iteration.

Appendix A has been attached to throw light on the bench-marking efforts undertaken to establish the efficiency of the ABAQUS to solve viscoelastic problems when *VISCOELASTIC keyword as compared to *CREEP is used for Maxwell materials. These efforts are essential to make sure parameters supplied to the numerical model exactly represent the equivalent analytical values. Careful efforts are made to derive the parameter values in the format that is supported by the ABAQUS.

Progressive Model Development

2.1 Introduction and Significance

While most of the earthquakes occur at plate boundaries, the occurrence of large intraplate earthquakes can have devastating consequences when their magnitude is comparable to plate boundary earthquakes. This statement evolved from the geologic evidence found in central United States, where three major earthquakes of magnitude $M > 7$ struck in the NMSZ, within 54 days in the winter of 1811-1812. These earthquakes are inferred to be amongst the largest known intraplate earthquakes in the US. As demonstrated by the Bhuj Earthquake 2001, $M \sim 7.7$, in Gujrat, India, very large earthquake do occur in intraplate regions and can cause widespread liquefaction with little expression of faulting or rupture at the ground surface. Paleoliquefaction data suggests at least three large seismic events in NMSZ in the last 2000 years, with the recurrence interval of 500-1000 years. The moment magnitude must have been at least 6.4 or larger to have been big enough to cause this severe liquefaction over large areas (Figure 2.1).

2.2 Geography of NMSZ

The NMSZ is situated within an ancient intraplate rift zone, known as Reelfoot rift, principally active during latest Precambrian and/or early Paleozoic time (*i.e.* about 550 million years ago) [Hamilton, Zoback and Mckeown, 1982]. The network catalogue of micro-earthquake reveals a clear pattern of intersecting planar active faults (Figure.1.3) consistent with those that presumably ruptured during 1811-1812. Two vertical southwest-northeast trending faults, ~ 50 km and ~ 150 km in length are offset by ~ 70 km long southwest dipping reverse fault known as Reelfoot fault (Figure. 2.1). The Reelfoot fault is approximately perpendicular to the two vertical faults. This dipping fault is the only one having observable features on surface. Aeromagnetic data provide evidence for the existence of the large mafic intrusions in the rift (Figure 2.3). The axis of rift trends

approximately N50E. The rift related faults are in a favorable position to fail within the regional stress field which has an approximately N60-65 direction S_{hmax} (maximum horizontal compression) [Zoback and Zoback, 1989].

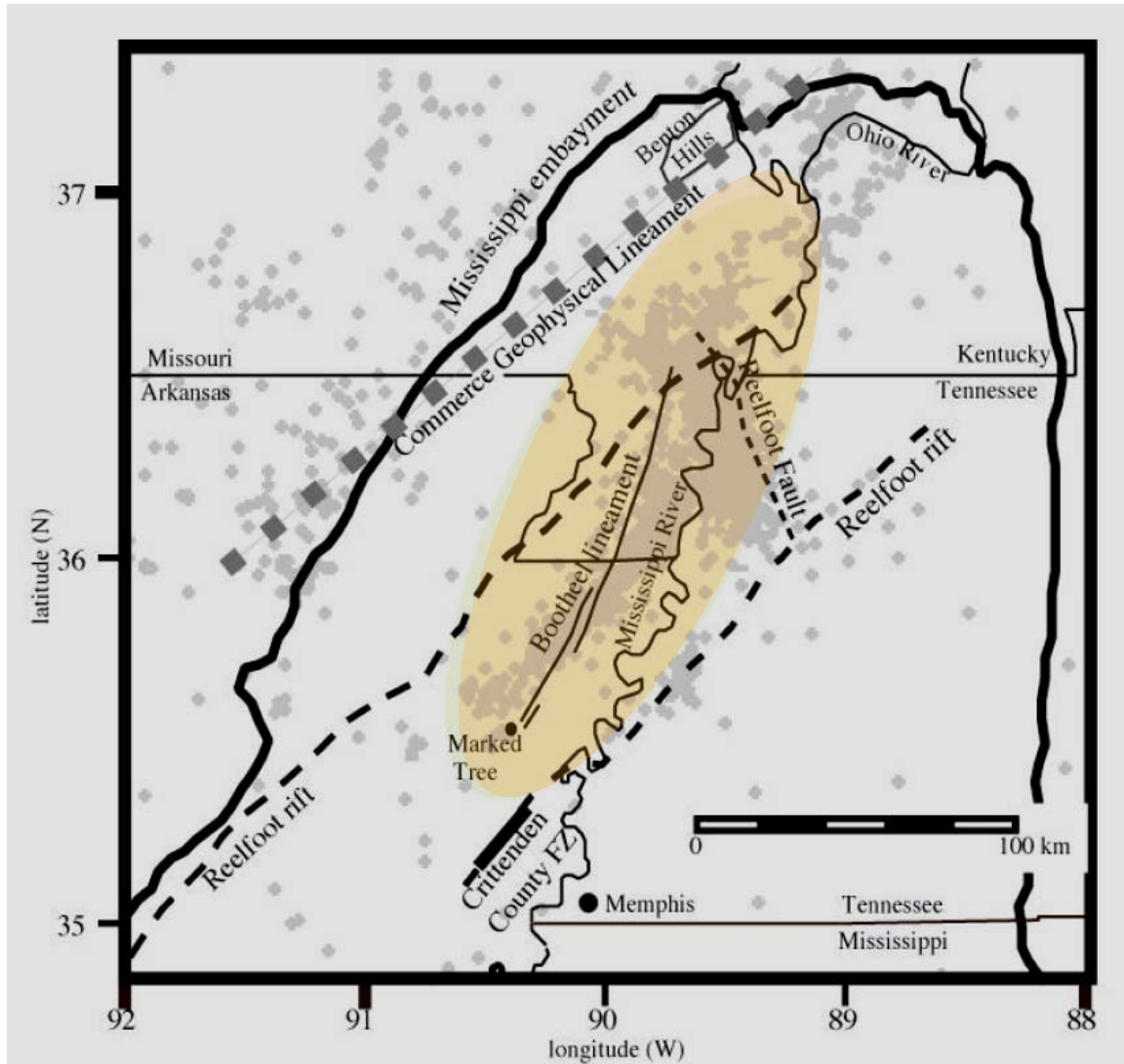


Figure 2.1. Schematic map of the NMSZ shows major tectonic features, state boundaries and major rivers. Instrumentally recorded seismicity (light dots at epicenters) delineates faults that probably ruptured in 1811-1812. Currently, aseismic structures (dashed lines) may also represent potential earthquake sources such as the Reelfoot rift boundaries, the Commerce geophysical lineament, the Crittendon county fault zone, and the Bootheel lineament. The shaded oval approximately covers the area where >1% of the surface is covered by sand blows of all ages, although liquefaction feature has been found far beyond this areas. The heavy dark lines represent the Mississippi embayment, a sedimentary basin, which continues into the gulf of Mexico. Altered from Atkinson, G. M. and 24 others [2000]

The boundaries of the failed rift are approximately 70 km wide and 300 km long [Hildenbrand and Hendricks, 1985], seismic refraction studies reveal an anomalously dense “rift pillow” at the base of the crust beneath the rift (Figure. 2.2 and 2.3) [Mooney *et al.*, 1983]. The “rift pillow” is characterized by high seismic velocity and high density material in the lower crust [Ginzburg *et al.*, 1983; Mooney *et al.*, 1983]. A Mississippi embayment in which the Reelfoot rift is located contains 5 km of late Precambrian/Paleozoic (From 250 to 550 million years ago) sediments, a major Mesozoic (50-250 million years) nonconformity, and 1 km of late Cretaceous/Cenozoic (from 150 million years to 10,000 years ago) sediments lying above the rift pillow [Ginzburg *et al.*, 1983]. The nonconformity represents a gradual period of uplift and extension accompanied by numerous magmatic intrusions (Figure 2.3). This shows that the Reelfoot rift was reactivated in the mid-Mesozoic [Ervin and McGinnis, 1975; Braile *et al.*, 1986]. Geological and geophysical evidence also indicates some episodes of Cretaceous magmatic activity [Zoback *et al.* 1980, Hildenbrand and Hendricks, 1985], hence crustal structure in NMSZ is anomalous as compared to surrounding region (Figure 2.3).

Recent focal mechanisms [e.g., Herrmann and Canas, 1978; Herrmann, 1979] and micro-seismicity studies [O’connell *et al.*, 1982, Stauder, 1982; Chiu *et al.*, 1992] reveal that the NMSZ is characterized by two zones of strike-slip faulting on vertical planes, and one zone of thrust faulting on a dipping plane lying between the strike-slip zones.

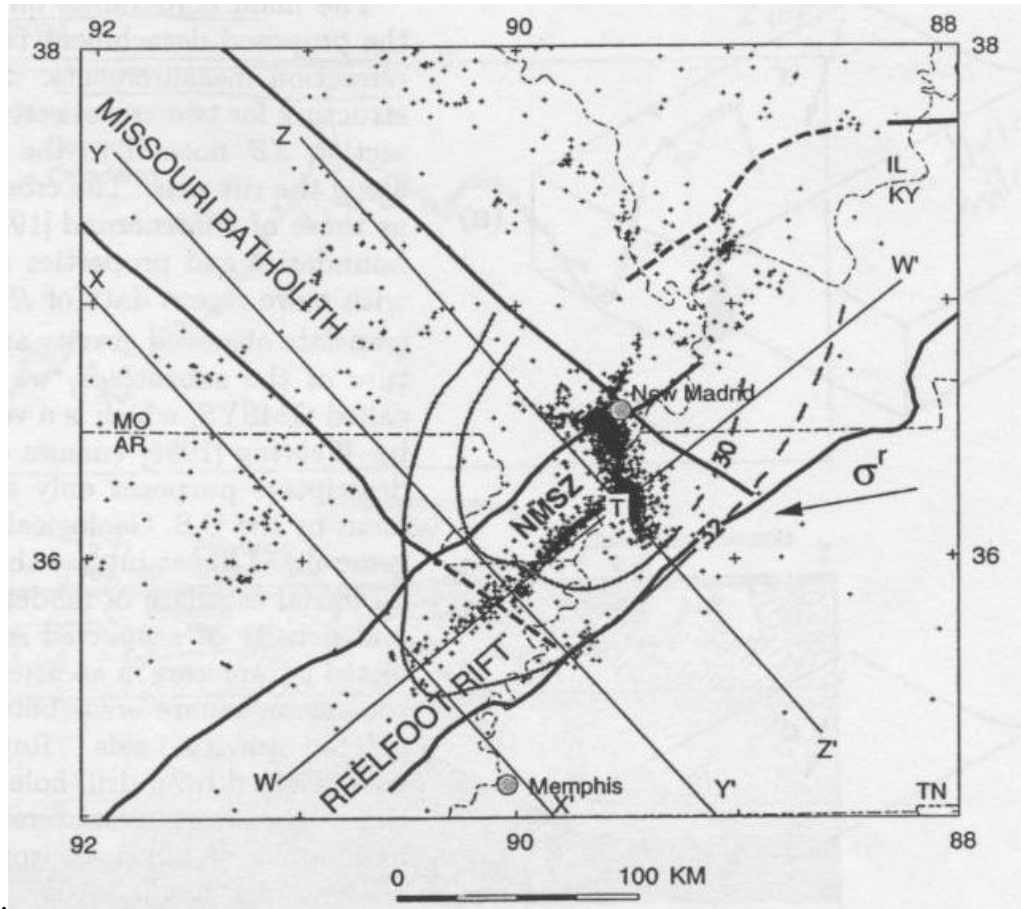


Figure 2.2 Small dots in the figure represents earthquakes of magnitude 0.1 to 5.2. Lines WW' is perpendicular to ZZ' which is parallel to rift axis. Location T is top of model perceived dome at the intersection of WW' and ZZ'. Heavy black lines trending northwest are the inferred edges of the Missouri batholith. It is not known how the Missouri batholith might affected seismicity in the NMSZ. Heavy gray lines are contours in depth (km) to top of rift pillow. The arrow is in the direction of far-field plate compression σ^r . [Stuart et al, 1997]

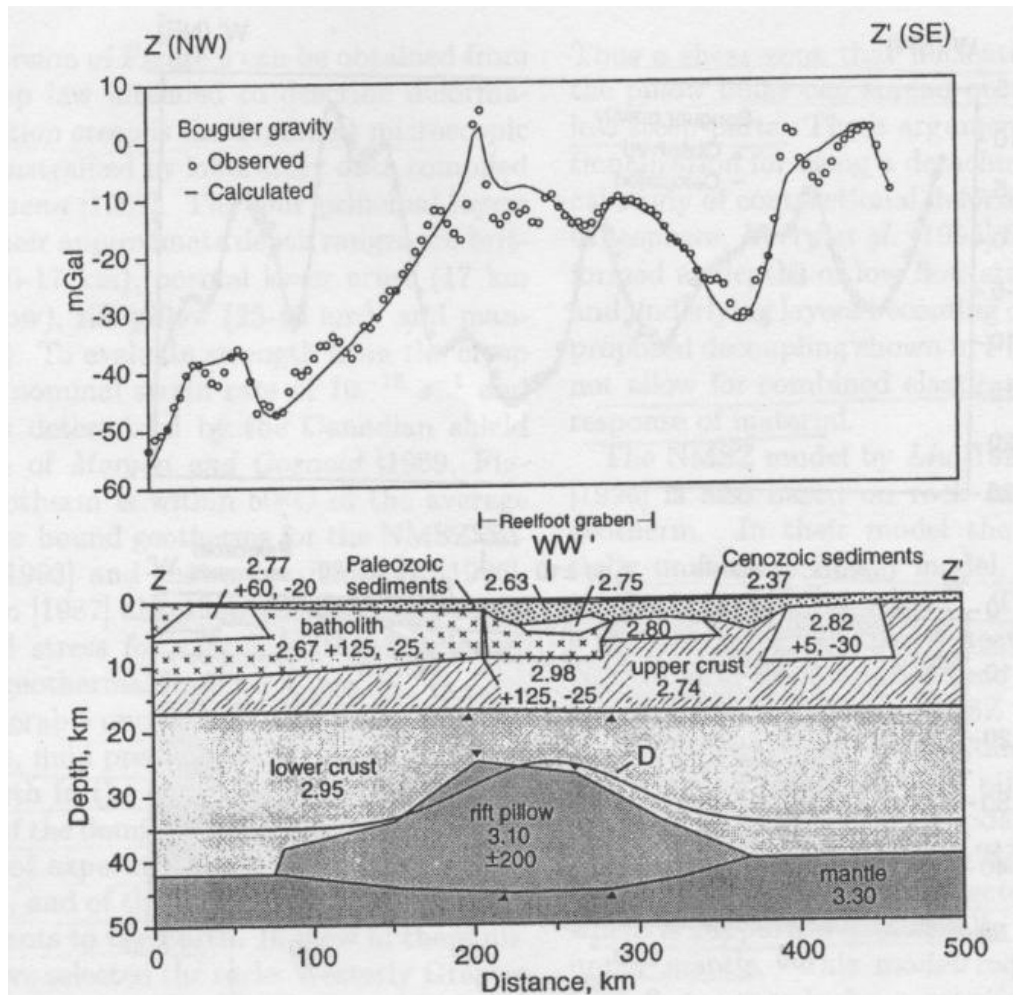


Figure 2.3 Bouguer Gravity profile and inferred crustal cross section normal to the Reelfoot rift along line ZZ' in figure 2.2, from Hinderbrand et al [1985]. The top figure shows actual and derived model for the gravity profile. Bottom figure shows inferred boundaries with densities in gcm^{-3} with labeled interpretation [Stuart et al, 1997]

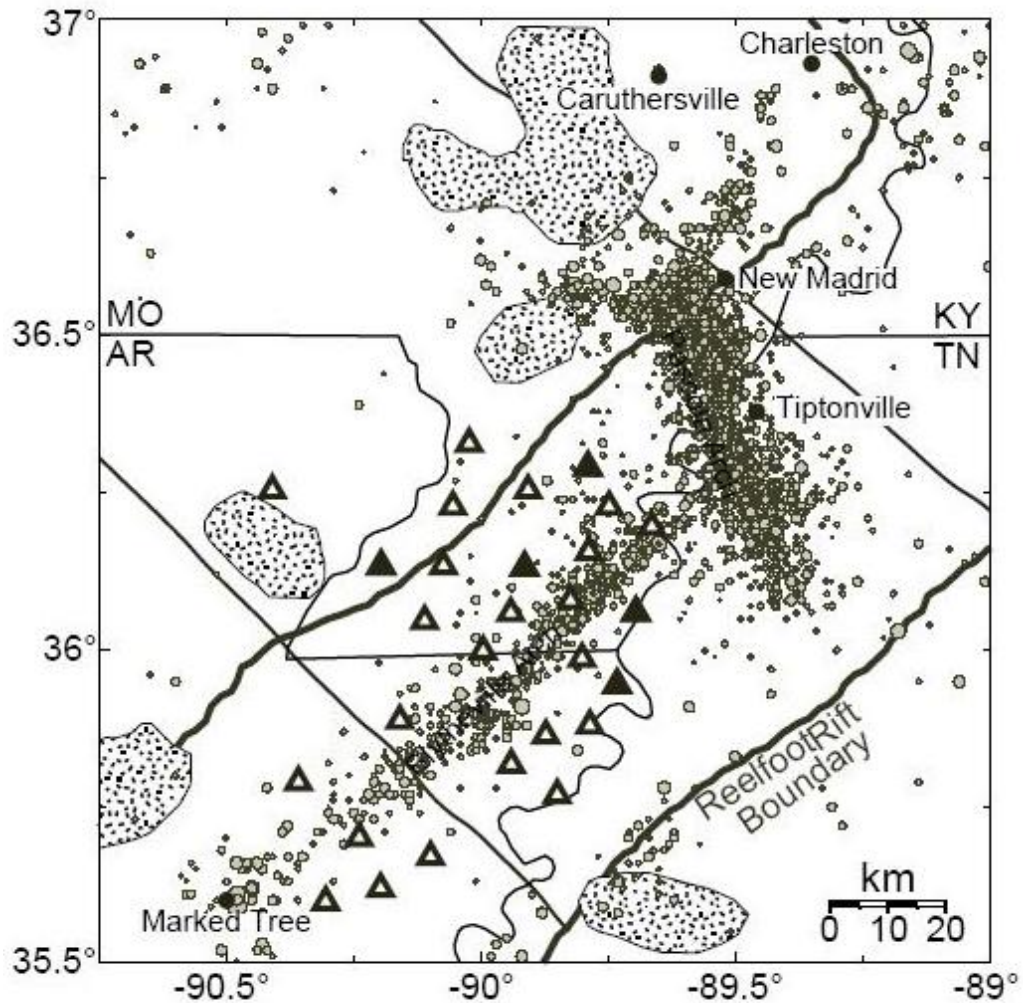


Figure 2.4 Regional setting and seismicity (filled circles) within the NMSZ. The hatched regions are plutons. Thick lines denote the boundary of the Reelfoot rift. Thinner northwest trending lines denote the approximate lateral extent of the Missouri batholith. Solid triangles denote sites in the hypothetical 5 station continuous network used in GPS uncertainty calculations [Kenner & Segall, 2000]. Both solid and open triangles are included in a 28 station yearly campaign network by Stanford University.

2.3 Rheological Properties of NMSZ

Recent studies have increased our knowledge of the structure and seismicity associated with the NMSZ. As discussed above, the seismicity observed in Figure 2.3, in the NMSZ seems to be associated with the anomalous state of a sub-horizontal crustal structure and its properties. A variety of geophysical techniques are being used to define the underlying structure and seismicity of the area and a number of hypotheses have been

proposed to explain the seismicity in NMSZ. The “zone of weakness” model, suggested by Braile et al., [1986] and Hinze et al., [1998] proposes to explain the major seismicity in the area. In this model contemporary earthquake activity is caused by the reactivation of ancient faults associated with the rift, which are favorably aligned for the failure within the current regional compressive stress field of eastern North America. These models can not provide for a 500 years repeat time as strain-rates in eastern North America are too low. Boundary element modeling [Gomberg, 1992; Gomberg and Ellis, 1994] suggests that morphologic and geologic features and the distribution of seismicity in the area are consistent with tectonic deformation, and slip on two left-stepping, right-lateral strike-slip faults that are coincident with the northeast trending zone of seismicity. Recent GPS study show no observable strain-rate within the uncertainties of the measurements [Neuman et. al., 1999, Kerkla et. al., 1998]. The lack of significant long term surface deformation has led to the suggestion that the NMSZ is possibly a very young geologic feature [Schweig and Ellis, 1994]

The spatial distribution and characteristics of liquefaction features, serve to estimate earthquake magnitude and affected areas. The enormity of the volume of sand mobilized at many of the liquefaction sites in the NMSZ implies that they could not have been formed by local events of moderate magnitude. The paleoliquefaction interpretation also suggests that large earthquakes like those of 1811-1812 may be characteristics earthquakes repeated in ~500 years. Multiple units of vented material are evident in many of the sandblows and have been interpreted as resulting from major events that have occurred within weeks to months of each other. Thus the paleoliquefaction records suggest that the clustering of earthquakes that occurred in 1811-1812 also occurred in prior events.

The earth’s geotherm plays an important role in controlling material properties of the crust and mantle. The heat flow of $\sim 60 \text{ mW/m}^2$, in NMSZ [Swanberg et. al., 1992, Liu and Zoback, 1997], is somewhat above average though not particularly abnormal. A crustal model based on relatively high heat flow is considered. An elevated increase in temperature with depth from high heat flow is believe to produce a relatively weak zone near the base of crust because of the ductile behavior of geological materials at this higher temperature [Chen & Molnar, 1983, Chen, 1988]. Based on the heat flow

measurement, the assignment of a geotherm based lower crustal viscosity is somewhat arbitrary and the results of this model should be considered carefully. That is why a range of rheologies is considered in this study.

2.4 Some Suggested Facts Derived from NMSZ Observations

- The rift structure is more developed on the southern arm than on the northern arm. The southern arm is aligned above the rift pillow. The area also contains the highest density of liquefaction, and sandblow features.
- Most of seismicity is concentrated between 4 -15 km depth.
- Length of strike-slip failure is greater for thrust faulting, although the thrust fault is easier to document geologically. As shown in figure 1.3 the 1811-1812 earthquake mainshocks are thought to have occurred in each of three fault segments in the NMSZ.
- Increased seismicity Late Quaternary (1 million year ago) and Holocene (10,000 years ago).
- Repeated occurrence of earthquake at fairly regular intervals.
- Presence of some zone of weakness

2.5 Weakening Mechanism

It is proposed that either thermal or pressure perturbations affected the region around NMSZ during the Holocene. The model presented requires a sudden perturbation which triggers seismicity due to relaxation in the lower crust and upper mantle. There is no specific cause that can be ascertained to trigger the seismicity given the current state of NMSZ.

One hypothesis for weakening is deglaciation at the beginning of the Holocene. The last North American glacial unloading took place a maximum of 10,000 years ago, and was relatively fast as compared with the time-scale of relaxation of mantle materials as

well as the time-scale of original loading [Karato & Wu, 1993, Peltier & Jiang 1996]. Thus even though the finally relaxed postglacial state should be close to the preglacial state, the rapidity of relaxation compared with the build-up of the ice load would be unique to the postglacial epoch. After unloading, during viscoelastic relaxation, pressure perturbations of several MPa may have been generated at shallow depths at a distance approximate 500 km outside the perimeter of former ice sheet.

1. Deglaciation produces increased pressure gradients, causing mantle material to slowly diffuse laterally in response to unbending of the North American plate as the glaciers recede. This would have resulted in a stress perturbation at the NMSZ causing it to weaken and initiate the young cycle of deformation.
2. Heating of the lower crust & upper mantle generated by postglacial flow raised the temperature of these regions and weakened them. This effect is generally small on laterally homogeneous viscoelastic models, but localization of flow within thin regions of the lower crust or upper mantle is possibly produced by heterogeneity in the mantle and lithosphere.

2.6 Previous Models of Tectonism/Seismicity

As pointed out earlier, any effort to produce a tectonic model applicable to NMSZ should be capable of producing multiple earthquakes having magnitudes comparable to those in 1811-1812 and recur in ~500 year increments. The fault should be ~200 km long, with very small surface strain-rates. Several models satisfying these criteria have been proposed, which are based on the assumption of uniform stress field and some sort of heterogeneity in the lower crust that produces deformation in NMSZ. A brief introduction to various model regimes is as follows:

1. Grana and Richardson [1996] proposed a finite element model without discrete faulting but with a stress concentration due to lateral density contrast within the crust *i.e.* the rift pillow as a possible reason for increased seismicity. This rift pillow is partially supported by the lithosphere, hence in this model the highest compression will occur above the thickest portion of the rift pillow generating the

thrust faulting. This implies high seismicity around thickest region. This hypothesis is supported by the observed seismicity in the southern arm of NMSZ located above the area where the rift pillow is the thickest [*Hildenbrand and Hendricks, 1985*] although this arm is predominantly a strike-slip feature. The model generates gravitationally driven body forces which contribute to both the present day tectonic stress field and intraplate seismicity. Consequently this model is attractive because the same mechanism is responsible for the local subsidence. The same hypothesis has been extended by Pollitz, Kellogg and Burgmann [2001]. The addition of local stresses associated with the rift pillow, however, results in an approximately 30% reduction in the resolved maximum horizontal shear stress. The main questions on this model are: a) How long has the rift pillow been gravitationally unstable? b) How is rift pillow support partitioned between the crust and mantle prior to the Holocene (when did it begin to sink)? and c) How weakening of these regions was accomplished?

2. Liu and Zoback [1997] proposed that the high rate of seismicity results from high ductile strain-rates in the lower crust and upper mantle due to locally elevated heat flow.
3. Cox and Van Arsdale [1997] hypothesize that the passage of the Bermuda hot spot in mid-Cretaceous time might have weakened the lithosphere as a result of accelerated heat exchange and thereby increase the potential for seismicity in the area.
4. Another hypothesis suggests lateral contrasts in elastic properties such as Young's Modulus within the crust may concentrate stress and promote seismicity within a zone of varying elastic moduli. This intrusion may be either stiffer (stress and seismicity concentrated in the intrusion) or less stiff (seismicity in the outer area) than the surrounding rock. The fractures associated with the rift intrusion may also serve as a zone of varying stiffness. Hence stress and seismicity can be transferred from the rift pillow in the lower crust to the upper crust. [*Malvern, Continuum Theory, 1969*]

5. Stuart et al [1997] presented an elastic boundary element model. They proposed that the cause of stress concentration in the NMSZ is slip on a weak sub-horizontal detachment fault in the lower crust (placed directly above the rift pillow). This leads to the observed seismicity. The model has far-field velocities of zero, a suitable boundary condition for intraplate regions. However, the model does not deal with time-dependent nature of faulting, hence repeated seismic events are not considered. Also this model generates a velocity field at the free surface near the fault that was found to be compatible with the geodetic data at the time of the paper [Liu, Zoback & Segall, 1992]. The data has been revised since that time. More accurate geodetic data indicates that surface velocities near the fault are effectively zero given the significantly smaller uncertainties associated with the GPS data.

The above models gradually try to cover observations in NMSZ, yet there are several potentially active forcing mechanisms in this region, which are still not understood. Following are a few examples of this.

1. The North American regional compressive stress field due to plate tectonics forces [Sbar and Sykes, 1973; Herrmann and Canas, 1978, Zoback and Zoback, 1989]. However the intraplate strain-rates due to plate tectonics is very small.
2. Body forces acting on the high density rift pillow in the lower crust [Ervin and McGinnis, 1975] and how these forces have been active long enough to produce seismicity in the Holocene.
3. The change in the Mississippi river course during the Holocene.

2.7 Conclusion

None of the hypotheses are completely able to explain the increased Holocene seismicity and lately discovered paleoliquefaction evidence in the NMSZ. Recent finite element modeling efforts by Kenner and Segall [2000] provides a step towards more realistic modeling resulting in the successful simulation of repeating sequences of earthquakes. In the present model no particular triggering mechanism has been proposed.

It is based on sudden weakening in the NMSZ, which took place approximately 10,000 years ago. This is the first modeling effort which successfully models all the observations from the NMSZ including surface strain-rates, cumulative fault offsets, earthquake magnitudes and coseismic fault slip. The model computed surface strain-rates in the mid-interseismic period would not be detectable in the NMSZ at the level of uncertainty which exists in recent measurement using GPS. The model postulates sudden weakening of the lower crust thereby concentrating stresses on the relatively thin upper crust. It is a time-dependent finite element model having an elastic crust and mantle with a viscoelastic embedded weak zone. Relaxation of this weak zone after a tectonic perturbation transfers stress to overlying crust, generating a sequence of earthquakes that continues until the zone is fully relaxed. In further analysis it was found that due to post-seismic reloading of stress during the earthquake cycle relaxation is generally prolonged by 10-30 times the relaxation time of weak zone [Kenner PhD Thesis, 2000]. The model also attempts to determine the magnitude and distribution of stress which can produce such conditions at the scale of the observations.

Previously the stress concentration idea had not been applied to the NMSZ to simulate fault slip and crustal deformation for successive stages of an entire earthquake cycle. One reason is a shortage of field data to constrain inter-seismic deformation, coseismic fault slip, and recurrence times. Secondly, numerical models had not been developed which could model multiple earthquakes without kinematically imposing their occurrence. Finally, there was little interest in intraplate seismicity as plate boundary earthquakes are more numerous and are clearly predicted by the theory of plate tectonics. In contrast, intraplate earthquakes are rare and not predicted by theory of plate tectonics. We feel that intraplate earthquakes are, therefore, the more interesting problem.

Rheology and Geometry of the New Madrid Region

Abstract

As seen in the previous chapter the New Madrid Zone is marked by its anomalous sub-crustal structures and their properties. Seismicity in the region is attributed to these variations in the geometry of the structure and its mechanical properties (rheologies). It is evident that mechanical properties of the material changes primarily with the depth. In this chapter a brief discussion on the variation of geological and rheological properties will be conducted and possible effective properties of the composite material behavior are discussed.

3.1 Foundation of Rheological Parameter Space

The bulk of earth consists of polycrystalline aggregate of various composition and properties occupying a continuum. As continuous bodies they can be and are subjected to movements during which elements change their relative position. Such relative changes results in deformation and flow of matter. Here comes rheology of earth materials in to picture. Rheology, originated from the Greek word, in its etymological sense, denotes the study of deformation and flow of matter. As a sub-discipline of geophysics, rheology, therefore, deals with both the study of the mechanical properties of our planet's material and their role in geodynamic processes. There exist a number of rheological behaviors which depend on a variety of responses to applied stress where the type of response depends not only on the material under consideration, but also on the external parameters such as pressure, temperature and time.

An important objective of the theoretical description of composite earth materials is the prediction of the effective material properties by means of the methods of continuum mechanics. The effective properties are taken from the macroscopic characterization and the material is replaced by an equivalent homogeneous continuum. The mathematical

characterization of the overall effective properties of heterogeneous materials can be done in various ways. The mechanical state of a body is defined by the means of kinematic and dynamic quantities. These are related by fundamental laws like Newton's second law ($F=m*a$) to form rheological equations of state or constitutive equations. The first step towards setting up these quantities is to know, identify and define kinematic quantities (quantities without regard to the causes of its variation) and dynamic quantities (quantities which are concerned with the causes affecting it). Rheologies include parameters related to properties of body such as rigidity, compressibility, viscosity and so on. These values change with changes in extrinsic conditions like pressure, temperature, and time. On the basis of experimental data from composite specimens it is possible to characterize the material behavior and ascertain appropriate rheological properties, but it is not always possible to have all the experimental data to fill the matrix defining the spatial material distribution. We must therefore characterize the behavior of the earth using idealized material like Maxwell and Voigt solids, the details of which are in Appendix B.

3.2 Linear Viscoelasticity.

The phenomenon of the time-dependent mechanical behavior of materials can show up in different ways: stress relaxation under a constant loading condition, decay of vibration or strain, and stress rate dependence are some examples of viscoelastic material behavior. Thus, as discussed above the constitutive equations come into the picture, forming the connectivity between the stresses and the strain in the material, as a function of time. For infinitesimal strain the material behavior can be described by linear viscoelasticity. The Boltzmann superposition principle gives the constitutive equations for linear viscoelasticity.

$$\varepsilon(t) = \int_{-\infty}^t J(t-\tau)\sigma'(\tau)d\tau \quad \text{And} \quad \sigma(t) = \int_{-\infty}^t G(t-\tau)\varepsilon'(\tau)d\tau \dots(3.1)$$

Where σ' and ε' are the time derivatives of the stress and strain history. The response of the material is a function of the preceding strain and stress history.

$J(t) = \varepsilon(t)/\sigma_0$ and $G(t) = \sigma(t)/\varepsilon_0$ are the creep compliance and relaxation modulus respectively, which describe the behavior of the material after the application of a constant stress and strain jump. A rheological network of springs and dampers provide a sum of exponential functions in time for these material functions. The parameters defining these material functions must be determined empirically.

3.3 Basic Rheological Models

Various viscoelastic models have been proposed like Maxwell, Voigt/Kelvin, Burger's and Standard Linear Solid (SLS) models. All the viscoelastic models are made up of combination of linear springs and linear viscous dashpots. Inertial effects are neglected in such models. The Burger's body has four elements comprising a Maxwell and Kelvin/Voigt body in series. These are the basic linear models for which the stress and strain relationship has been well developed. In the earth material, although most data can be fit with basic viscoelastic materials, earth materials are more likely to be nonlinear. Depending on these analytical solutions, computational models have been developed. In this study material definitions like Creep, Power-Law (PL) and Standard Linear Solid (SLS) have been implemented computationally using ABAQUS. We consider the viscoelasticity in which the dilatational response is elastic and the deviatoric is viscoelastic.

Since the composite material consists of one or more polymeric phases, the time dependency of the mechanical behavior must be taken into account. The rate dependency can be described by means of linear viscoelasticity. The independent viscoelastic material function for earth materials is determined with the macro-mechanical model presented. Viscoelastic analysis problems are more involved than elastic problems, due to inclusion of time variables as well as spatial variables in the differential equation. However, in many problems where the type of boundary condition and temperature remains constant in time, the time variable can be removed by employing Laplace transformations. The method is known as the correspondence principle in which viscoelastic problems are converted into equivalent static elastic problem. The solution for desired variable is achieved in the form of Laplace variable "s". Then inversion of

this solution back into time domain yields the required solution. This method can be applied to solve a large set of problems but in some places it is not acceptable. Following are the steps involved in carrying out this method.

- a) Develop the relationship to obtain the desired quantities in the corresponding elastic problem.
- b) Take the Laplace transform of the elastic solution.
- c) Replace the Laplace transform of the elastic moduli with the viscoelastic moduli.
- d) Solve for the desired quantities as functions of the Laplace variable.
- e) Take the inverse Laplace transform.

The correspondence principle is applicable to only those boundary conditions where the interface between the boundary on which stress is prescribed and the boundary on which displacement prescribed are independent of time.

3.4 Viscoelastic Materials Used and Their Implementation in ABAQUS

Earlier *CREEP has been used to model the viscoelastic Maxwell model. The equivalent power law material has been used to implement linear creep models.

$$\dot{\epsilon} = A \tilde{q}^n t^m \text{ (Time Hardening Form)} \dots \dots \dots (3.2)$$

Where

$\dot{\epsilon}$ is uniaxial equivalent creep strain-rate

\tilde{q} is the uniaxial equivalent deviatoric stress

t is the total time and

A , n , and m defined by user as function of temperature.

We consider only temperature independent Maxwell bodies, such that only the deviatoric response is viscoelastic. We neglect elastic response in following the equation.

$$\dot{\bar{\epsilon}}_{ij} = \frac{1}{2\mu} \dot{\bar{\sigma}}_{ij} + \frac{1}{2\eta} \bar{\sigma}_{ij} \dots\dots\dots(3.3)$$

where $\bar{\sigma}_{ij}$ is the deviatoric stress, $\dot{\bar{\sigma}}_{ij}$ is deviatoric stressing rate, $\dot{\bar{\epsilon}}_{ij}$ is the deviatoric strain-rate, μ is the shear modulus, and η is the viscosity. The creep strain-rate $\dot{\bar{\epsilon}}_{ij}^{cr}$ is the defined as viscous part of above equation.

$$\dot{\bar{\epsilon}}_{ij}^{cr} = \frac{1}{2\eta} \bar{\sigma}_{ij} \dots\dots\dots(3.4)$$

While \tilde{q} and $\bar{\epsilon}^{cr}$ can be defined as

$$\bar{\epsilon}^{cr} = \sqrt{\frac{2}{3} \dot{\bar{\epsilon}}_{ij}^{cr} \dot{\bar{\epsilon}}_{ji}^{cr}} \dots\dots\dots(3.5)$$

$$\tilde{q} = \sqrt{\frac{3}{2} \bar{\sigma}_{ij} \bar{\sigma}_{ij}} \dots\dots\dots(3.6)$$

We find

$$\bar{\epsilon}^{cr} = \frac{1}{3\eta} \tilde{q} \dots\dots\dots(3.7)$$

Hence the constants in ABAQUS creep law are $A = \frac{1}{3\eta}$, $n=1$, and $m = 0$. Use of standard viscoelastic material definitions would require a similar analysis to determine an appropriate definition of A. For all linear material $n = 1$ and time hardening behavior is neglected ($m= 0$). When we consider nonlinear materials that are power-law we just need to vary the value of n like 1.5, 2.0, 2.5, 3.0, 3.5, 4.0, 4.5 to ascertain appropriate values in the various models that need to be run. Power-law, Maxwell bodies and SLS (see Figure 4.1) are considered in this thesis.

Benchmarks have been run to show that *VISCOELASTIC can be used to formulate Maxwell viscoelastic material as well as SLS (for details see section 3.5). Maxwell model has characteristics of having no long term strength and hence it behaves as fluid at large time-scales, but with earth materials it does not seem to be the most appropriate

definition. Rather a material model having some long term finite strength seems more feasible, hence SLS appear as the best potential choice for crustal earth materials.

A SLS body is modeled with the combination of a simple spring in series with a Voigt body (spring and dashpot in parallel). Hence instantaneously the body behaves as an elastic body, but as the time increase its viscoelastic nature come in to picture. After long time (several cycles of relaxation) when damping effect dies down, it becomes elastic with some long term strength.

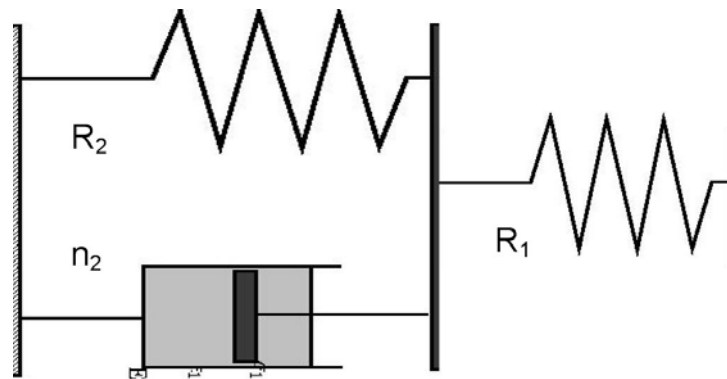


Figure 3.1 *Standard Linear Solid*

3.5 ABAQUS Numerical Implementation of SLS

For small-strain applications elastic response can be defined with a linear elastic material model. For the viscoelastic material like SLS, which has “long term strength”, *i.e.* when a constant strain is applied the response settles down to constant stress. The shear relaxation modulus can be written in dimensionless form as

$$g_R(t) = G_R(t) / G_0 \dots\dots\dots(3.8)$$

where $G_0 = G_R(0)$ is the instantaneous shear modulus. This function has limiting values of $g_R(0) = 1$ and $g_R(\infty) = G_\infty / G_0$. ABAQUS assumes that the viscoelastic material is defined by a Prony series expansion of the dimensionless relaxation modulus

$$g_R(t) = 1 - \sum_{i=1}^N g_i^{-P} (1 - e^{-t/\tau_i^G}) \dots\dots\dots(3.9)$$

where N , g_i^{-P} and τ_i^G $i=1,2 \dots N$ are numerical constants. Substitution in small strain in the small-strain expression for the shear stress yields.

$$\tau(t) = G_0 \left(\gamma - \sum_{i=1}^N \gamma_i \right) \dots\dots\dots(3.10)$$

where,

$$\gamma_i = \frac{g_i^{-P}}{\tau_i^G} \int_0^t e^{-s/\tau_i^G} \gamma(t-s) ds \dots\dots\dots(3.11)$$

The γ_i are the state variables that control the stress relaxation. For details of this derivation please refer to ABAQUS 6.4 user's manual section 10.7.1 which shows that relaxation parameters can be defined by direct specification of the Prony series parameters. The Prony series parameters g_i^{-P} , k_i^{-P} and τ_i can be defined directly in the data line for *VISCOELASTIC keyword. The value of these parameters can be found by comparison with the analytical solution.

The creep compliance for a three body SLS model is analytically based on basic elements found in Table 5.1 of *Creep and Relaxation of Nonlinear Viscoelastic Material* [Findley, Lai, and Onaran, 1990]. We start with a Burger's body which has a Maxwell and a Voigt body in series. The Burgers body can be converted to a SLS by removing the damper from the Maxwell portion. Numerically this can be achieved by assuming the damper to be of infinite viscosity.

The Laplace transform of the relaxation modulus for a Burgers body is given by

$$\hat{E}(s) = \frac{q_1 + q_2 s}{1 + p_1 s + p_2 s^2} \dots\dots\dots(3.12)$$

where

$$p_1 = \frac{\eta_1}{R_1} + \frac{\eta_1}{R_2} + \frac{\eta_2}{R_2} \quad \text{and} \quad p_2 = \frac{\eta_1 \eta_2}{R_1 R_2} \dots\dots\dots(3.13)$$

$$q_1 = \eta_1 \quad \text{and} \quad q_2 = \frac{\eta_1 \eta_2}{R_2} \dots\dots\dots(3.14)$$

as $\eta_1 = \infty$ for SLS element. On substituting this value in equation (3.12) we get

$$\hat{E}(s) = \frac{A}{s} + \frac{B}{(R_1 + R_2/\eta_2 + s)} \dots\dots\dots(3.16)$$

where

$$A = \frac{R_1 R_2}{R_1 + R_2} \quad \text{and} \quad B = R_1 - \frac{R_1 R_2}{R_1 + R_2} = \frac{R_1^2}{R_1 + R_2} \dots\dots\dots(3.17)$$

Taking the inverse Laplace transform of equation (3.16) we have

$$E(t) = Au(t) + Be^{-(R_1+R_2)t/\eta_2} \dots\dots\dots(3.18)$$

where $u(t)$ is unit step function such that $u(t) \begin{cases} 1 & \dots\dots t \geq 0 \\ 0 & \dots\dots t < 0 \end{cases}$. Hence the relaxation modulus for weak body at any time is given by

$$G_R(t) = E(t) = \frac{R_1 R_2}{R_1 + R_2} + \frac{R_1^2}{R_1 + R_2} e^{-(R_1+R_2)t/\eta_2} \dots\dots\dots(3.19)$$

In ABAQUS the dimensionless index is defined as

$$g_R(t) = G_R(t) / G_0 \dots\dots\dots(3.20)$$

where $G_0 = R_1$, Hence we get

$$g_R(t) = \frac{R_2}{R_1 + R_2} + \frac{R_1}{R_1 + R_2} e^{-(R_1+R_2)t/\eta_2} \dots\dots\dots(3.21)$$

$$g_R(t) = 1 - \frac{R_1}{R_1 + R_2} (1 - e^{-(R_1+R_2)t/\eta_2}) \dots\dots\dots(3.22)$$

On comparing equation (3.8) and equation (3.22) we get

$$g_i^{-P} = \frac{R_1}{R_1 + R_2} \dots\dots\dots(3.23)$$

$$\text{Relaxation Time } \tau_i^G = \frac{\eta_2}{R_1 + R_2} \dots\dots\dots(3.24)$$

3.6 Geometrical Parameters

As seen in chapter two, field seismic exploration results, in the NMSZ seems to indicate high seismic velocities and correlating high densities in the lower crustal body *i.e.* the “rift pillow”. The shape of this zone is defined by gravity measurements which are less certain. Inversion of gravity data in the absence of geometrical constraints yields non-unique solutions because an infinite number of geometrical combinations can produce an associated field that closely matches the measured field. Still both gravity and seismic data have been used to define the dimension of rift pillow. The steep change in gravitation data helps in getting preliminary information along a north-west south-east direction (normal to axis of pillow). Very high gravity can be seen in the range of 190 km to 260 km in Figure 2.3. In the north-east south-west direction (along the axis of pillow) the variation is seen in the range of 200 km to 400 km. As seen in (Figure 2.3) this lens shaped rift pillow is about 300 km wide and 20 km thick. This layer is interpreted as a solidified intrusion or under plating of partial molten material derived from decompression of the asthenosphere. It is thought that this layer was emplaced during late Precambrian to early Paleozoic (about 550 million years ago) rifting event. For modeling purposes an average height of 25 km was considered starting from depth of top of pillow at 15 km to the depth of the bottom of pillow at 40 km depth. Various widths are analyzed starting from 3 km wide to 75 km wide. For 2D models the fault is assumed to be of infinite length. In 3D models the fault length has been constrained to 200 km as per observation in the NMSZ (Figure 2.3).

There is considerable uncertainty about the composition, temperature, fluid pressure, strain-rate and other conditions at depth in the NMSZ area. There is great uncertainty regarding the dominant rheologies in the NMSZ, but in our model everything except weak zone is considered elastic

3.7 Generation of Anti-plane Model

A model has been developed to approximate a sequence of earthquakes in the NMSZ in the last two thousand years. The model is composed of a vertical single strike-slip fault along the rift axis. During the occurrence of the earthquake, one surface slides

against the other surface and all displacements occur only in the strike direction (z direction in model). This type of deformation is anti-symmetric about the fault. In 2D this is known as anti-plane deformation. ABAQUS contains special plane-stain and plane-stress elements, but anti-plane elements are uncommon in engineering analysis and don't exist in ABAQUS. As a result, anti-plane models are generated using standard 3D elements and applying requisite boundary conditions. These boundary conditions are XSYMM and YSYMM which impose symmetry along the X and Y plane respectively. All in-plane displacements (*i.e.* fault normal and fault parallel in the depth direction) must also be set to zero. This is currently done by applying appropriate symmetry conditions to all the nodes. At least three node layers in the strike direction are required for the definition of contact surfaces. Constraint equations are then used to require the strike-direction displacement to be the same in each layer. "APMODEL", a script that has been written in MATLAB [Kenner, PhD, 2000] generates the input file for ABAQUS, as per the parameters required by the user.

3.8 Model Pre-stressing

In order to approximately apply the ambient tectonic stress field, great care must be taken to initialize the stresses in finite element mesh. It becomes critical when repetitive earthquakes are going to be considered. Also, nodal displacements should be minimized when initializing the stress in the model. This helps in minimizing the errors due to undue distortion of the finite element mesh.

Because of the observed seismicity, the model considers the sudden weakening of the underlying intraplate region. Before the occurrence of weakening, the whole system is assumed to maintain stress equilibrium. Hence, it is necessary to implement a steady state pre-stress condition while initializing the model. These stresses must be in equilibrium with the boundary conditions. If there is any difference in these stresses then the finite element mesh will deform to a new equilibrium state (new location of nodes) during the very first step of analysis. This would result in unnecessary non-geologic deformation. The background stress in the model is 60 MPa (which has been arrived at

empirically). The model is pre-stressed using *INITIAL CONDITION, TYPE=STRESS. Details of this are discussed in following sections.

3.9 Geologically Appropriate Boundary Conditions

Far-field stress boundary conditions are applied in each direction independently. As discussed above this should be in equilibrium with the internal body stresses. Normal boundary conditions can be applied to each face with *DLOAD. A non-uniform pressure distribution can be applied to prescribed node sets with a user-defined *DLOAD subroutine. Tangential tractions are more complicated as they cannot be applied with *DLOAD. Though a concentrated tangential load can be applied to each node set with *CLOAD, this is not appropriate for applying surface tractions. To properly apply surface tractions, concentrated nodal-load values must be interpolated using the appropriate shape function such that, when integrated over the surface, net tractions on each element face converge to the appropriate value. Alternatively, all nodes on the specified boundary can be constrained to have same displacement in the direction of applied shear (using a constraint equation). Then using *CLOAD, a concentrated load can be applied to a single node (to which all other nodes have been tied), with a magnitude ($\tau \cdot A$), where τ is the required shear traction and A is total area of specified boundary. Though this approach may not be strictly appropriate, if the far-field boundaries don't deform significantly it is a reasonable approximation. This means that it is essential to place the model edges well away from the loci of deformation.

One of the problems with only applying stress boundary conditions (*i.e.*, no displacement or velocity boundary conditions) is to constrain rigid body motion. If the applied boundary tractions do not sum to zero the finite element model will deform and accelerate due to the unbalanced forces. Even if the applied tractions sum to zero, rigid body motions may still be present because the model, as formulated, remains ill-constrained and can rotate about its axis. Thus, additional constraints needed to be applied which prohibit rigid body motions. If they are incorrectly applied, using displacement or velocity conditions, motions may be eliminated but stress will concentrate at the constraint point. To determine a suitable constraint first consider an

initially stress free rectangular body which is subjected to pure shear boundary tractions. The body's central point must remain stationary and net horizontal displacements at any corner of the mesh must be oriented along a line connecting that corner in with its opposite corner at the same depth. With this in mind, it turns out that if two opposite corners in a pre-stressed finite mesh are constrained to 1) move in the direction described above and 2) have motions which are equal and opposite, rigid body motions are eliminated and there are no unwanted side effects. This has been incorporated in the APMODEL program [Kenner, *PhD 2000*]. Constraint equations are used to tie the necessary degrees of freedom to one another. While applying these various boundary conditions, care must be taken to avoid constraining particular degrees of freedom more than once to avoid over-constraining errors. This is particularly hard to do along the trace of the fault.

The embedded time-dependent material initially has the same distribution of stress as the surrounding elastic body. Given this condition the time-dependent zone is transparent and no deformation should take place during the initial equilibrium step. Once the embedded zone is perturbed and allowed to relax the model should transiently deform, but eventually equilibrium is should be re-established and deformation should cease. If the lower crust (excluding the weak zone) is time dependent and constant stress boundary conditions are applied then as the weak zone relaxes and the stress become heterogeneous the time-dependent lower crust will no longer be in equilibrium with the boundary condition. This will drive model dependent deformation that is not geologically realistic. For models in which the weak zone is embedded within an elastic body, changes in internal stresses will not drive continuous deformation in the lower crust. Unfortunately a viscoelastic lower crust is geologically more reasonable. We use an elastic body because methods for maintaining stress equilibrium at the boundary of a viscoelastic lower crust have not yet been developed. Obtaining the required balance between internal stress, applied constraints, and external stress boundary conditions is a difficult thing. This demonstrate that before the finite element model can be taken seriously, it should be thoroughly tested to make sure that it behaves as you expect it to behave, especially when time dependent materials are included.

3.10 The Model

The present model incorporates a lower crustal zone of weakness embedded within an elastic lithosphere. In this model the mantle is also considered as an elastic body. This eliminates any possibility of considering rheological variations with depth. This is done to achieve increased computational efficiency and avoid model dependent transients. This helps to get the first order response of the model so it can be compared with the observations. The possible impact of using an elastic mantle would be on the number of earthquakes on the fault, which would be increased if a viscoelastic material had been used. Following a perturbation in the weak zone stress, the system tries to re-establish equilibrium. Since the weak zone can not support any shear stress, it relaxes by transferring stress to the upper crust. This may trigger slip on overlying seismogenic faults, potentially generating a sequence of earthquakes. This continues until the weak zone reaches its fully relaxed state. Slip on the fault in turn partially reloads the lower crustal weak zone causing cyclic stress transfer, which prolongs the relaxation process. Relaxation of the weak zone could be induced by variations in rheology, due to, for example, a thermal or fluid perturbation, or by a transient change in the regional stress.

The model formulation is true to first order observations from the NMSZ. Since the length of weak zone is finite and constant stress boundary conditions have been applied, the net fault offset remains finite as the weak zone relaxes. This implies that there is finite number of slip events. Also deformation rates far from the fault are zero. Finally, seismicity is confined to a localized region. In order to calculate the influence of post-seismic transients which re-load the seismogenic fault, time dependent calculations have to be performed. Computational efforts are required to quantify the amount of coseismic slip, earthquake magnitudes, earthquake recurrence intervals, and surface deformation rates.

In present finite element models, a rectangular weak zone (Figure 5.1) with various types of rheological properties is defined. Rheologies include a Maxwell model, a standard linear solid and various power-law formulations. Also geological parameters like weak zone width and depth is also varied. Details of these properties have been discussed at length in section 3.4 and Appendix B. This type of variation is necessary to

be considered in order to incorporate all the possibilities. Since the exact material properties can not be firmly ascertained and allocated in the space matrix as it exists, it makes numerical approximations necessary to adopt. Each model must then be evaluated against the other models and geological observations. Previous modeling efforts considered only Maxwell materials for the weak zone, which have no long term strength and linear dissipation properties. Other material options may have more realistic rheological properties, and also match observed distributions of earthquake repeat times and observed magnitudes in the NMSZ.

3.11 Conclusion

As discussed in the previous section we apply the boundary conditions on the model by initially stressing entire model uniformly ($\sigma_{11} = \sigma_{22} = \sigma_{33} = \sigma_{12} = \sigma_{21} = \sigma_{31} = 0$) while $\sigma_{13} = \sigma_{\infty}$, which maintains equilibrium with far field stress “ τ_{∞} ”. Fault slip occurs when the resolved stresses on the seismogenic fault reach τ_{\max} and stress on the fault then drops to a stress that satisfies one of the chosen friction criteria explained in chapter four.

Model behavior, as function of various fault friction criteria, geometrical, rheological and stress parameters, is thoroughly evaluated. In order to improve the computational efficiency 2D models are run to derive a first hand knowledge base of the system. 2D results are then used to refine the set of 3D model parameters. This improves the computational efficiency of obtaining results which becomes crucial as the computational cost is very high in 3D models.

Initial estimates of the weak zone geometry were made using the rift zone geometry as derived from topographic, seismic and gravimetric investigations of the NMSZ. Order of magnitude estimates of the remote stress, τ_{\max} , were obtained using the simple elastic crack relation plate tectonic theories.

Estimates of stresses in the NMSZ are not available. Maximum horizontal stress in the upper 300 m and surrounding regions of the NMSZ lie between ~ 7 and ~ 25 MPa. Deviatoric stresses from hydro-fracturing experiments in the deep boreholes are much

larger [Zoback & Zoback, 1989]. Shear stresses inferred from these measurements are only 2-3 times higher than our estimates using elastic crack relations.

If the upper mantle also relaxes then cumulative offsets on the fault will change but the fundamental behavior of model will be untouched. Then to generate the equivalent cumulative offset remote stress magnitudes must be reduced. Since earlier studies have been extended using the same model formulation, we will use the same remote stress, 60 MPa. The relaxation time of the material in the weak zone is important in governing the rate of stress transfer from the weak zone to the seismogenic upper crust. We are going to consider a range of relaxation times ranging from 90 years to 9000 years

Fault Friction Behavior

Abstract

In order to model a discontinuous fault in an otherwise continuous model (finite element mesh) we use contact surfaces. Fault friction behavior is the tool for modeling coseismic faulting or discrete slipping surfaces past each other at depth. Various friction relations can be applied to these surfaces and theoretically user-defined subroutines ultimately allow almost any possible combination of choices of fault constitutive relations to be defined. To date, normal stresses have not been included in any of the models and fault normal motion has been prohibited. In future models normal stresses can be incorporated.

4.1 Discrete Faults Using Contact Surfaces and User Subroutines

ABAQUS works in such a way that the main program supplies values for the existing shear stress (τ_1), maximum allowed shear stress (τ_{\max}) and possible stress drops ($\Delta\tau_1$) and then ABAQUS estimates the increment in sliding motion ($\Delta\gamma_1$). These estimates are based on the discretised partial derivatives ($\partial\Delta\tau_\alpha/\partial\Delta\gamma_\beta =$ Fault Stiffness, $\partial\Delta\tau_\alpha/\partial\Delta\rho =$ zero) supplied to ABAQUS. Where $\partial\Delta\tau_\alpha/\partial\Delta\gamma_\beta$ (DDTDDG) is the partial derivative of the frictional stress in direction α with respect to relative motion in direction β , and $\partial\Delta\tau_\alpha/\partial\Delta\rho$ (DDTDDP) is the partial derivative of the frictional stress in direction α with respect to the contact pressure. The subroutine then generates new values for τ_1 and $\Delta\gamma_1^{sl}$. These values are assigned to variables when a non-recoverable sliding motion is allowed in the subroutine. If equilibrium is not established in the model then ABAQUS re-iterates the increment using modified values for the time-increment until equilibrium is achieved. In the subroutine the residual shear stress is calculated first and then ABAQUS calculates the amount of slip using internal methods.

ABAQUS uses a master-slave algorithm to define contact conditions. The master surface defines the geometry and orientations of the contact relationship. Slave nodes are not allowed to penetrate the master surface, while master surface nodes can penetrate slave surface. In 2D models a contact surface is used to define the master surface and contact node set to define the slave surface. It is because 2D models consist of only one layer with active degrees of freedom. The other two layers are tied to the first layer. In 3D models contact surfaces are used to model both mater and slave surfaces. The ABAQUS subroutine is called for all slave nodes in a contact pair in 2D models and at integration points in a contact surface element in 3D models. ABAQUS has the option of including user-defined parameters in the subroutine, through which the user can pass on values which directly affect the control of subroutine. This also gives capability on the users end to direct the decision taking capability of ABAQUS. Section 4.4 details the list of parameters which have been passed on to subroutine.

4.2 Surface Behaviors

Presently, there are three basic surface behaviors that can be applied through the APMODEL program.

1. The fault can be permanently locked and no contact surfaces or friction relations are defined. Nodes on either side of the mesh are tied to one another using *TIE and differential motions are not allowed.
2. In 'ROUGH' friction, the coseismic fault is either locked or freely slipping. This is implemented through *FRICTION, ROUGH which allows no relative motion between the slave and master surfaces. When freely slipping fault behavior is required, the *ROUGH friction can be temporarily deactivated. The fault friction can be inactivated by invoking the *MODEL CHANGE, CONTACT PAIR, REMOVE command in time-step definition portion of the input file. The contact surfaces can be reactivated again by the *MODEL CHANGE, CONTACT PAIR, ADD command invoked during a subsequent step and the *ROUGH friction relation is reapplied. Note that, when *ROUGH friction is inactive, other boundary conditions can be applied to the fault surface (like kinematically

prescribed earthquakes). Currently, if *ROUGH friction is inactive and other boundary conditions are not applied, the fault surfaces slip freely past one other. The freely slipping fault can be constrained to slip in only the dip or strike directions. If these conditions are not satisfied, zero pivots will result and job will fail during analysis.

3. The third surface behavior is a maximum shear stress criterion. This friction relation is defined using a user-defined friction subroutine which is described in detail in the following section. User-defined parameters can be changed during analysis using the *FRICTION, CHANGE command.

4.3 Maximum Shear Stress Criteria Friction Subroutine

To model a fault which fails at a prescribed maximum resolved shear stress and continues to slip until the stress drops to some residual level, it is necessary to implement a user-defined friction subroutine. Without using user-defined subroutine, ABAQUS allows the specification of a maximum shear stress rupture criteria with slip continuing until the stress drops below the failure stress. In this formulation nodes on the rupture surface slip freely when the maximum stress at nodes are greater than or equal to the failure stress. In our case, once the surface is sliding increases in the resolved shear stress due to continued tectonic loading cause the surface to keep sliding. Since the peak stress on the fault never drops below that required sliding, the surfaces never relock. Eventually all the nodes on the fault plane slip continuously at the failure stress. Thus there is never a sudden stress drop as required in an earthquake. This eliminates the default ABAQUS maximum shear stress criteria for use in geological problem since stick-slip behavior can not be produced.

A variety of maximum shear stress friction subroutines have been developed which are capable of stick-slip behavior. These are described below:

1. [Type1, MXSHRFRC] This allows motion in the strike-slip direction only. Slip occurs when the resolved shear stress reaches a user-specified maximum shear stress. The fault continues to slip until the shear stress value on the fault falls at

user-defined residual shear stress. No aseismic slip is allowed. Dip-slip motion is not considered and fault perpendicular motions are not allowed. Any changes in normal stress across the fault are neglected. The subroutine evaluates stress independently at each node, such that nodes can fail independently or in groups. This subroutine can be used in anti-plane or 3D models. An effort has been made towards more efficient methods for cutting back the time-step. During the analysis ABAQUS continuously augments the time-step values but when shear stress on the fault falls in super stress region (Figure 4.3) the subroutine requires ABAQUS to consider a smaller time-step. The time reduction factor was supplied as user input parameter. This was inefficient way of obtaining stress in desired window as use of user supplied values often required more iterations. This subroutine implements a mechanism of slip occurrence which is more realistic, but computationally it is more expensive. It takes longer time to compute since each node is considered. The cut back ratio is calculated as

$$rtime = \frac{\tau_{max} - \tau_{in}}{\tau_{out} - \tau_{in}} .$$

where,

τ_{in} = stress at the start of step.

τ_{out} = stress at the end of step.

τ_{max} = stress at the failure.

2. [Type 2, AVGMXSHRFRC] This subroutine follow all the rules explained above except that instead of calculating the stress at each node separately, an average is calculated using all the slave nodes on the fault. It is used in 2D anti-plane or plain strain models. This utilizes the fact that there is a low variation of stress as nodes rise above the fault tip. If desired the average can be taken over some subset of nodes, for instance nodes near the fault tip need not be included in the average. This modeling of average stresses in certain circumstances can save large amounts of computation time, giving indicative results for first order modeling. The average is calculated as

$$\frac{\sum_{n=1}^n \sigma_n \nabla_n}{\sum_{n=1}^n \nabla_n}$$

σ_n = Shear stress at node

∇_n = Area associated with the node

We used the fixed earthquake stress drop in this subroutine (which is geologically less realistic) and got interesting first order results which will be discussed in chapter 5 in section 5.9.

3. [Type 3, PERDPMXSHRFRC] This version of the friction subroutine controls the stress drop. This subroutine has been developed to overcome the shortcomings of the above two subroutines. Stress change during an earthquake event has been previously calculated as either dropping to a constant value of stress (say 50 MPa) or constant stress drop (say drop by 10 MPa). We know that values of stress can not be the same at the top and bottom of fault after an earthquake. Secondly, all earthquakes can not be of same magnitude and release the same amount of stress. This subroutine calculates the amount of stress drop as a user-defined value of “percentage drop of stress” at the node. A constant value of percentage stress drop can be considered throughout the fault, and represent a more realistic geological model. This has been considered under the assumption that the variation of the percentage stress drop, being a second order quantity, would have less effect on model. This is applicable with both the calculation of stress at each node (type 1) and the average of stress on fault (type 2) versions of subroutines discussed above. This has been used for most of 3D model run for this thesis.
4. [Type 4] Apart from above, some other propositions are under consideration but have yet to be tested. One such subroutine would calculate average stress on the group of nodes at different locations (average of small areas a compared to whole

fault at once) on the fault and when maximum allowed limit of stress is reached on that patch of nodes the stress is dropped. This is mid way between the above tested methods (type 1 and type 2). This would have advantages of both methods, a speed close to method type 2 and accuracy close to method type 1. Over all it could be a more efficient subroutine.

5. [Type 5] Book-keeping is the most important key to generate a successful subroutine and particular book-keeping schemes can result in very efficient computations, while other times could end with unpredictable outcomes or deterioration in results. I have tried some of the schemes but so far did not get success to generate an efficient subroutine. Advanced understanding of ABAQUS numerical scheme is required to manipulate the ABAQUS's internal variables which control the computation at high level. It has been very difficult to understand the trends in the models which I have run. They are very large and consume huge computational time as well.

A version of the friction subroutines has been developed by Kenner [2000, *PhD*] which allows both dip-slip and strike-slip motion along with the fault plane. Dip-slip faulting does occur in the NMSZ but it is an area for further study. First, strike-slip user-subroutine must be optimized for both computational efficiency and geological realism.

All the subroutines that have been produced are variation in the above discussed subroutines. Only a few have been used in the models presented in this thesis. The study presented in this thesis shows that subroutine type 3 has high capability to be realistic. We do, however need to find a middle ground between average and individual calculation of shear stress.

4.4 Input Parameters

The values conveyed to the different friction subroutine typically require the following criteria given by user.

1. Maximum resolved shear stress at failure [τ^{\max}].

2. Residual resolved shear stress after failure [τ^{resd}].
3. Fault zone stiffness [*fltstiff*]
4. Fraction of failure stress which specifies the maximum allowable deviation [*sdiff*] from the maximum shear stress, τ^{\max} , at the time of rupture.
5. The minimum time-step at which rupture at one node is allowed to trigger rupture at neighboring nodes [*eqtimemin*].
6. When a node is satisfying the rupture criteria but the time-step is more than the *eqtimemin*. The [*ritme*] is taken as ratio specifying the reduction in time-step when iterating towards the failure stress. In later versions efforts have been made to give the program more intelligence in choosing the value of *rtimeeq* such that computation time and the cost of additional iterating can be saved.
7. The ratio [*rtime*] specifying the reduction in time-step, used when nodal stresses are in superstress zone.
8. Number of slave surface nodes on the fault plane. (APMODEL determines this number).

Parameters 4-7 directly influence the time-stepping scheme adopted by ABAQUS such that it meets geological requirements. Through this subroutine we try to pass on information like the stress value at which earthquake/slip should take place, possible stress drops in such events, and nodes lying on fault surface. For a given model, during rupture the sequence in which nodes will break and the timing of the rupture is dependent on the time-stepping scheme and critical friction parameters. Small slip events may be due to numerical limitations and uncertainties. Hence they are less liable to be ascertained as an earthquake. Bigger rupture events are more robust and rise above numerical uncertainties. Their magnitudes are less sensitive to some of friction parameters and time-stepping schemes. In general, a big event is characterized by its occurrence in a set of 2 to 3 slip events during consecutive iterations.

4.5 Logic

The basic logic governing the frictional failure is the same in all the three subroutines. ABAQUS calls the friction subroutine twice for each node on the fault, for each equilibrium iteration in each increment of each time-step. This ensures that the

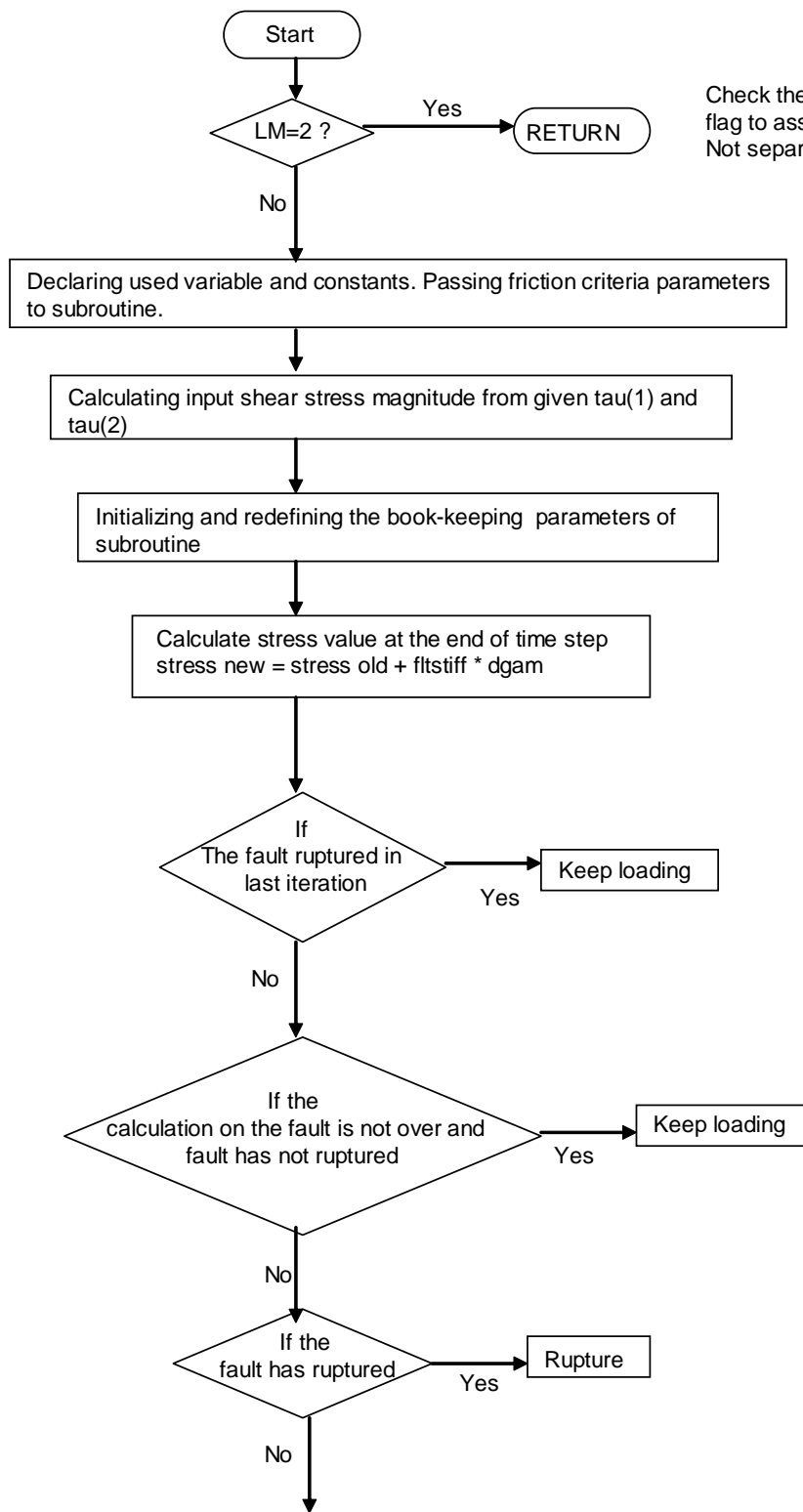
computation has converged. This methodology also poses problems, in that it is hard to control time-stepping and failure criteria in the user subroutine.

A node ruptures when the shear stress, τ_{out} , at the end of increment falls in the “failure window” (see Figure 4.3). This window, which is defined using user-specified parameters is between $(\tau^{max} - sdiff * \tau^{max})$ and $(\tau^{max} + sdiff * \tau^{max})$. The τ_{in} is the shear stress at the node at the beginning of the increment and τ_{out} is stress at the end of time-step. After rupture this τ_{out} could be redefined using a fixed stress drop, a fixed residual stress value, or the stress drop can be defined as some percentage of τ_{in} stress at the node. The last method seems to be the best formulation.

In the subroutine when a rupture takes place we set `ddtdg(1,1)` and `ddtdg(2,2)` to zero. When the rupture does not occur the stressing continues and we set these values to an elastic stiffness. Any stress or pressure across the fault is neglected. The change in shear stress for a locked node in a given time increment in a given slip direction is defined as `fltstiff*dgam`, where `dgam` is the expected change in sliding motion during the current increment if node is allowed to slip freely. The `dgam` is automatically calculated by ABAQUS and passed to the subroutine. A bookkeeping procedure needs to be adopted to methodically decide whether a node does or does not slip. The book-keeping method must also save the increment’s initial conditions so that the increment can be restarted if the time-step is changed.

4.6 Flow-Chart Representation of the Subroutines

The logic for the 2D model (plane-strain or anti-plane), which employs an average maximum shear stress (type 2, Figure 4.1) and the 3D/anti-plane model which employs the shear stress at each node (type 1, Figure 4.2) is explained in flow charts Figure 4.1 and Figure 4.2. They show how the control is governed in both the subroutines



Check the Lagrange Multiplier flag to assure that surfaces Not separate.

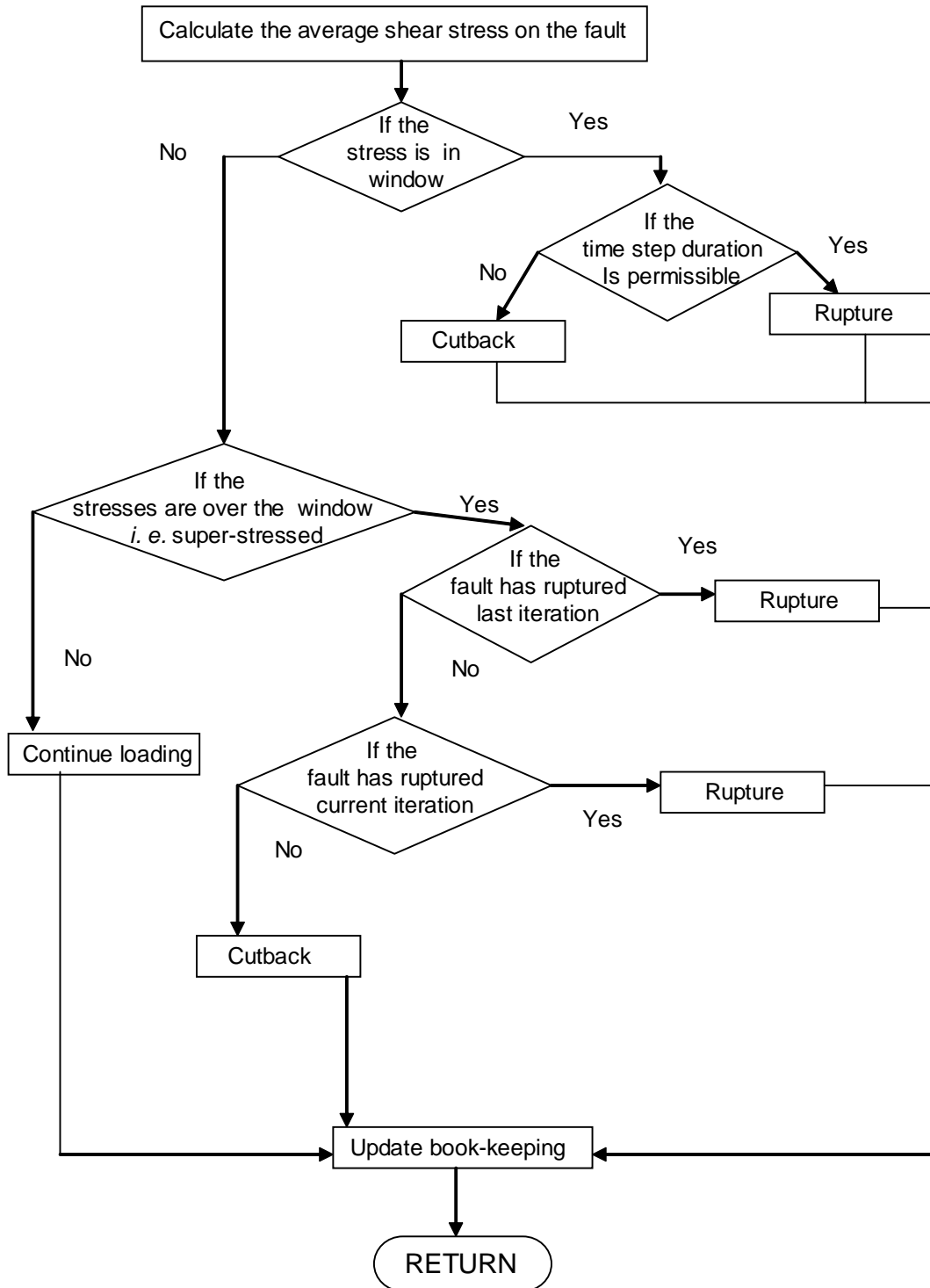
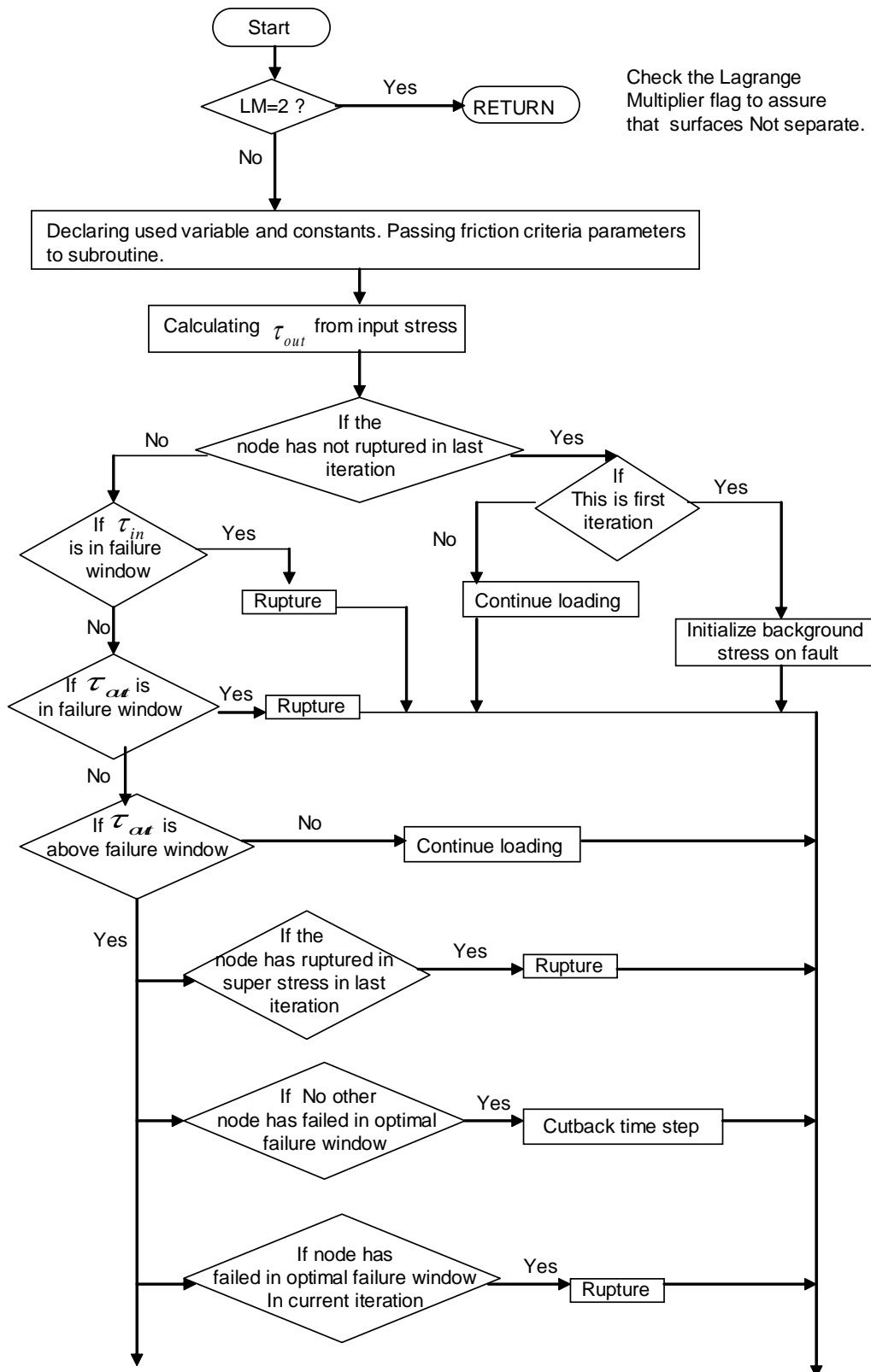


Figure 4.1 Logic for the friction subroutine used in the 2D models (plane-strain or anti-plane). This makes use of average shear stress on the fault (Type 2).



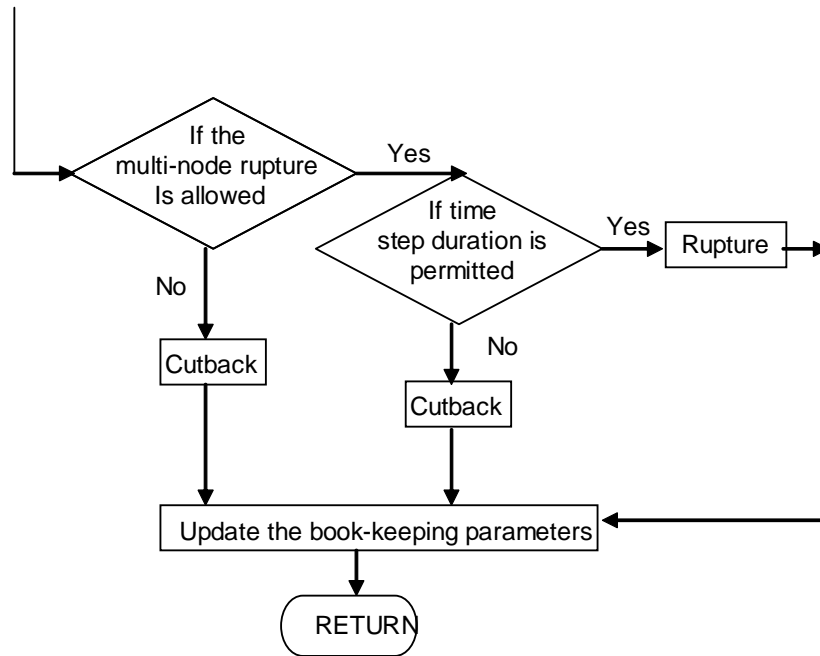


Figure 4.2 Logic for the friction subroutine used for 3D/anti-plane models. The criterion is applied to individual nodes and on satisfying the criteria a single node is capable of slipping (Type 1).

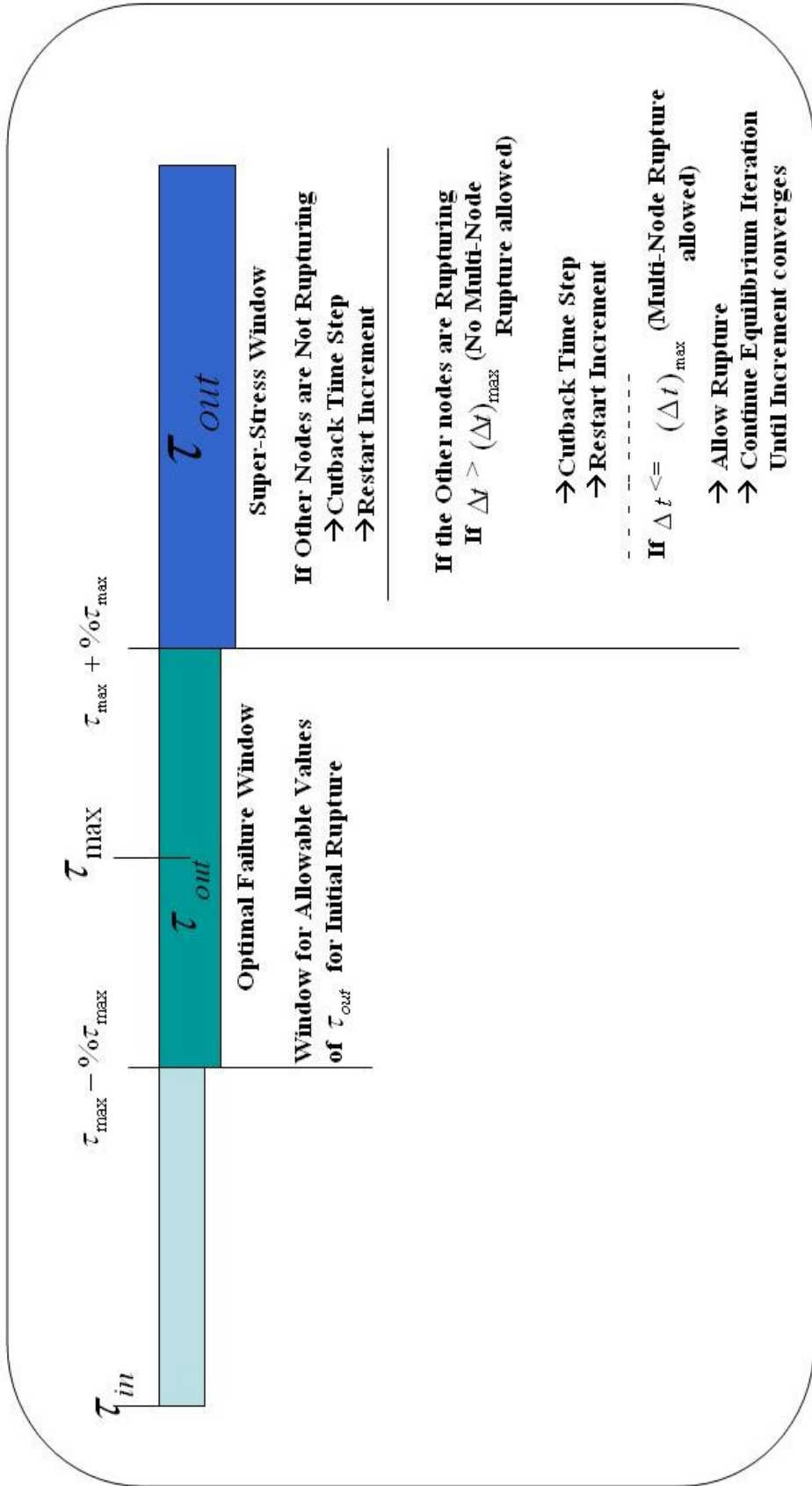


Figure 4.3 Figurative representation of the failure criteria. This is based on a user-defined maximum shear stress at the fault. Middle section of above scale represents failure window where node can potentially rupture. Above this window i.e. in the super-stress region nodes can rupture only when other node are also rupturing, i.e. in multi-node rupture.

2D Model Results and Discussion

5.1 Introduction

2D models provide guidelines which help to constraint the parameter space (both rheological parameters and weak zone width) for 3D models. 2D models run faster, thereby saving computational time and cost by eliminating parameter sets which are unlikely to produce useful information in 3D model. Table 5.1 gives the values which were successfully tested in 2D models. Since we were more interested in non-linear results, plots of linear Maxwell and SLS models were not extensively searched. Kenner [PhD Thesis, 2000] did extensively search the Maxwell parameter space.

In the 2D models, the remote shear stress of 60 MPa is assumed in all models. With use of fault friction criteria slip on the fault is automatically (*i.e.* not kinematically) initiated when the average maximum shear stress criteria is satisfied. The maximum shear stress of 62 MPa has been chosen for all the models. Constant stress drop of 10 MPa (friction subroutine of type 2) is applied for initial models. It evolved not to be the most appropriate condition as discussed in section 5.9. Friction subroutine of type 3 is used for the models presented in the following sections.

A variety of 2D models (Figure 5.1) have been developed to study how changes in geometry and rheology affect the number of earthquakes generated over 10,000 years (Table 5.2). Results produced are shown below.

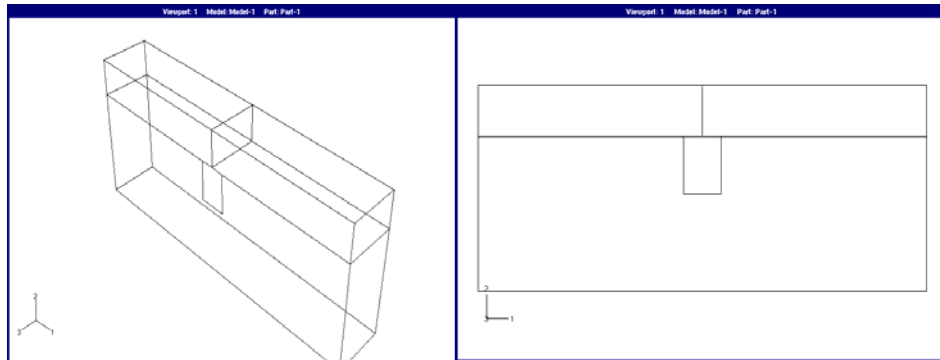


Figure 5.1: 2D models in ABAQUS. Since ABAQUS doesn't support anti-plane elements, 3D bricks must be used which are then constrained to deform as an anti-plane model.

Details of the model are discussed in section 3.11. Numerical calculations are completed in ABAQUS. The APMODEL program, by Dr. Kenner, has been used to generate the input file for ABAQUS as well as to post-process the data file generated by ABAQUS.

Table 5.1 Range of Parameter Space Searched

Rheology Type	Maxwell		Power-law		SLS	
Width, W(Km)	3		6		12	
Power-law, stress exponent, n	1.0	1.5	2.0	2.5	3.0	3.5
Effective Viscosity (Pa-s)	10e20	10e21	10e22	10e23	10e24	
Relaxation time, Tr(Yrs)	90	900	9000	90000	900000	

The graphs below are the results generated by APMODEL. Moment is defined as multiplication of shear modulus, slip magnitude and area that slipped. Cumulative moment is sum of the moments in each earthquake. While plotting the diagram lumped cumulative moment has been used, which calculates sum of moments released in events for each node failure in consecutive increment. Big events of multiple node failure are then represented as one earthquake. This reduces the computational uncertainties of cumulative moment. Results shown below compare variation of one parameter at a time in one graph, keeping the other two parameters fixed. Sometimes a curve has been used in more than one comparison as it falls under other criteria as well. Each figure is an independent comparison between the curves. Each section handles comparison for one parameter.

5.2 Viscosity Variation for 3 km Wide Weak Zone

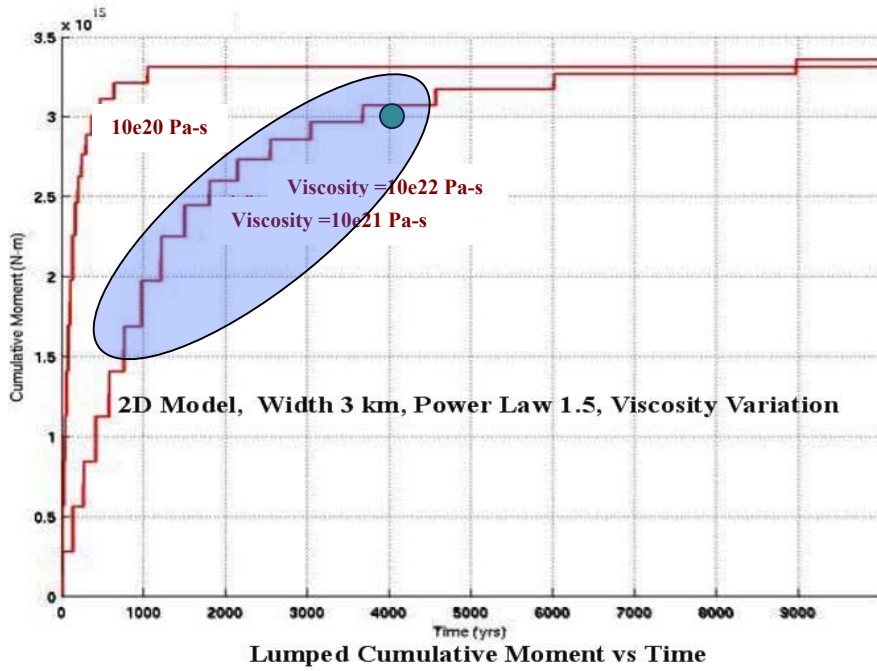


Figure 5.2.1 Width 3 km, Power-law exponent 1.5, Viscosity variation . Y axis of graph represents the cumulative moment in N-m release on the fault (the stress relaxation) and the X axis represents the time in years. Green dot on the curve indicates that the model satisfy the observation from NMSZ i.e. 3-4 earthquakes in 2000 years window. Blue shaded area shows the duration of time in which 2000 year window can be spotted.

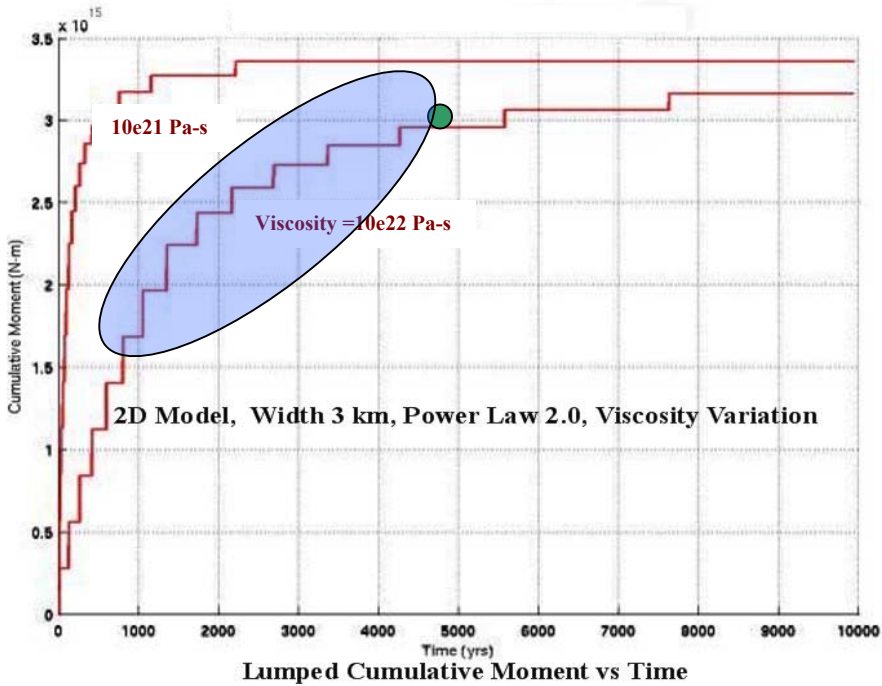


Figure 5.2.2 Width 3km, Power-law exponent 2.0, Viscosity variation

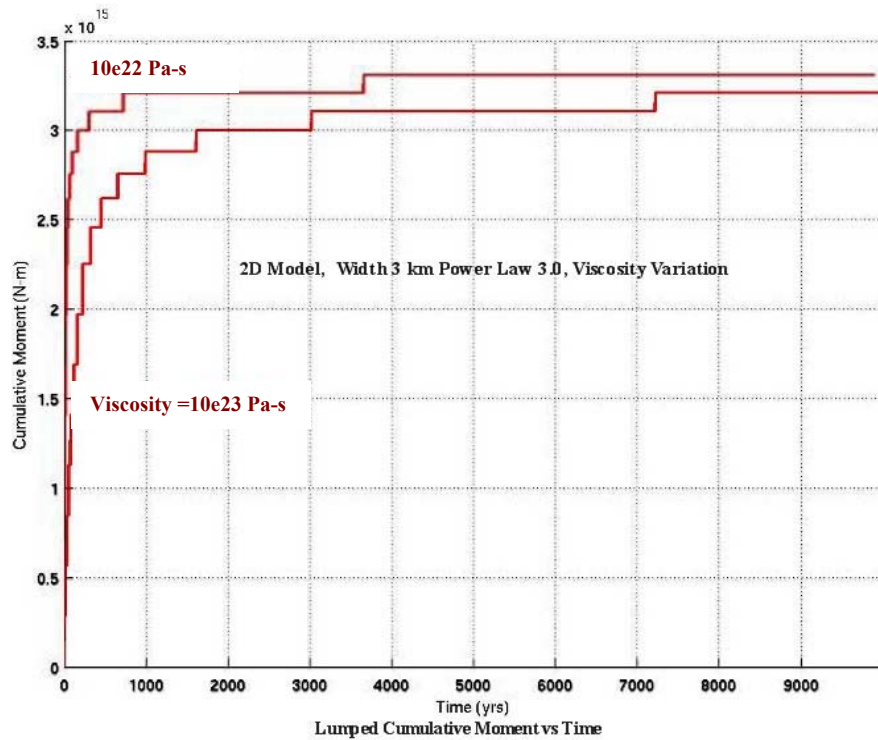


Figure 5.2.3 Width 3 km, Power-law exponent 3.0, Viscosity variation

Figures 5.2.1 to 5.2.3 show variations in stress relaxation pattern (as cumulative moment release on the fault) for increasing values of viscosity and a fixed power-law stress exponent. When viscosity is increased total time before the model cease to produce earthquake increases. Values of viscosity beyond $10e23$ Pa-s results in relaxation times of more than 10,000 years for the models. Present model limits viscosity values to $10e23$ Pa-s since Holocene is only 10,000 yrs long. As we increase the viscosity to higher values, the rate of relaxation decreases and the relaxation curve becomes less steep. We found that in Figure 5.2.1 and 5.2.2 total relaxation of weak zone extends till $\sim 10,000$ years and we note that there are ~ 15 earthquakes with recurrence time intervals of ~ 500 for first 6000 to 8000 years. We can therefore select a window of 2000 years having 3-4 earthquakes with recurrence interval of ~ 500 years

5.3 Power-law Variation for 3 km Wide Weak Zone

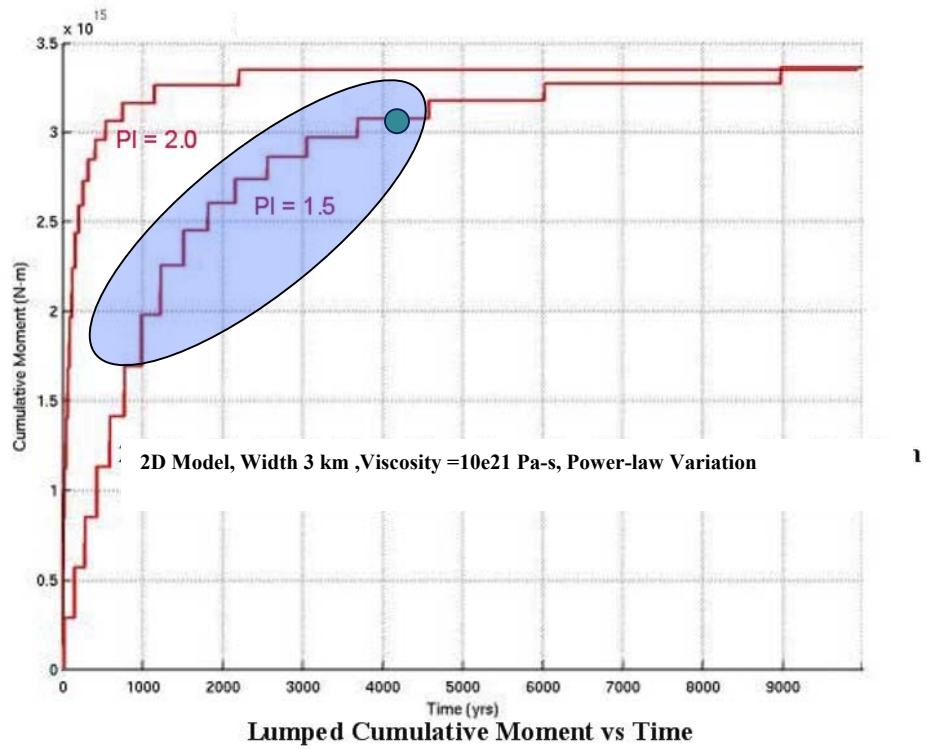


Figure 5.3.1 Width 3km, Viscosity 10e21 Pa-s, Power-law exponent variation

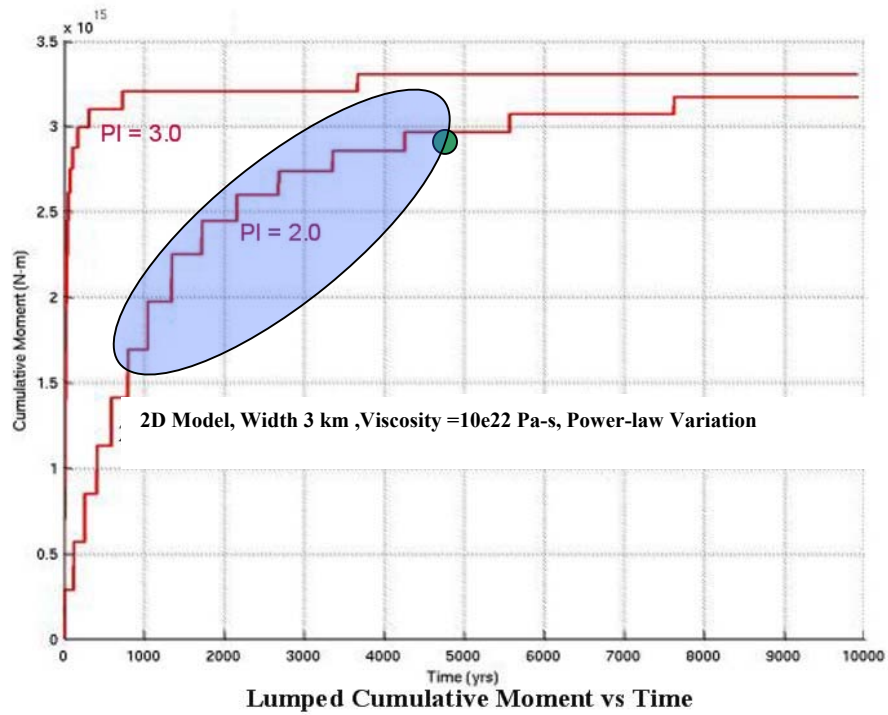


Figure 5.3.2 Width 3 km, Viscosity $10e22$ Pa-s, Power-law exponent variation

Figures 5.3.1 to 5.3.2 show variations of power-law exponent for fixed material viscosity. We have results for three different power-law exponents used with a weak zone width of 3 km. For the same viscosity, use of higher power-law exponents increases the slope of the relaxation curve. Power-law value can not exceed beyond a certain value as the relaxation curve becomes so steep that a numerical singularity results. For 2D models, we found use of power-law higher than 3.0 results in such rates of stress relaxation as to results in a computational singularity. Curves which satisfy the observation from the NMSZ have a green spot on them, while other curves don't as they are steeper and get most of relaxation in first 1000 years.

5.4 Viscosity Variation for 6 km Wide Weak Zone

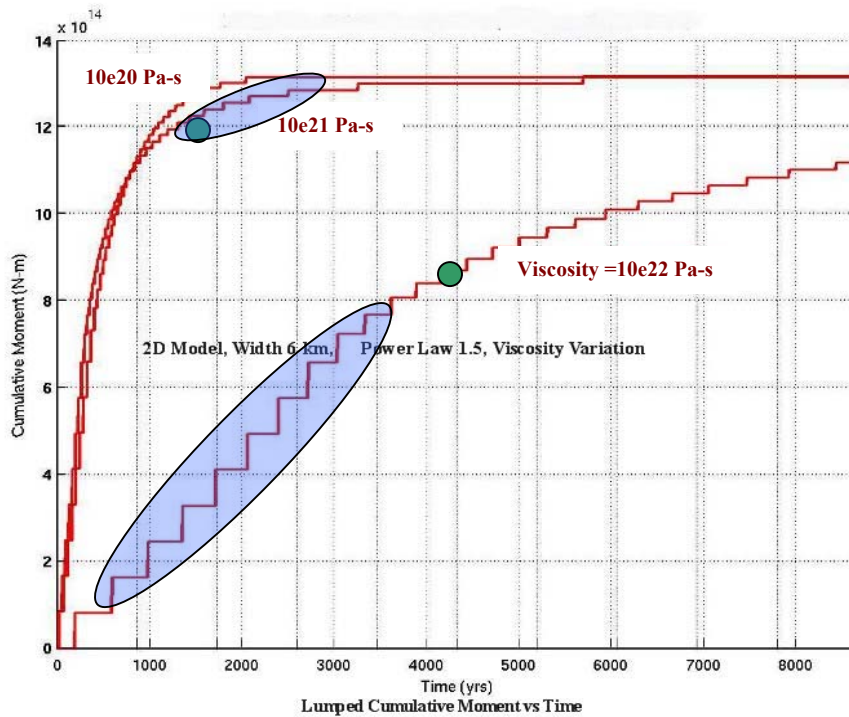


Figure 5.4.1 Width 6 km Power-law exponent 1.5, Viscosity variation

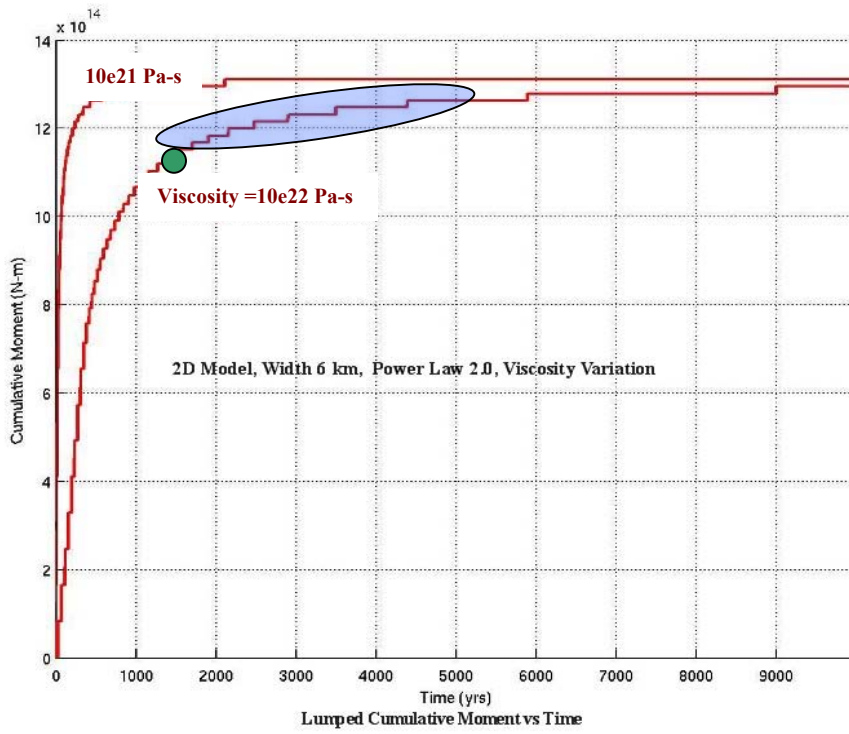


Figure 5.4.2 Width 6km, Power-law exponent 2.0, Viscosity variation

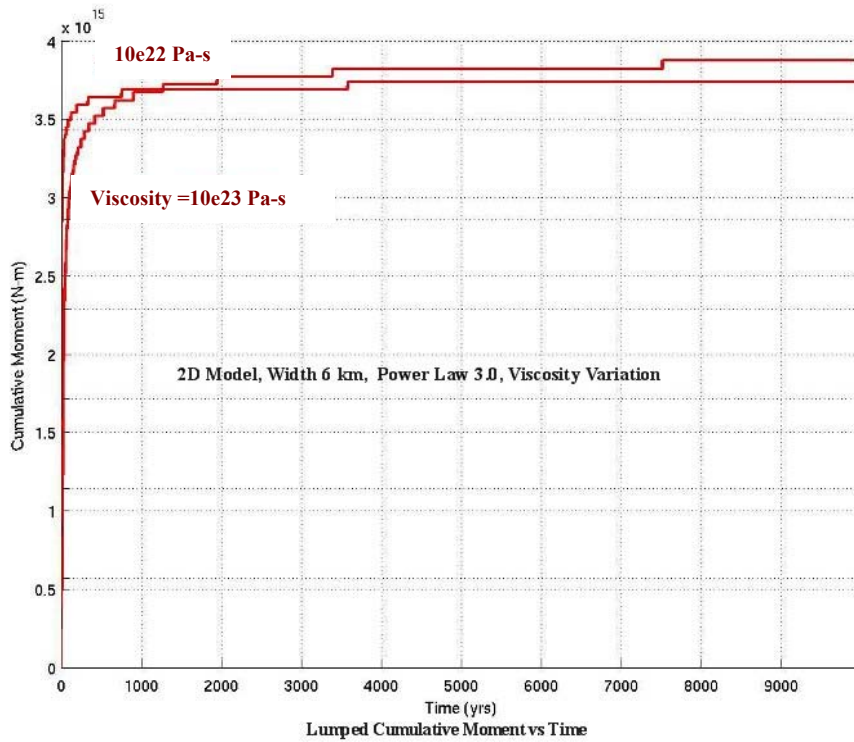


Figure 5.4.3 Width 6 km, Power-law exponent 3.0, Viscosity variation

Figures 5.4.1 to 5.4.3 show effect of variation in viscosity on relaxation of stress for 6 km weak zone width. As seen section 5.2 increasing viscosity decreases the relaxation rate. We used a maximum viscosity of $10e23$ Pa-s for getting results for the power-law exponent of 3.0. As viscosity increases total time before earthquakes cease to occur also increases. Variation of power-law exponent is dominant over variation of viscosity. (compare Figure 5.4.2 and 5.4.3). The model does not completely relax for viscosity $10e22$ Pa-s and a power-law exponent of 1.5. Curves in Figure 5.4.1 and 5.4.2 with green spot can have a window of 2000 years located where we can find 3-4 earthquakes which satisfy the observations from the NMSZ.

5.5 Power-law Variation for 6 km Wide Weak Zone

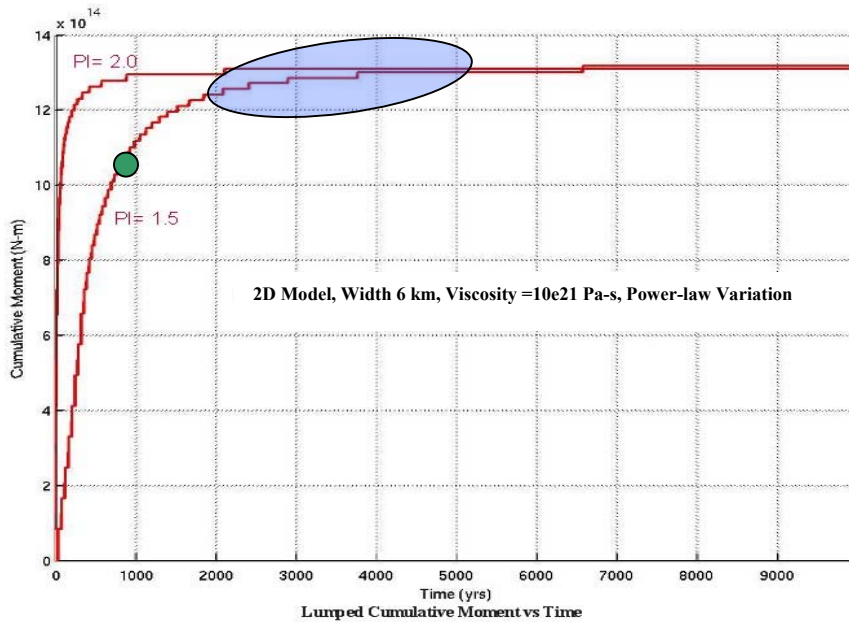


Figure 5.5.1 Width 6km, Viscosity $10e21$ Pa-s, Power-law exponent variation

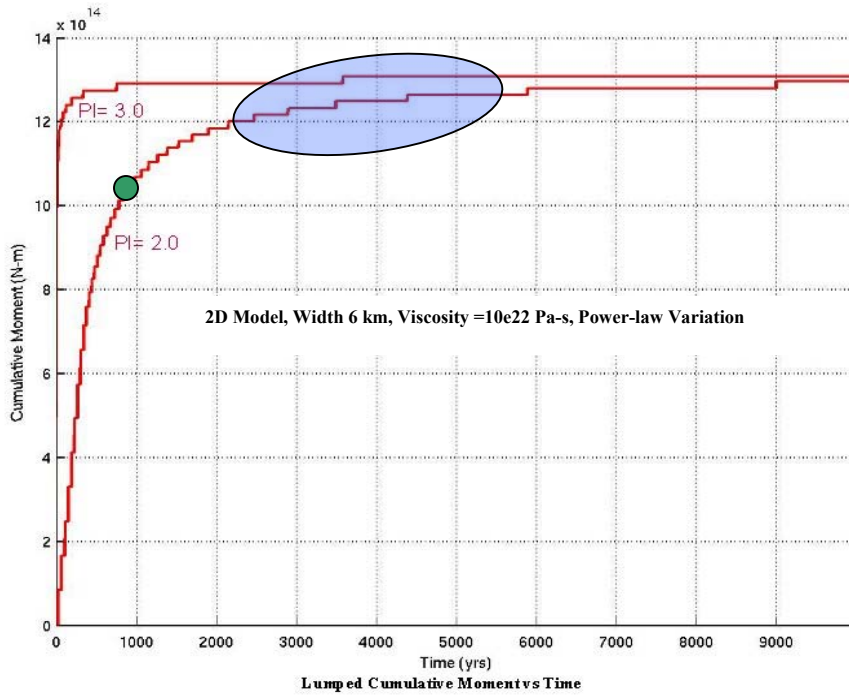


Figure 5.5.2 Width 6km, Viscosity 10e22 Pa-s, Power-law exponent variation

Figures 5.5.1 to 5.5.2 show variation of power-law exponent for given viscosity values for a 6 km wide weak zone. All curves are pretty much completely relaxed in about 5000 years. Curve having green spot satisfy NMSZ observation. As seen in section 5.3 slope of the relaxation curve increases with increase in power-law. A power-law exponent of 3.0 can be used before computational singularity is reached.

5.6 Viscosity Variation for 12 km Wide Weak Zone

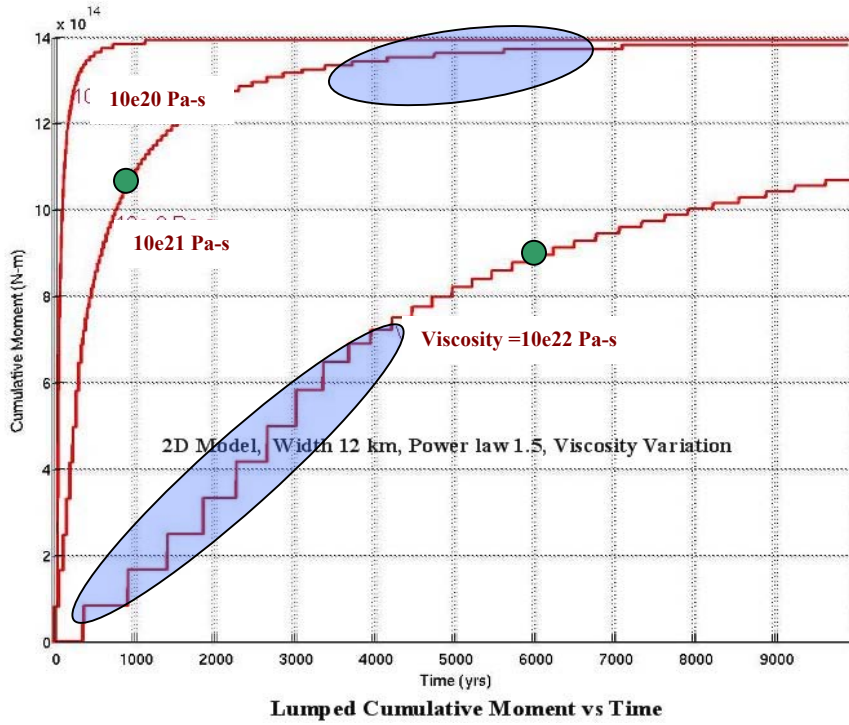


Figure 5.6.1 Width 12 km, Power-law exponent 1.5, Viscosity variation

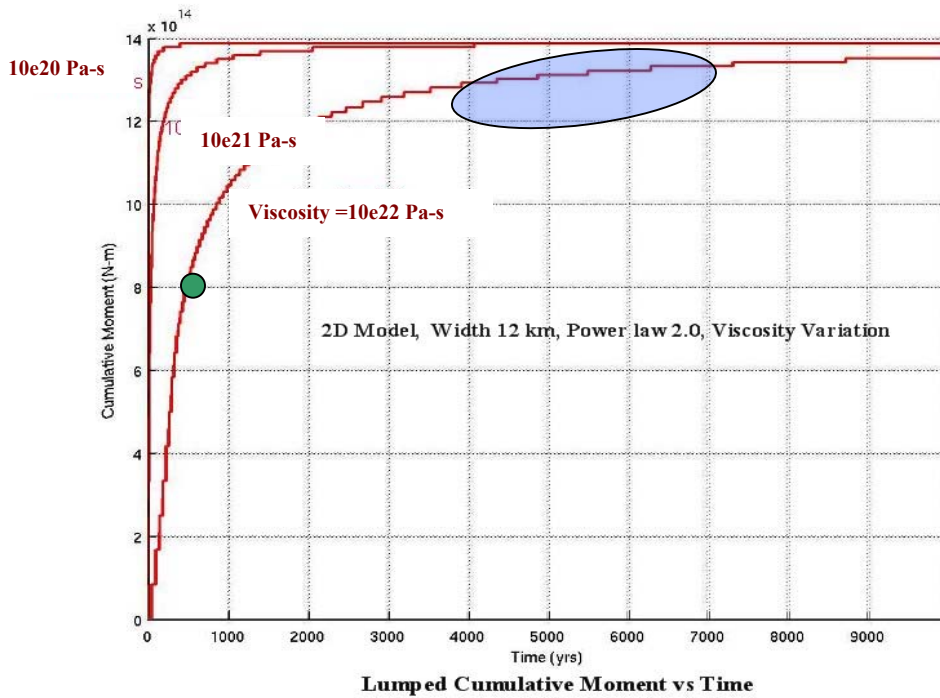


Figure 5.6.2 Width 12 km, Power-law exponent 2.0, Viscosity variation

Figures 5.6.1 to 5.6.2 show variation of viscosity for a given power-law and a weak zone width of 12 km. Again, we see that increasing viscosity decreases the dissipation rate as seen in section 5.2 and 5.4. The total number of earthquakes occurring has increased by great amount in time period of 1000 years. For viscosity $10e20$ Pa-s relaxation is very steep. Curves that satisfy the NMSZ-observation are marked with green spot [viscosity $10e21$ Pa-s; power-law 1.5] and [viscosity $10e22$; power-law 2.0]. As we have observed, increases in power-law and viscosity have opposite effect on the slope of the relaxation curve. The two green spotted curves depict the effect when both the viscosity and power-law exponent is increased. Thus, models matching the NMSZ observations seem to be achievable by increasing viscosity and power-law exponent simultaneously.

5.7 Power-law Variation for 6 km Wide Weak Zone



Figure 5.7.1 Width 12 km, Viscosity $10e20$ Pa-s, Power-law exponent variation

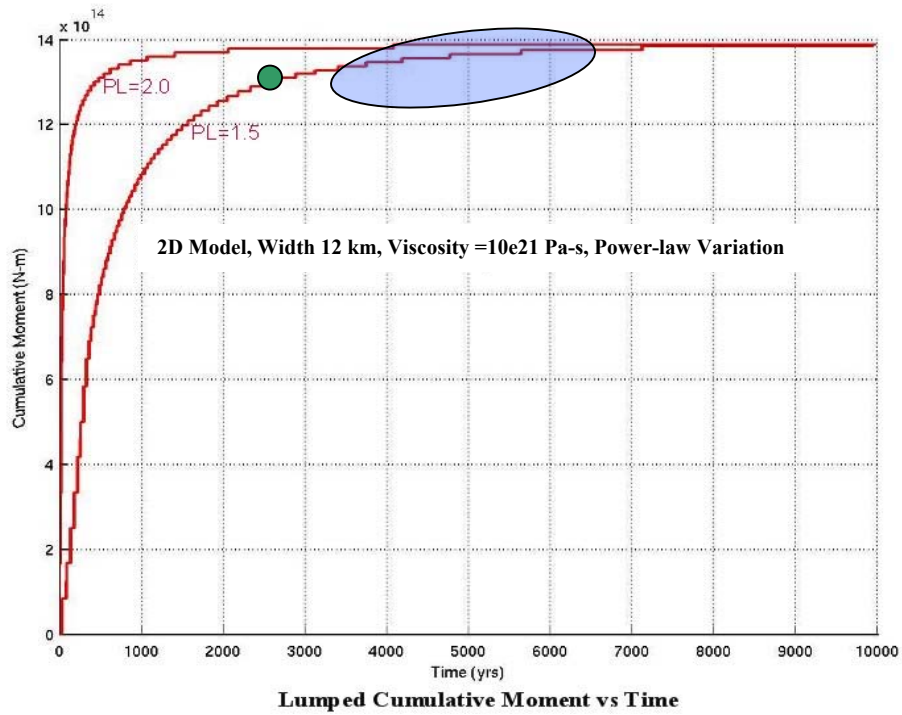


Figure 5.7.2 Width 12 km, Viscosity $10e21$ Pa-s, Power-law exponent variation

Figures 5.7.1 to 5.7.2 show variation of power-law exponent for weak zone width of 12 km. As seen in section 5.3 increasing power-law increases the slope of the dissipation curve. Except for higher viscosity models, all other models relax in 1000 years. Only high viscosity model satisfy NMSZ observation.

5.8 Geometric Variation with 3, 6, 12 km Wide Weak Zones

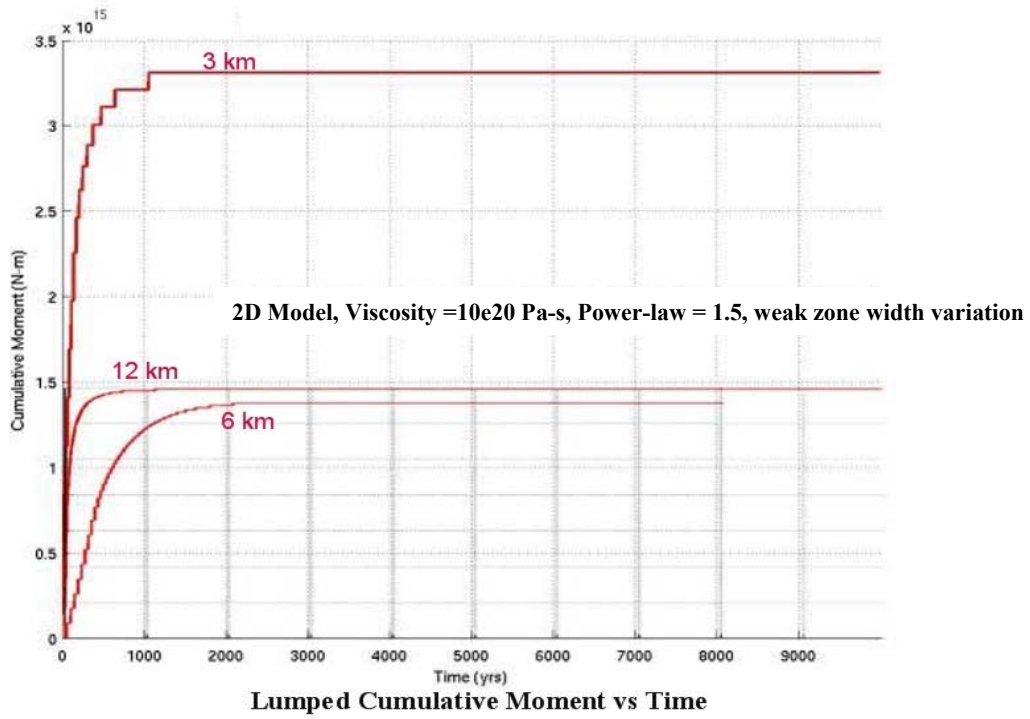


Figure 5.8.1 Power-law exponent 1.5, Viscosity $10e20$ Pa-s, Width variation

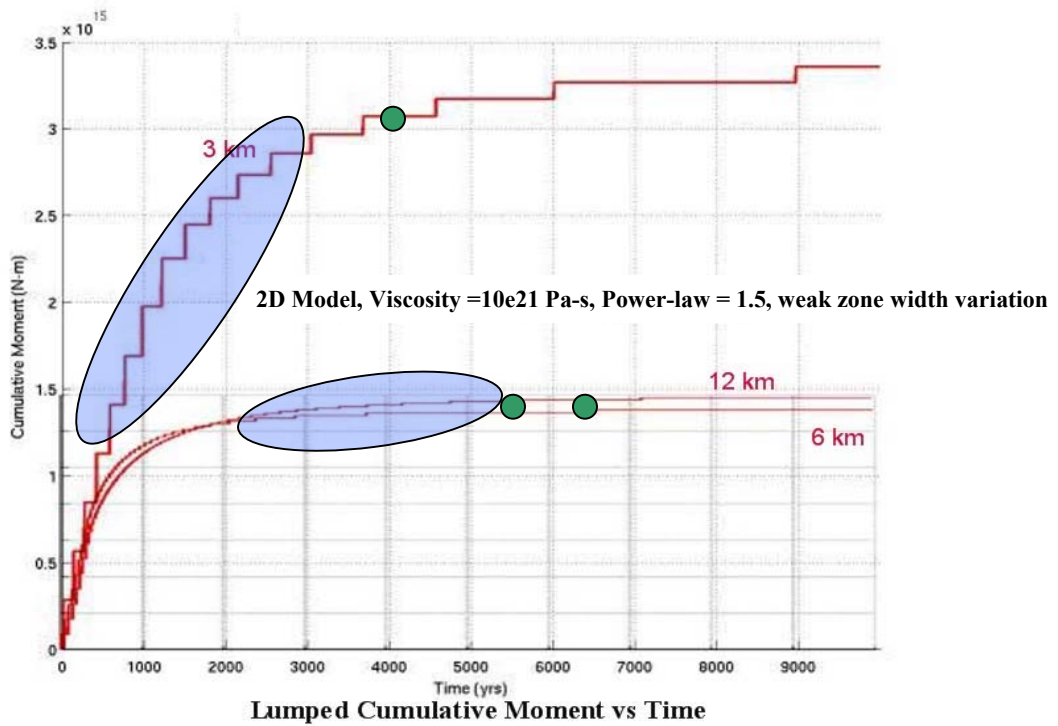


Figure 5.8.2 Power-law exponent 1.5, Viscosity $10e21$ Pa-s, Width variation

Figures 5.8.1 to 5.8.2 give the comparison among different weak zone widths for constant set of the other two parameters. The number of earthquakes which occurred increases as the width of weak zone increases. For the viscosity 10^{20} Pa-s all the models relax completely in 2000 years having ~15 earthquake which does not satisfy NMSZ observations. For a viscosity 10^{21} Pa-s we can find a window of 2000 years having 3-4 earthquakes, hence satisfy the NMSZ observations. In general as the width of weak zone is increased, cumulative moment released at the fault gets drops. This drop is very high when we go from 3 km to 12 km and 3 km to 6 km. The drop from 6 km to 12 km is considerably smaller. We don't know why 3 km wide weak zone behaves so differently. It may be non-linear effects from post seismic stress relaxation in a narrow weak zone. A thorough investigation of the output would be necessary to determine the exact cause.

Table 5.2 2D models run for 10,000 years with Maximum Average Shear Stress criteria on whole fault.

No	Width km	Power-law exponent 'n'	Viscosity Pa-s 'η'	Cumulative Moment (N-m)	No. of Earthquake (Approx.)	Relaxed after 1000 Years (Yes or No)	Time for full Relaxation years	Satisfy NMSZ Observation
1	3	1.5	10e20	3.25e15	~15	Yes	1200	No
2	3	1.5	10e21	3.25e15	~14	No	NA	Yes
3	3	2.0	10e21	3.25e15	---	Yes	2300	No
4	3	2.0	10e22	3.25e15	~16	No	NA	Yes
5	3	3.0	10e22	3.25e15	---	Yes	3700	No
6	3	3.0	10e23	3.25e15	~14	Yes	7300	No
7	3	3.5	10e23	3.25e15	---	Yes	2000	No
8	6	1.5	10e20	1.30e15	~34	Yes	2200	No
9	6	1.5	10e21	1.30e15	~38	Yes	6600	Yes
10	6	1.5	10e22	1.10e15	~24	No	NA	Yes
11	6	2.0	10e21	1.30e15	---	Yes	2200	No
12	6	2.0	10e22	1.30e15	~34	No	NA	Yes
13	6	3.0	10e22	1.30e15	---	Yes	3600	No
14	6	3.0	10e23	1.37e15	~15	No	NA	No
15	12	1.5	10e20	1.40e15	---	Yes	1200	No
16	12	1.5	10e21	1.40e15	---	Yes	7300	Yes
17	12	1.5	10e23	1.10e15	~30	No		Yes
18	12	2.0	10e20	1.40e15	---	Yes	600	No
19	12	2.0	10e21	1.40e15	---	Yes	4200	No
20	12	2.0	10e22	1.35e15	---	No	NA	Yes
21	12	3.0	10e22	1.40e15	~50	No	NA	No

“---“ No. of earthquake could not be counted due to lack to resolution.

“NA” Weak zone was not fully relaxed.

5.9 2D Model with Constant Stress-drop

A number of initial model have been run with constant stress drop. Eventually we decided that this was not the most optimal fault constitutive law. In the constant stress drop version, the failure criteria were based on average shear stress on the fault. During earthquake the stress on the fault is dropped by a constant stress-drop of 10 MPa on whole fault. This results in the same magnitude of earthquake every time. Hence better and more geologically reasonable failure criteria could be developed. Also this method causes stress profiles on the fault to increasingly diverge giving unrealistic values of stress in the bottom half of fault as seen in the Figure 5.9.1. Still this model can be used to obtain preliminary conclusions similar to the paleoliquefaction observations suggesting the magnitudes to be around $M \sim 7$.

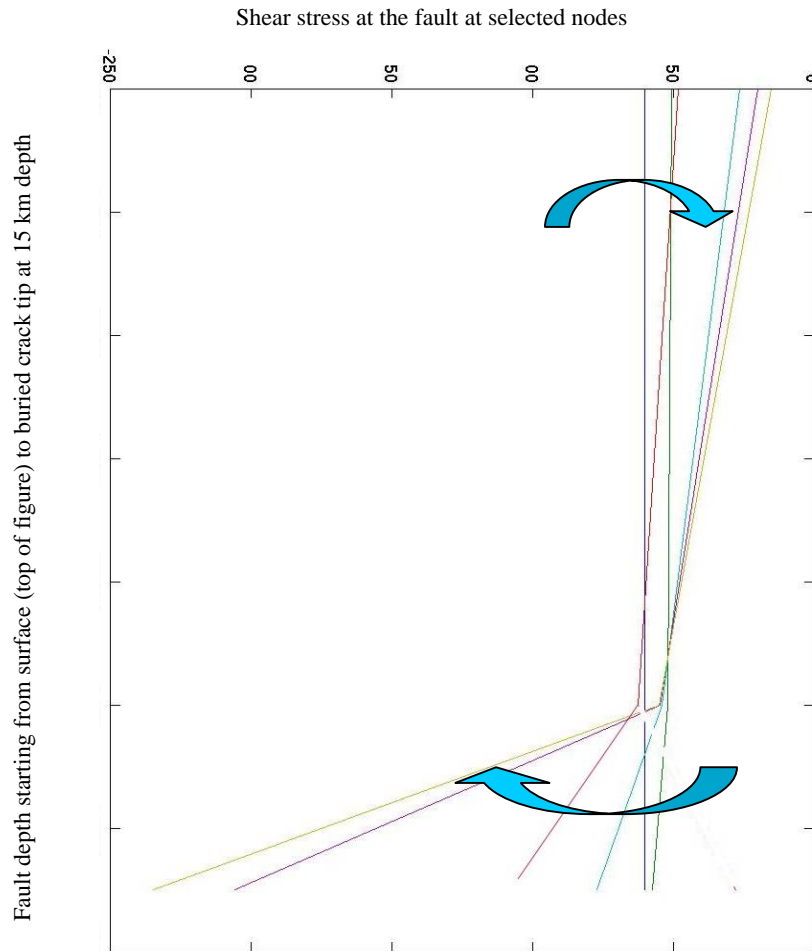


Figure 5.9.1 *Variation of stress profile along the depth on the fault section with time. Failure criteria is average shear stress on the fault, constant stress drop on the fault at every earthquake (Depth not to scale).*

As we see in Figure 5.9.1, when the time increases and the weak zone relaxes the stress profile on the fault changed to lower stresses on the upper zone while much higher stresses in lower fault and towards tip of the fault. Stresses at the last nodes are neglected, being situated in the crack tip (we bury the fault tip in the viscoelastic material to try to minimize the effect of singularity of crack tip). This is an expected numerical result but is also consistent with fact that the earthquakes have foci at the base of

seismogenic zone. Still unrealistic values of the stresses at the lower fault speak of a numerical singularity. As we are not interested in stress near the crack tip this is reasonable approach.

5.10 Conclusions

Table 5.1 and 5.2 show outcome of numerous experiments. We have recognized three possible rheology type of material for weak zone. For geometrical variation we have considered just width of the weak zone. We found that for power-law materials widths beyond 12 km the occurrence of earthquakes becomes so frequent that it can not match with observation of the NMSZ unless viscosity is larger than $10e21$ Pa-s. We have not run models for wider weak zone but infer that above trend continues. Wider weak zone require higher viscosities. We found that limiting values for power-law exponent is 3.5 as after this relaxation of stress becomes so fast that individual events can not be identified. Hence such model can not represent the NMSZ in this limiting case.

On analyzing Table 5.2 we can state that earthquakes do occur with weak zone widths as low as 3 km for 2D results. The rate of dissipation of stress is proportional to the stress exponent and inversely proportional to viscosity. Increase in viscosity increases the total relaxation time. For higher viscosities we found that some of the models were not fully relaxed in 10,000 years. The number of earthquakes in the model increases with the increase in weak zone width even though increase in cumulative moment do not seem to be monotonic with increasing weak zone width (Figure 5.8.1 to Figure 5.8.2). Increasing width satisfy NMSZ observation only with increasing viscosity.

3D Model Results and Discussion

6.1 Introduction

3D models more realistically represent the geometry of the NMSZ and are designed to study the variation in weak zone width and coseismic stress drop within the relaxing weak zone. We require a finite number of number of major earthquakes occurring over a period of 10,000 years. The remote stress in the 3D models is always 60 MPa. In present models, a stress drop of 30% is used (type 3). The effect of other stress drops is under consideration in future work.

On the down side, 3D models are more computational intensive (Figure 6.1). Depending upon which model parameters are used it can take 1-3 days on a Dell 2003, Xeon processor workstation to complete a job.

Parameters from successful 2D results (Table 5.2) are considered. The 2D results indicate that, in general, low power-law exponents (1.0 to 3.0) coupled with average viscosity values ($10e20$ to $10e23$ Pa-s) are found to give suitable results. A power-law exponent of 3.0 is found to be an upper bound. A viscosity corresponding to a relaxation time of 9,000 years is found to be an upper bound. (Young's modulus of 35 GPa and Poisson's ration 0.25 is assumed.)

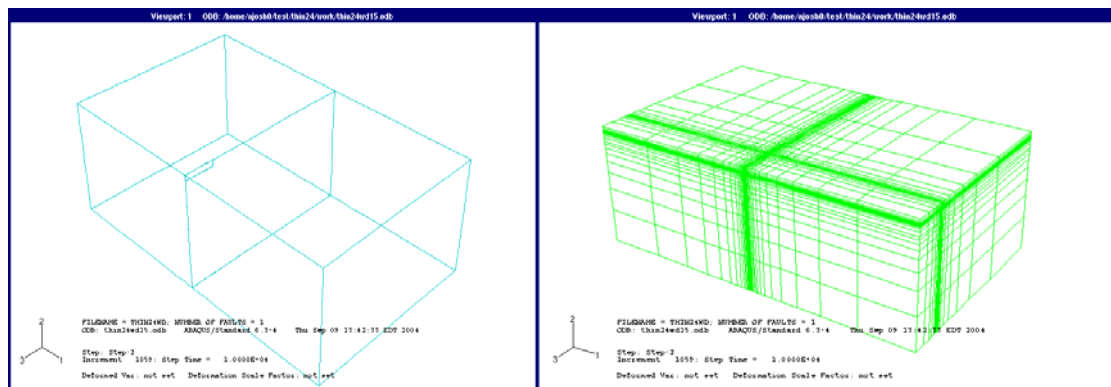


Figure 6.1: 3D models in ABAQUS. A symmetry plane is imposed perpendicular to the fault at it's midpoint. Brick elements are employed.

Figure 6.1 shows the 3D model geometry considered. We have used geometrical symmetry across x-axis. Fault perpendicular boundary conditions have been applied on the front face seen in Figure 6.1. The model uses brick element. Element sizes vary from 0.25 km to maximum of 300 km in any direction. A typical mesh generated is shown Figure 6.1. The model covers the seismically affected area shown in Figure 6.1. Further details of the model have been discussed in section 3.10. In the analyses shown below some of the curves may repeat in different comparisons. A comparison of nearby values of same parameter is presented in every figure.

6.2 Viscosity Variation for 24 km Wide Weak Zone

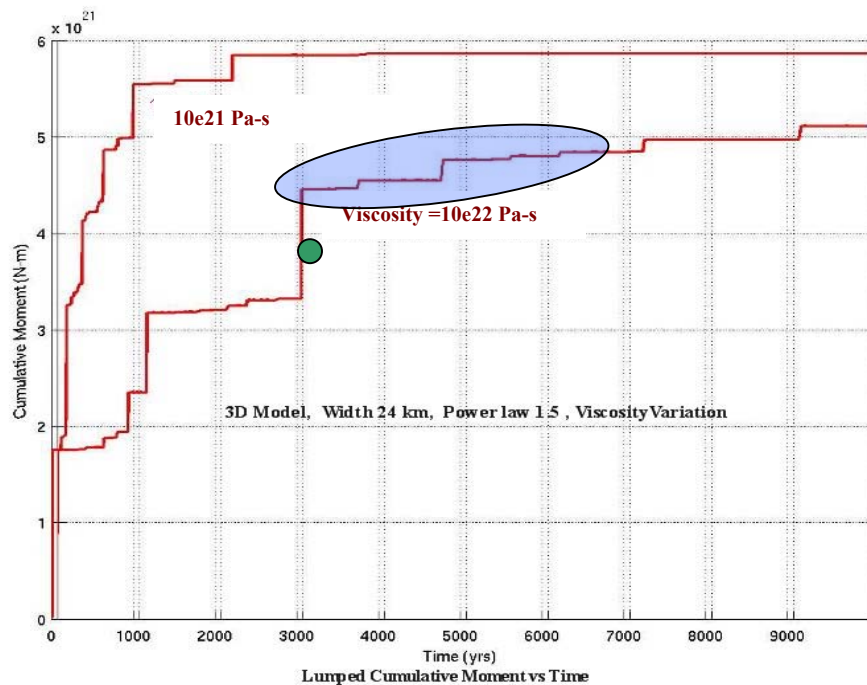


Figure 6.2.1 Width 24 km, Power-law exponent 1.5, Viscosity variation. Y axis of graph represents the cumulative moment in N-m release on the fault (the stress relaxation) and the X axis represents the time in years. Green dot on the curve indicates that the model satisfy the observation from NMSZ i.e. 3-4 earthquakes in 2000 years window. Blue shaded area shows the duration of time in which 2000 year window can be spotted.

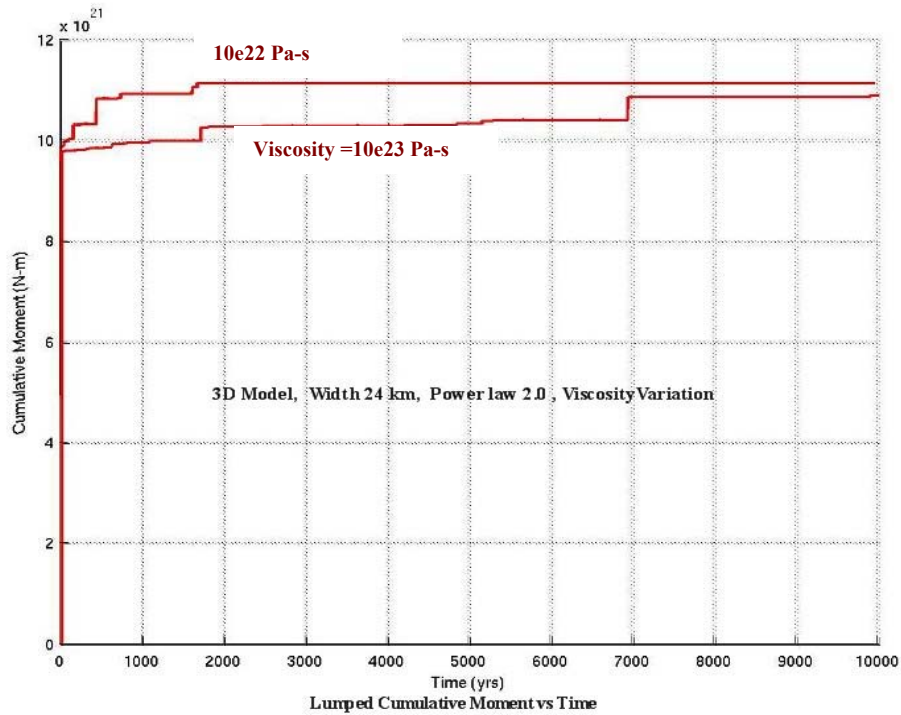


Figure 6.2.2 Width 24 km, Power-law exponent 2.0, Viscosity variation

Figure 6.2.1 to 6.2.2 show variation of viscosity for 3D model with weak zone width of 24 km for a fixed power-law exponent. In the above models as viscosity increases the relaxation time increases as seen in section in section 5.2. It also increases the earthquake recurrence time. We found that viscosity of $10e20$ Pa-s is no more capable of producing earthquake in 10,000 years we are considering. While we considered an upper limiting value of $10e23$ Pa-s, the only models producing suitable results close to the NMSZ observations was found in to be $10e22$ Pa-s. Model found to match the NMSZ observation are marked with a green spot. One remarkable trend noticed in these models is that when a combination of higher power-law exponent and higher viscosity is used we get higher dissipation of cumulative moments on the fault. This phenomenon needs further study to satisfactory explained.

6.3 Power-law Variation for 24 km Wide Weak Zone

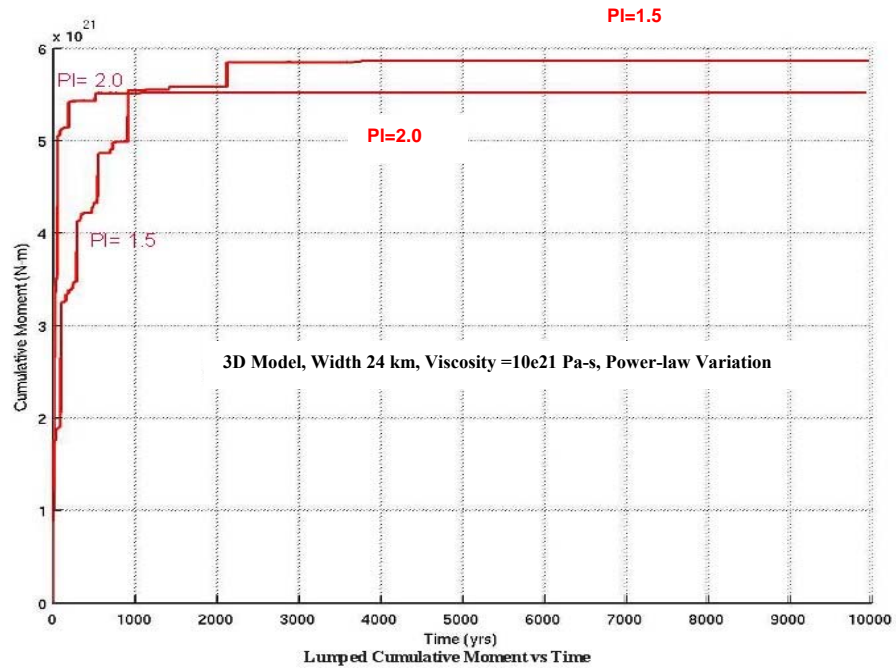


Figure 6.3.1 Width 24 km, Viscosity 10e21 Pa-s, Power-law exponent variation

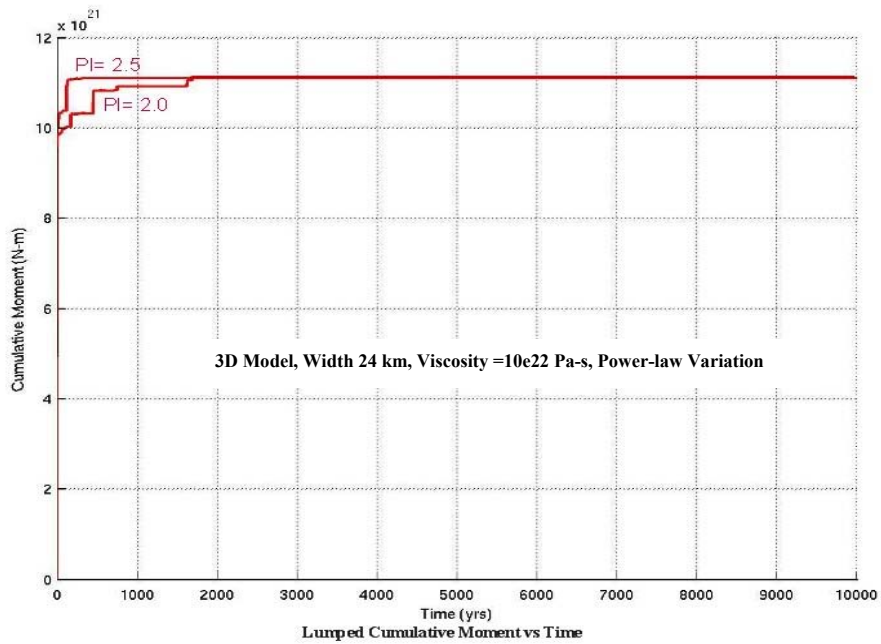


Figure 6.3.2 Width 24 km, Viscosity 10e22 Pa-s, Power-law exponent variation

Figure 6.3.1 to 6.3.2 show variation of power-law exponent for 3D models with weak zone width of 24 km. As we move to higher values of power-law exponents stress dissipation rates on the fault are almost doubled. This trend might indicate that 3D models are more sensitive to power-law variations than 2D models. In Figure 6.3.1 and 6.3.2 there is increase in viscosity as well power-law exponent, and increase in power-law is dominant over viscosity variation, hence model in Figure 6.3.2 relaxes faster even with higher viscosity.

6.4 Viscosity Variation for 54 km Wide Weak Zone

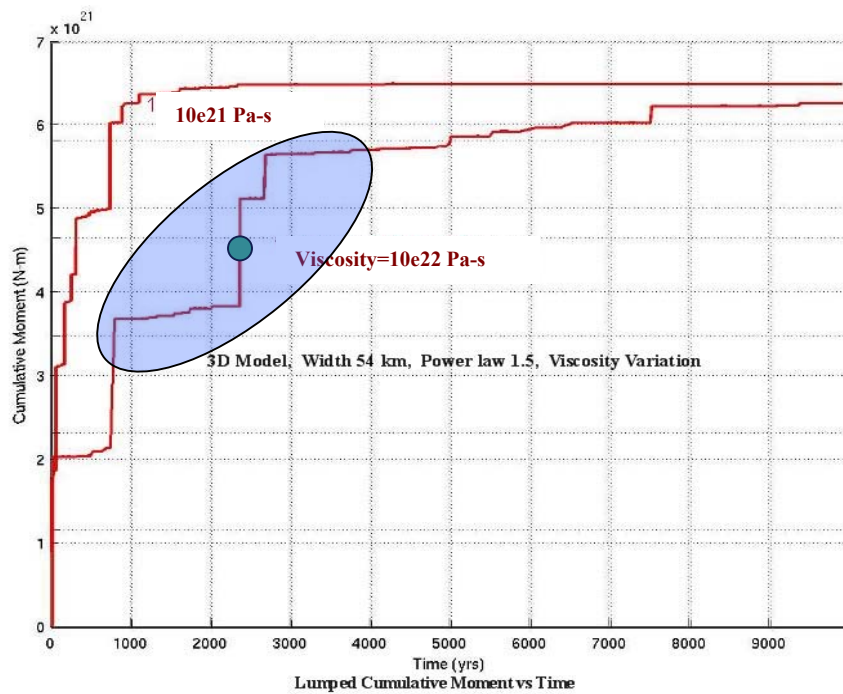


Figure 6.4.1 Width 54 km, Power-law exponent 1.5, Viscosity variation

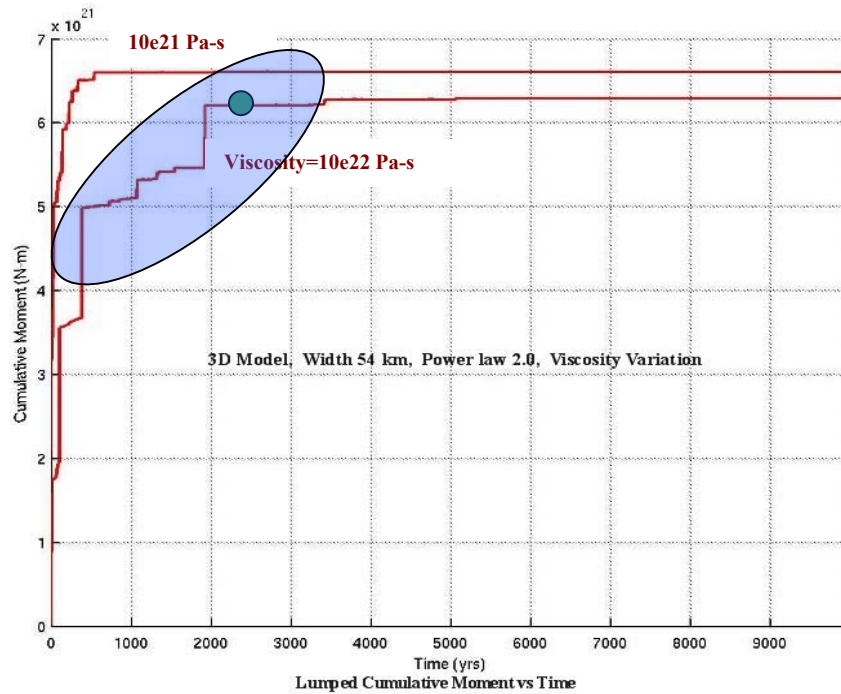


Figure 6.4.2 Width 54 km, Power-law exponent 2.0, Viscosity variation

Figure 6.4.1 to 6.4.2 show variation of viscosity for 3D model for weak zone width of 54 km. Each figure shows comparisons for fixed power-law exponent. As seen in the previous section, increase in viscosity increases the relaxation time and changes the stress relaxation pattern. The slope of relaxation curve decreases when viscosity is increased. Models for values 10e21 Pa-s and higher can be run for this width of model. For values below this viscosity the models do not satisfy the convergence criteria.

6.5 Power-law Variation for 54 km Wide Weak Zone

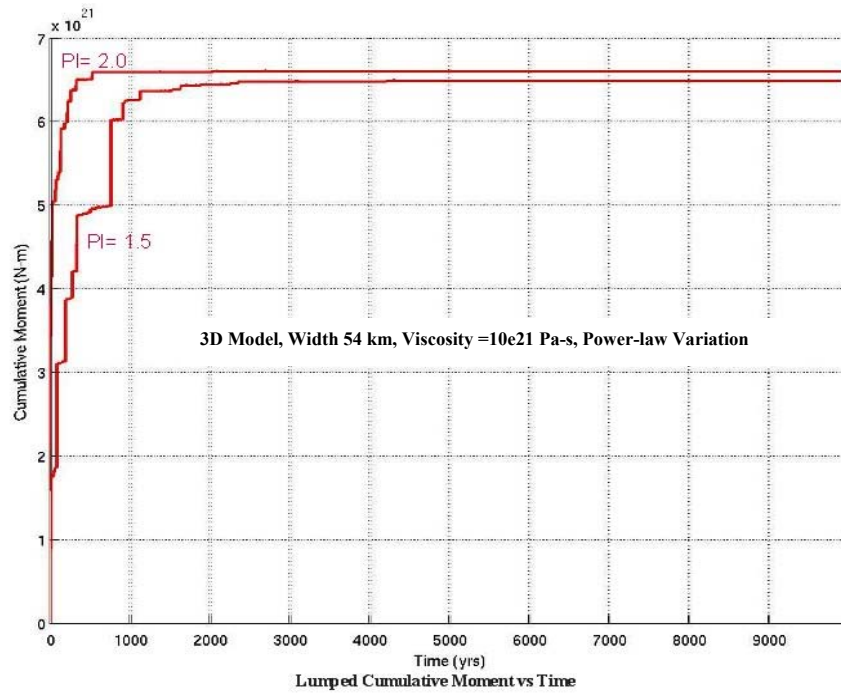


Figure 6.5.1 Width 54 km, Viscosity 10e21 Pa-s, Power-law exponent variation

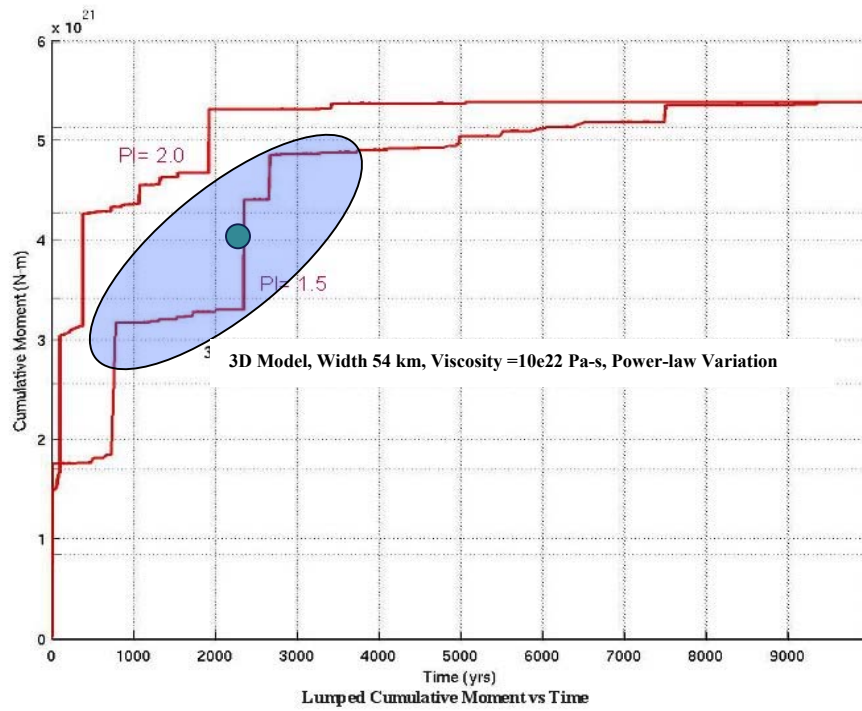


Figure 6.5.2 Width 54 km, Viscosity 10e22 Pa-s, Power-law exponent variation

Figure 6.5.1 to 6.5.2 shows the variation in power-law exponent for 3D model with 54 km weak zone width. Again each figure shows comparison for fixed value of viscosity. Only one curve is found to satisfy the NMSZ observation. As noted earlier, with higher weak zone width, models become sensitive to power-law exponents and higher power-law exponents result in fast stress dissipation rates. As per the trend seen in Table 6.1, a suitable value set is found in the lower power-law exponent range. With the variation in power-law exponent, models with the same geometry can have very different stress relaxation curves.

6.6 Viscosity Variation for 75 km Wide Weak Zone

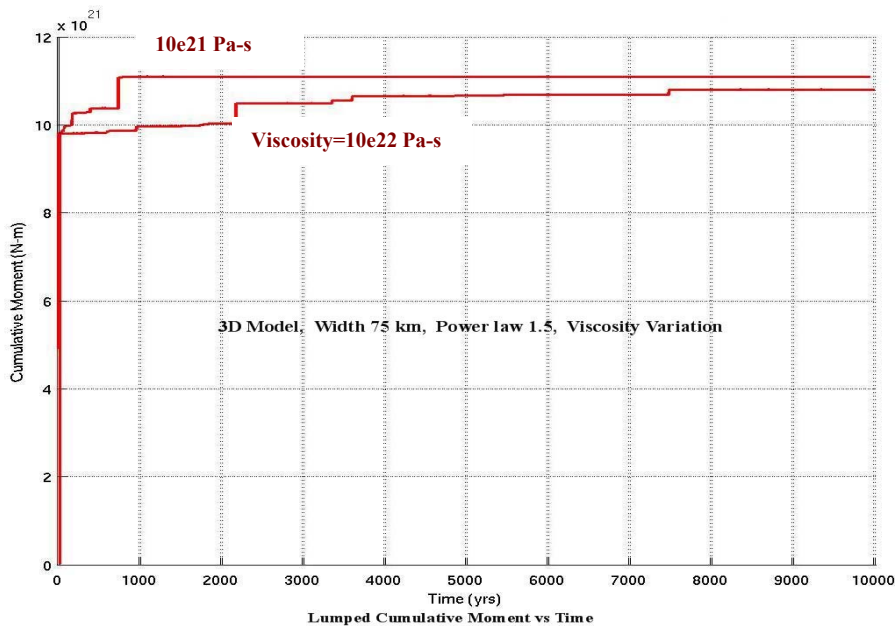


Figure 6.6.1 Width 75 km, Power-law exponent 1.5, Viscosity variation

Figure 6.6.1 shows viscosity variation of the 3D model for a weak zone width of 75 km. Only two model can be run for this width both having power-law exponent of 1.5. The general trend seen in viscosity variation follows previous results yielding a greater number of earthquakes with increase in viscosity. None of the models found satisfy the NMSZ trend for this weak zone width and power-law exponent, and viscosity combination.

6.7 Geometric Variation with 24, 54 and 75 km Wide Weak Zone

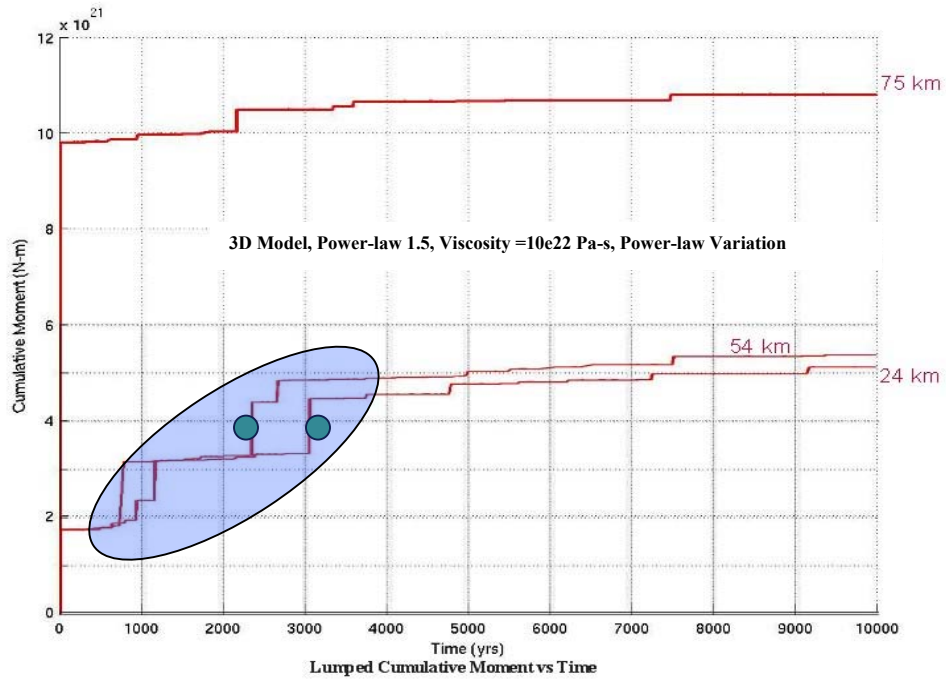


Figure 6.7.1 Power-law exponent 1.5, Viscosity 10e22 Pa-s, Width variation

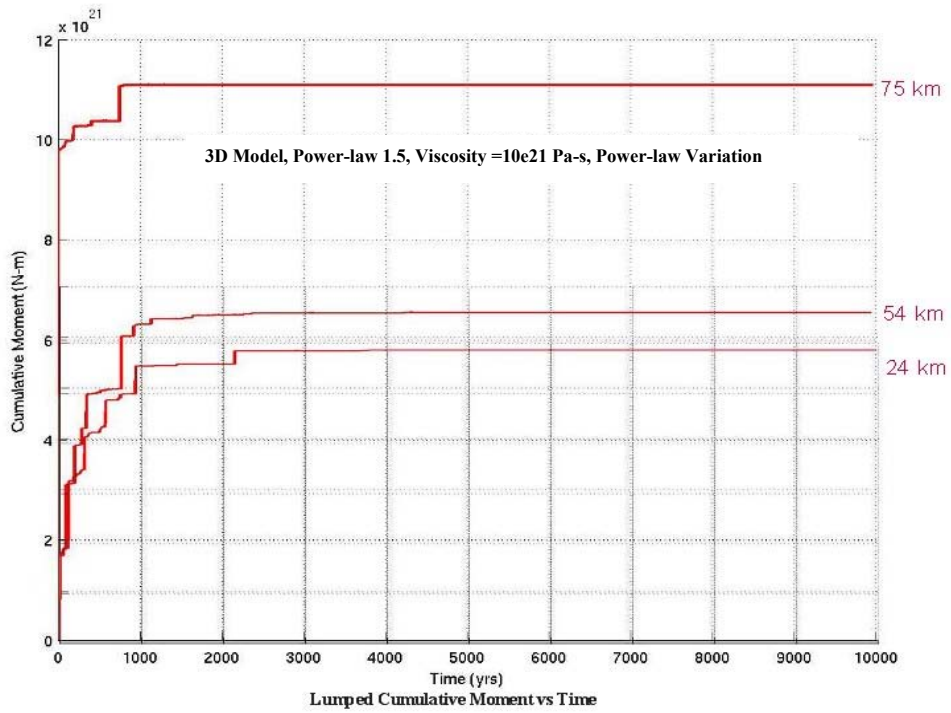


Figure 6.7.2 Power-law exponent 1.5, Viscosity 10e21 Pa-s, Width variation

Figures 6.7.1 to 6.7.2 show variation in width of the weak zone for 3D models, we have compared the variation for constant power-law exponent and viscosity values. For lower values of viscosity models are found to be relaxed in first couple of thousands of years. None of lower viscosity model satisfies the observations from NMSZ. If we move to higher viscosity models with less width, they do satisfy the observations from the NMSZ. Note the difference in stress release on the fault between the 24 km to 54 km models (30 km jump) and the 54 km to 75 km models (21 km jump). A likely reason for the 3D case could be the effect of the characteristics lengths. The 3D problem has two characteristic lengths 40 km as the depth of bottom of weak zone and 100 km as half of length of fault. The 24 and 54 km model are close to characteristic length 40 km *i.e.* depth of the bottom of the weak zone, hence stress release on the fault is controlled by depth of the bottom of weak zone. The 75 km model is close to characteristic length of 100 km hence stress release on the fault is proportionally increased. Because they are of infinite length this argument does not apply to the 2D models.

6.8 Conclusions

We found that as we move towards the higher weak zone width higher amounts of stress is released on the fault. Use of power-law exponents as high as 1.5 to 2.0 may need very high viscosity values in order to produce models having resemblance with the NMSZ observation. Suitable results can be obtained with the moderate values of width about 24-54 km, power-law exponents of 1.5 -2.0 and viscosities of $10e22$ Pa-s to $10e23$ Pa-s. We ran some models with weak zone widths of 3 km and 6 km but did not result in successful convergence of model. Due to time constraints and computational constraints models could not be revised. Thus we cannot comment on the model with widths below 24 km. Given the time constraints 24 km was lowest weak zone width that ran successfully. Thus we have no models run for widths of 3, 6, 12 km so we don't have any comment on them. Table 6.1 shows data for parameters which resulted in model satisfying the NMSZ observation.

Table 6.1 These 3D models were run for 10,000 years with Maximum Shear Stress criteria on each node with 30 % drop in stress on fault.

No	Width km	Power-law exponent 'n'	Viscosity Pa-s 'η'	Cumulative Moment (N-m)	No. of Earthquake (Approx.)	Relaxed after 1000 Years (Yes or No)	Time for full Relaxation years	Satisfy NMSZ Observation
1	24	1.5	10e21	6e21	6	Yes	2500	No
2	24	2.0	10e21	6e21	3	Yes	800	No
3	24	1.5	10e22	6e21	7	No	NA	Yes
4	24	2.0	10e22	11e21	4	Yes	2000	No
5	24	2.0	10e23	11e21	4	No	NA	No
6	54	1.5	10e21	7e21	8	Yes	2000	No
7	54	1.5	10e22	6e21	5	No	NA	Yes
8	54	2.0	10e21	7e21	4	Yes	700	No
9	54	2.0	10e22	6.5e21	4	Yes	4000	Yes
10	75	1.5	10e21	11e21	2	Yes	800	No
11	75	1.5	10e22	11e21	2	Yes	8000	No

Results and Discussion

In this section we test the model against field data. The most useful data for testing the model are the 1811-1812 earthquake sequence and two other pre-historic events which took place in last two thousand years. There is also a small set of geodetic data measured in the last decade by Stanford University, Northwestern University, and Memphis University. The observations in the NMSZ include 15 m of uplift on the Reelfoot fault [Van Arsdale and TenBrink, 2000] and dramatic increase in slip-rate during the Holocene (Table 1.1). The sequence of earthquakes was extremely large, $M > 7$ with a felt area extended to Boston (Figure 1.1). In part, seismic waves travel much farther in the central and eastern US as compared to the western US (Fig 1.2) but the 1811-1812 earthquakes are still extremely large. The sizes of sandblows which are located in the NMSZ region are the largest ever recorded.

The study shows that a simple model of the earthquake cycle in the NMSZ, based on the phenomenon of stress relaxation in a weak zone, can explain the first order observations from the NMSZ. Results in Chapter 5 and Chapter 6 indicate that we can find models using narrow weak zone widths and power-law and viscosity values which can produce earthquake sequences as seen in the NMSZ. Given a combination of certain parameters an earthquake cycle close to the observed one can be produced with negligible surface strain-rates. Though the solution is non-unique, we can still rule out parameter combinations that don't work. A smaller set of parameters can be obtained when an additional constraint of number of earthquakes produced in the last 2000 years is used.

One of the goals of this study was to see how narrow a weak zone could get and still satisfy observations from the NMSZ. Figures in Chapter 5 show that in certain windows of time a weak zone as low as 3 km width can produce earthquake sequences similar to those in the NMSZ. The model uses nonlinear power law rheologies. All the models producing required observation have been marked with green spot, other models can be eliminated.

The second goal was to develop more computationally efficient and rheologically realistic fault friction subroutines. We investigated various possibilities. Fault friction is a complex geological phenomenon. Efforts have been made to integrate these phenomena and reach optimal utilization of computation resources. Friction criteria type 1 and type 2 enforce predetermined stress drops. Type 3 criteria use a percentage stress drop and may be more geologically realistic approach. In all cases computational efficiency must be improved. Book-keeping parameters are the key to performing friction simulations of earthquakes. Further streamlining of the book-keeping can be investigated to improve efficiency.

A final goal was to identify the trends in the parameter space which might help to limit future studies. For constant width and power-law exponent, increases in viscosity increase the total relaxation time for the same geometry but the trend of occurrence of earthquake changes. For a given set of the other two values, higher and lower viscosity value can be decided where average recurrence time for earthquakes can be resolved on the time scale ~ 500 years.

For the constant width of the weak zone and viscosity, increases in power-law exponent accelerate the occurrence of earthquake. Criteria of ruling-out a value of the power-law is same as discussed above for viscosity. We found that large values of weak zone widths are incompatible with large values of power-law exponents. The same results are seen in both 2D and 3D models. Finally, many of the models produce geological impossible results and can be eliminated.

After we have obtained these values, further parameter set can be constraints by limiting magnitude of earthquake and slip on the fault. This could be scope of future work. Concurrent development of fiction subroutines will help to investigate more realistic values and further restrict parameter set being constrained. As see in Chapters 5 and 6 we can also produce positive results using narrow weak zones and power-law rheologies to match observations in the NMSZ.

Limitations

Following are limitations on the result that are applicable to the finite element modeling of the NMSZ.

1. Approximations used in the modeling which result from a lack of precise geometrical and rheological information in the NMSZ. These uncertainties are dealt with by attempts to bound the range of geologically reasonable parameters.
2. There are certain limitations in the friction subroutines used both in the 2D and 3D calculations. For example, in 2D problems the whole fault will rupture every time there is an earthquake. There also errors which are introduced by variations in the numerical convergence criteria. More precise friction subroutines are currently being developed.
3. We have used simplified fault geometry in the model *i.e.* the NMSZ is modeled as one strike-slip fault of span 200 km, while in actual it is composed of three faults two strike-slip and one dip-slip as discussed in Chapter 2. In future both thrust faulting and strike-slip faulting can be included to obtain more realistic results.
4. Earthquake magnitude are uncertain (though certainly $M > 7$) because they are based on felt reports and the amount of shaking necessary to form observed paleoliquefaction feature.
5. Earthquake repeat times are uncertain because they are based upon dating of paleoliquefaction features. Further more there is no historical record of a complete earthquake cycle. Finally, earthquake repeat times are highly variable in any tectonic setting.
6. The results are restricted to an elastic crust and mantle.
7. We have considered steady state stress boundary conditions, where in real life remote stress would be slowly changing.

Conclusions

As we review the 2D and 3D model results, we can draw the following conclusions:

- 1) As the power-law exponent increases, the frequency of earthquakes is initially very high and the weak zone reaches a fully relaxed state relatively quickly. Thus, higher power-law exponents produce higher energy dissipation rates. See results in sections 5.2 and 6.2
- 2) In the 2D model, as weak zone width increases, the total number of earthquakes occurring before total relaxation increases. This trend is not as clear in 3D may due to width values used. See Table 5.2 and 6.1.
- 3) For 2D models as weak zone width increases the time required for full relaxation of the weak zone increases although the total moment release after 10,000 years is decreased (see Figure 5.7.1 and Figure 5.7.2). This is because energy is initially transferred to parts of the crust which are far from the fault. Very narrow weak zones (3 km) have much higher moment release compared to models with wider weak zone (6-12 km). This may be the result of the increase in efficiency of postseismic stress recycling in the narrow non-linear weak zone.
- 4) At its fully relaxed state for 3D power-law models with wider weak zone have higher moment release (see Figure 6.7.1 and Figure 6.7.2).
- 5) Increases in weak zone viscosity lead to lower initial slopes in the moment vs. time curves. This produces lower initial energy dissipation rates. See section 5.3 and 6.3.
- 6) Using power-law rheologies in 2D, we can have 10-12 earthquakes in weak zones as narrow as 3 km over 1200 years with lower values of viscosity. 3D models using a weak zone width of 24 km yield 5-6 earthquakes in 5000 years. This difference in number of earthquakes is mainly because of the way the modeling is done, as 2D models have infinite weak zone length while 3D model have limited weak zone length.

- 7) This is a non-unique problem. A specific set of parameters satisfying the observation can not be considered as solution. If we are given two of the following three parameters, power-law exponent, weak zone viscosity, and weak zone width, a range of the third parameter can always be found which matches geological observations in the NMSZ. However, if we can make realistic, independent assessments of two of these parameters, we can place more restrictive bounds on the range of possible third parameter values
- 8) We find that weak zone as narrow as 3 km for 2D models and 24 km for 3D models can fit the observations in the NMSZ using the power law rheology. Unfortunately 3D weak zone models with width smaller than 24 km with power-law rheologies experienced numerical convergence difficulties.
- 9) We have developed and refined 4-5 different fault friction subroutines, though some them have not been used in the reported results. Preliminary testing indicated that subroutine using average shear stress values for calculation is the fastest but the friction subroutine which is implemented through shear stress at each node seems geologically more realistic. Hence a friction model having a median (type 3) between the two features would be more appropriate. As suggested in Chapter four, research using type 4 and type 5 subroutines can yield very efficient subroutines and more realistic results.
- 10) Stress drop is one of the important parameters in deciding the whole earthquake cycle. Earlier constant stress drop and stress drop to a constant value has been used which does not reflect the true behavior of process and give more unrealistic stress profiles.
- 11) Benchmarking efforts have been made to compare *CREEP and *VISCOELASTIC keywords for representing linear materials and *VISCOELASTIC keyword was found to be more computationally efficient when Maxwell material is considered.
- 12) Standard linear solid has been proposed as an alternative choice for material representing the crust weak zone material. Analytical calculations were performed to calculate Prony series coefficients for SLS model in ABAQUS.

Appendix A

Comparison of *VISCOELASTIC & *CREEP Keywords

The Nur-Mavko model has been used to compare two keywords. The Nur-Mavko model comprises of geometry as seen in Figure 5.1. It has two layers. The top layer is elastic representing the lithosphere while bottom layer is a viscoelastic half-space representing the asthenosphere. The Nur-Mavko model can be used to find the surface displacements through an analytic method. Earlier a benchmark for this analytical and *CREEP keyword has been done. I proceed further and compare surface displacement for *VISCOELASTIC and *CREEP keyword for same setup.

Following are the plots of difference in the displacement at nodal points on the surface between the models using *CREEP and *VISCOELASTIC keywords. These graphs have been plotted at different times starting from first occurrence of earthquake.

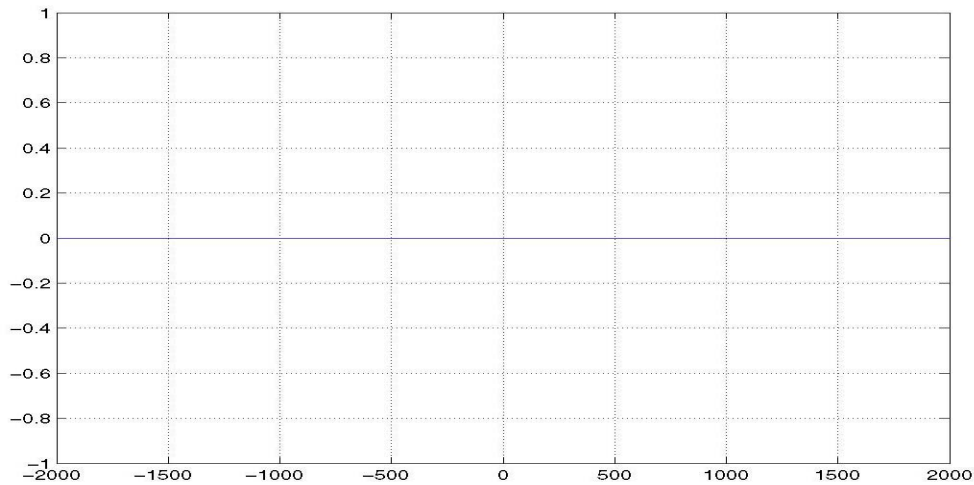


Figure A.1 Displacement difference at top surface at Time $t = 0.000$ Years. X axis shows distance from fault in km and Y axis shows the difference in displacement in mm at the elapsed time in years given in the figure caption.

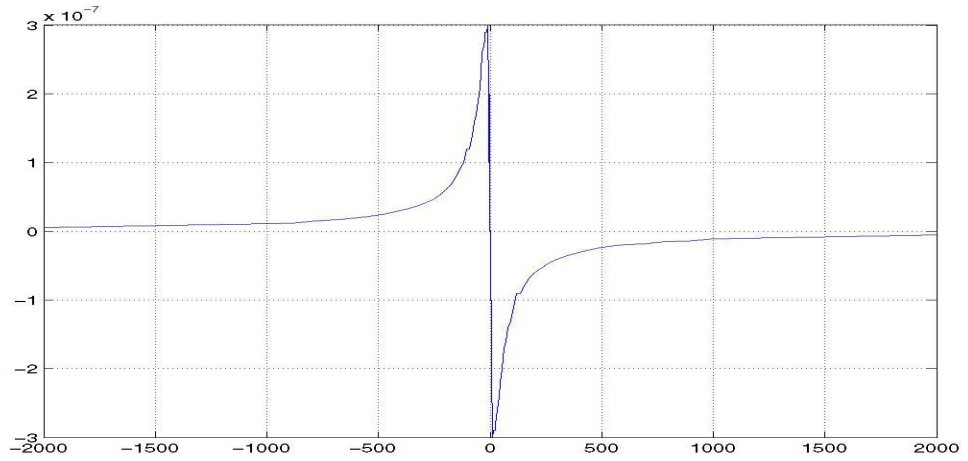


Figure A.2 Displacement difference at top surface at Time $t = 0.236$ Years

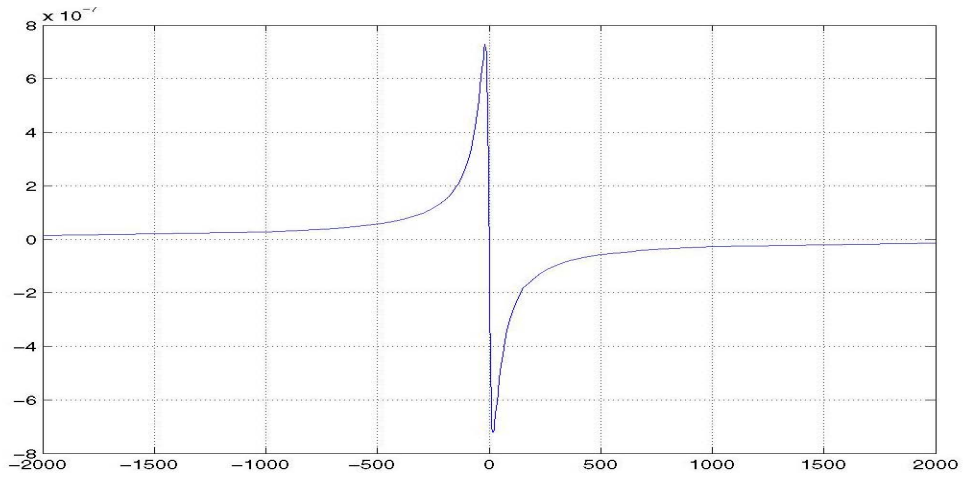


Figure A.3 Displacement difference at top surface at Time $t = 0.540$ Years

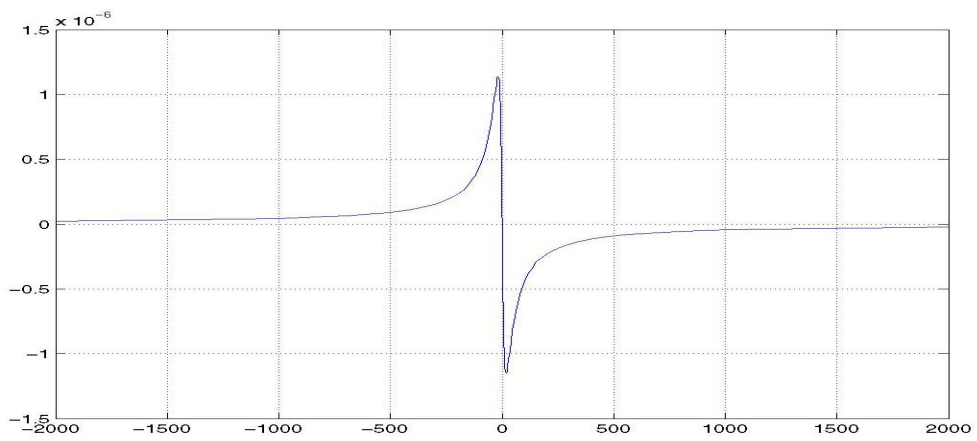


Figure A.4 Displacement difference at top surface at Time $t = 0.800$ Years

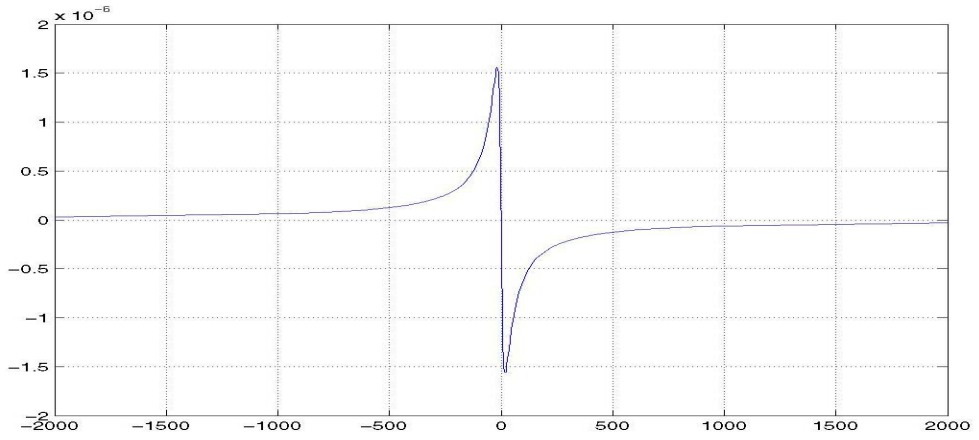


Figure A.5 Displacement difference at top surface at Time $t = 1.080$ Years

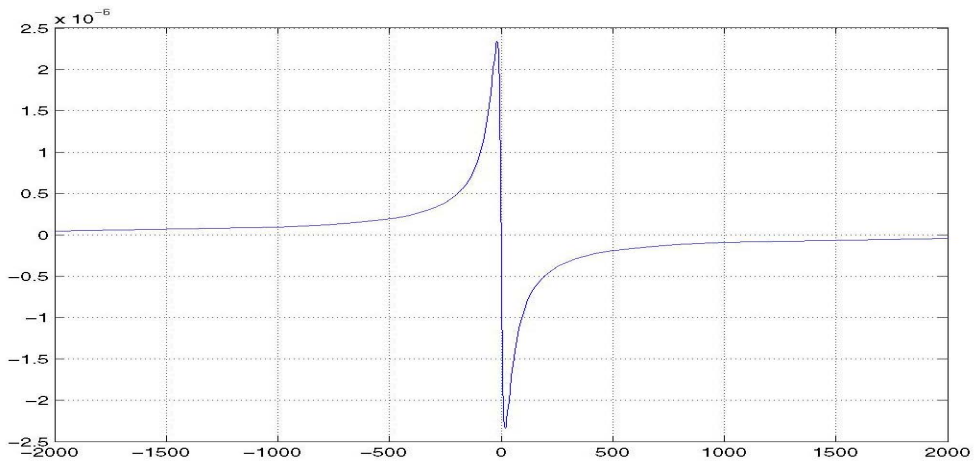


Figure A.6 Displacement difference at top surface at Time $t = 1.720$ Years

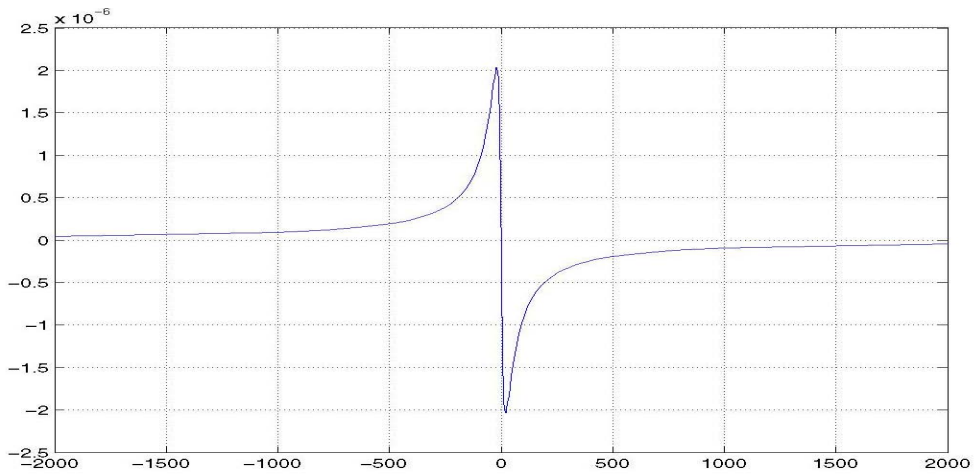


Figure A.7 Displacement difference at top surface at Time $t = 2.700$ Years

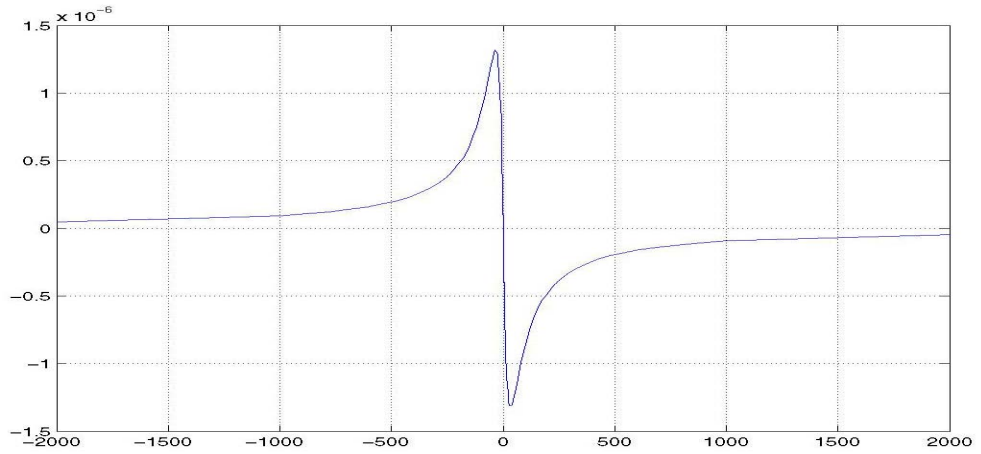


Figure A.8 Displacement difference at top surface at Time $t = 5.600$ Years

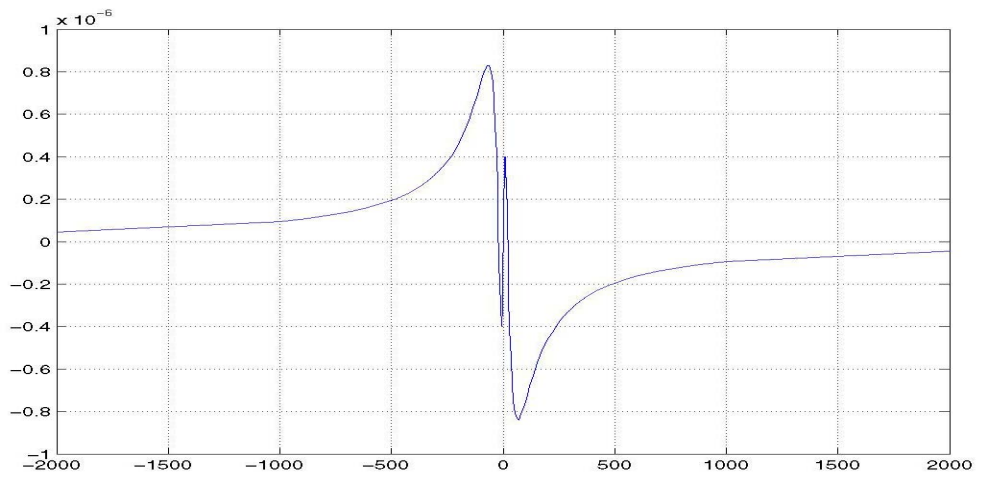


Figure A.9 Displacement difference at top surface at Time $t = 10.600$ Years

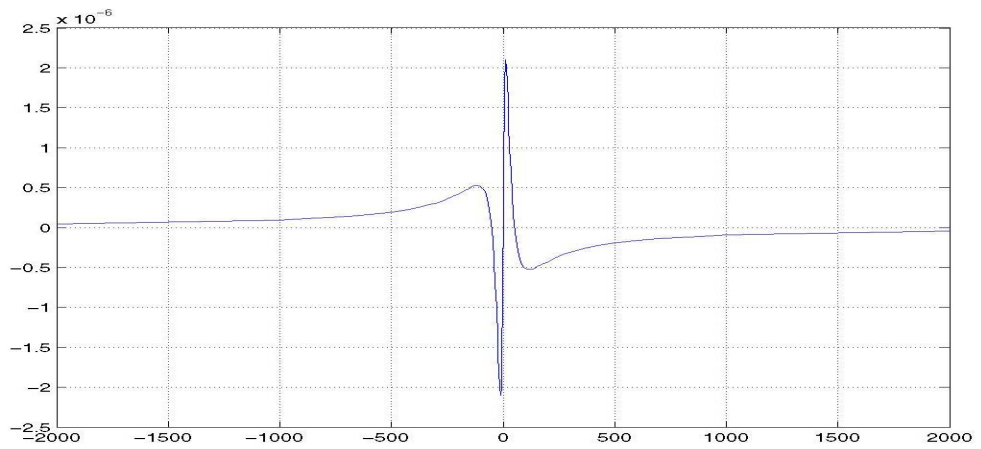


Figure A.10 Displacement difference at top surface at Time $t = 20.000$ Years

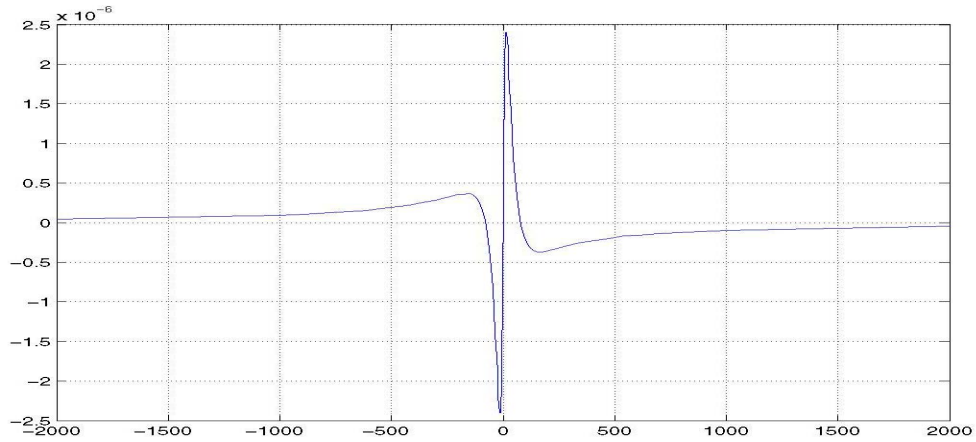


Figure A.11 Displacement difference at top surface at Time $t = 40.000$ Years

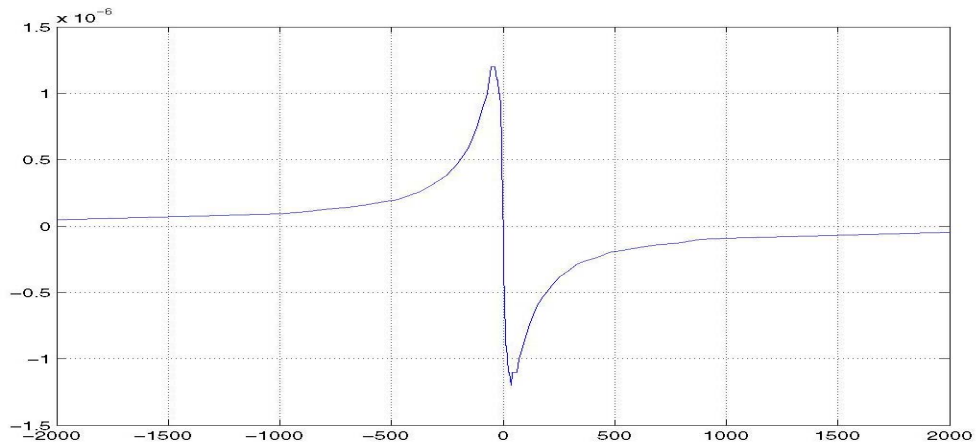


Figure A.12 Displacement difference at top surface at Time $t = 80.000$ Years

After reviewing these results we find the maximum difference of 2.5 mm in displacement after 40 years. When viscoelastic body is fully relaxed after 80 years, this difference becomes 1.5 mm. This difference goes down as we go from 40 to 80 years because both models tend to achieve fully relaxed state. When we are talk at the scale of hundreds of km this difference is negligible. Hence *VISCOELASTIC keyword can replace *CREEP keyword without any difference in the result. It is also found that *VISCOELASTIC take 10 % less iterations to complete the time-step

Analytical Models of Viscoelastic Behavior

B.1 Introduction

In following model springs and dashpots are used to simulate the elastic and viscous components of the stress/stain response. The spring (elastic component of the response) obeys the relations for tensile and shear stress. The dashpot (viscous component of the response) obeys the relations for tensile and shear stress

$$\sigma = E.\epsilon \quad \tau = G.\gamma \dots\dots\dots(B.1)$$

$$\sigma = \eta.\dot{\epsilon} \quad \tau = \mu.\dot{\gamma} \dots\dots\dots(B.2)$$

Simple models using combinations of springs and dashpots are used to understand viscoelastic material response for stress/strain variations using tensile stress conditions. In general, more complex the model is better the experimental fit are, but greater numbers of experimental constants are involved. Note that E, G, η , and μ depend not only on the material but also on pressure and temperature. Following analysis was taken in large part from <http://www.see.ed.ac.uk>.

B.2 Maxwell Model

A Maxwell model consists of a spring and dashpot in series (Figure B.1). Each of the Equations in the section B can be used for shear.

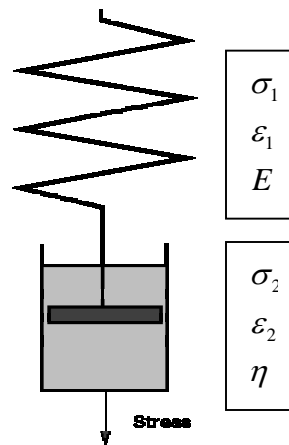


Figure B.1 Maxwell Model

B.2.1 Governing Equation

Assuming constant area, at equilibrium condition of forces, stress and strain in each element is given by following equations

$$\text{Stress} \rightarrow \sigma = \sigma_1 = \sigma_2 \dots \dots \dots (B.3)$$

$$\text{Strain} \rightarrow \epsilon = \epsilon_1 + \epsilon_2 \dots \dots \dots (B.4)$$

Using Equations B1, B.2 and B.4 we get

$$\dot{\epsilon} = \frac{1}{E} \cdot \dot{\sigma}_1 + \frac{1}{\eta} \cdot \sigma_2 \dots \dots \dots (B.5)$$

Now putting values from B.3

$$\dot{\epsilon} = \frac{1}{E} \cdot \dot{\sigma} + \frac{1}{\eta} \cdot \sigma \dots \dots \dots (B.6)$$

This is the governing equation of the Maxwell Model.

B.2.2 Creep for Maxwell Model

Deformation under constant stress σ_o is known as creep. For a Maxwell Body the creep equation can be found by integrating equation B.6. If the strain increases linearly with time, and a constant applied stress,

$$\epsilon(t) = \frac{\sigma_o}{E} + \frac{\sigma_o}{\eta} \cdot t \dots \dots \dots (B.7)$$

B.2.3 Stress Relaxation

For a constant strain, equation B.6 becomes

$$0 = \frac{1}{E} \cdot \dot{\sigma} + \frac{1}{\eta} \cdot \sigma \dots \dots \dots (B.8)$$

Solving this equation with $\sigma = \sigma_o$ at $t = 0$,

$$\sigma(t) = \sigma_o \exp\left(\frac{-E}{\eta} \cdot t\right) \dots \dots \dots (B.9)$$

B.2.4. Strain Recovery

When the stress is removed there is instantaneous recovery of the elastic strain. The dashpot is no longer creeping the strain is constant and given by

$$\epsilon_R = \frac{\sigma'}{E} \quad \text{for tensile stress(B.10)}$$

Where σ' is time derivative of stress

B.3 Kelvin /Voigt Model

This consists of a spring and dashpot in parallel (Figure B.2). This model is acceptable as a first order approximation to creep and recovery behavior, but is inadequate for prediction of stress relaxation. Each of the equations in Section C can also be used for shear

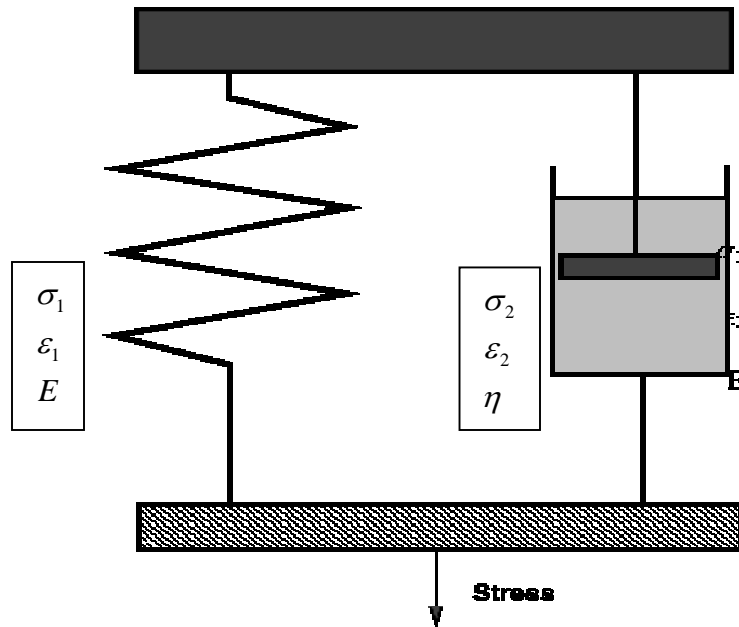


Figure B.2: Kelvin/ Voigt Model

B.3.1 Governing Equation

The applied load is supported by both the spring and the dashpot simultaneously

$$\sigma = \sigma_1 + \sigma_2 \dots \dots \dots (B.11)$$

Further the strain and stress can be given by

$$\text{Strain} \rightarrow \epsilon = \epsilon_1 = \epsilon_2 \dots \dots \dots (B.12)$$

$$\text{Stress} \rightarrow \sigma = E.\epsilon_1 + \eta.\dot{\epsilon}_2 \dots \dots \dots (B.13)$$

From above equations B.12 and B.13 we get

$$\sigma = E.\epsilon + \eta.\dot{\epsilon} \dots \dots \dots (B.14)$$

This is the governing equation of the Kelvin/Voigt Model.

B.3.2 Creep for Kelvin/Voigt Model

For a constant applied stress, σ_o , Solving differential equation (B.13) for total strain, ϵ We get

$$\epsilon(t) = \frac{\sigma_o}{E} [1 - \exp(\frac{-E}{\eta}.t)] \dots \dots (B.15)$$

B.3.3 Stress Relaxation

For a constant strain

$$\sigma = E.\epsilon \dots \dots \dots (B.16)$$

i.e., the stress is constant, which is the predicted response being that of an elastic material. There is no relaxation

B.3.4 Strain Recovery

When the stress is removed, Equation B.13 becomes

$$0 = E.\epsilon + \eta.\dot{\epsilon} \dots \dots (B.17)$$

Solving this equation with the initial condition $\epsilon = \epsilon'$ at the time of stress removal

$$\epsilon_R(t) = \epsilon' \exp\left(\frac{-E}{\eta} \cdot t\right) \dots\dots\dots(B.18)$$

B.4 General Equations

Various compromises between the Maxwell and Kelvin/Voigt models have been proposed. More complex models are also used.

In general, equations of the form

$$a_n \frac{\partial^n \sigma}{\partial t^n} + a_{n-1} \frac{\partial^{n-1} \sigma}{\partial t^{n-1}} + \dots + a_0 \cdot \sigma = b_m \frac{\partial^m \epsilon}{\partial t^m} + \dots + b_0 \cdot \epsilon \dots\dots\dots(B.19)$$

are used to define the governing equations for all linear viscoelastic materials. a_i and b_i are determined from constitutive relations, boundary and initial conditions

Appendix C

Geological Time Scale

Geologic time is often discussed in two forms:

- **Relative time** ("chronostratic") → subdivisions of the Earth's geology in a specific order based upon relative age relationships (most commonly, vertical/stratigraphic position). These subdivisions are given names, most of which can be recognized globally, usually on the basis of fossils.
- **Absolute time** ("chronometric") → numerical ages in "millions of years" or some other measurement. These are most commonly obtained via radiometric dating methods performed on appropriate rock types.

Think of relative time as physical subdivisions of the rock found in the Earth's stratigraphy, and absolute time as the measurements taken upon those to determine the actual time which has expired. Absolute time measurements can be used to **calibrate** the relative time scale, producing an integrated geologic or "geochronologic" time scale.

In addition, like any good scientific measurement, every dated boundary has an uncertainty associated with it, expressed as "+- X millions of years" which can be found in Harland *et al.*, [1990].

This geological time scale is based upon Harland *et al.*, 1990, but with the Precambrian/Cambrian boundary modified according to the most recently-published radiometric dates on that interval, revising the boundary from 570+-15 million years to 543+-1 million years ago [Grotzinger *et al.*, 1995].

The time scale is depicted in its traditional form with oldest at the bottom and youngest at the top, the present day is at the zero mark. Geologic time is finely subdivided through most of the Phanerozoic [Harland *et al.*, 1990], but most of the finer subdivisions (e.g., epochs) are commonly referred to by non-specialists only in the Tertiary. Because of the vast difference in scale, the younger intervals have been successively expanded to the right to show some of these finer subdivisions.

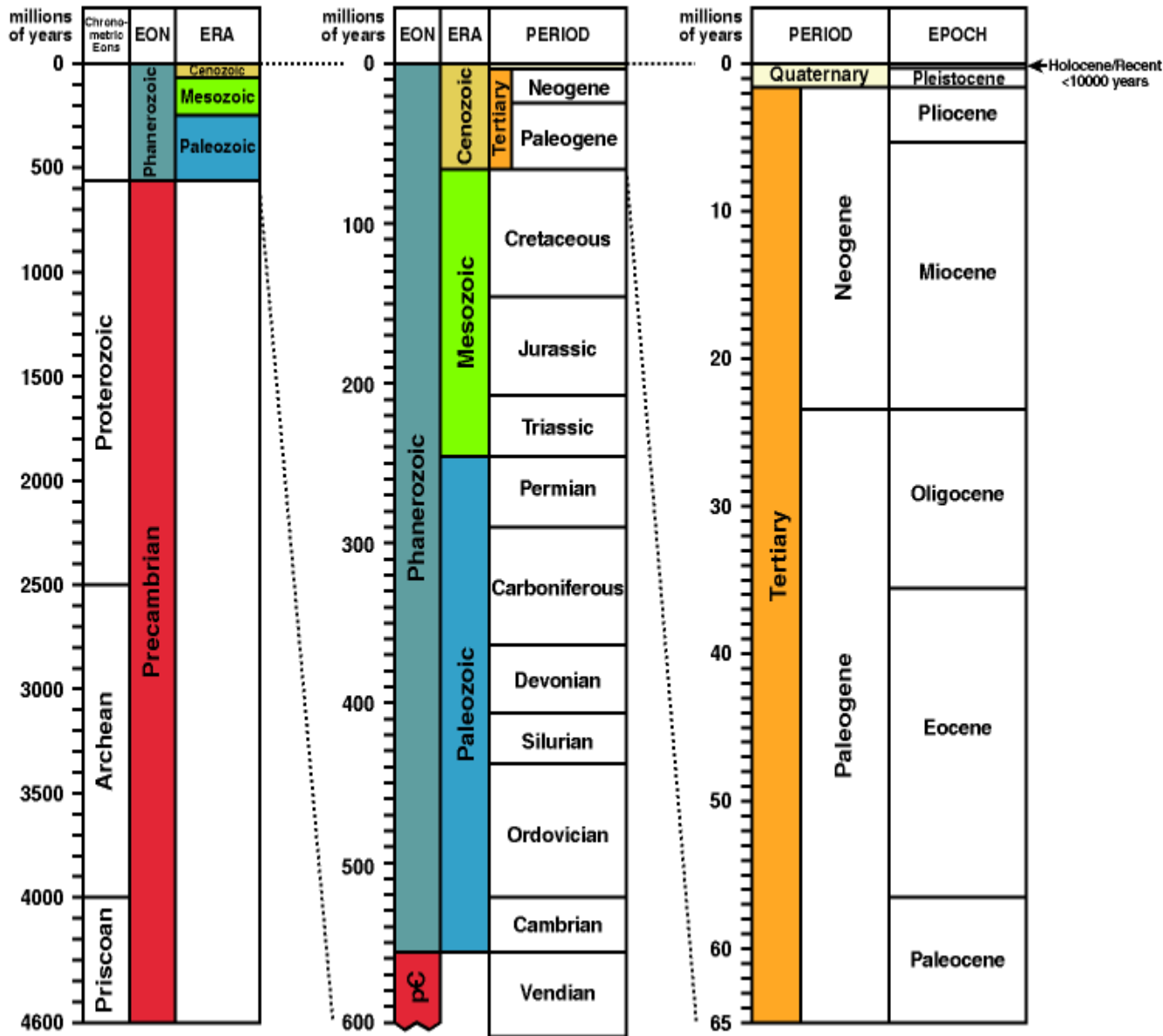


Figure C.1 Geological Time Scale

References

Blatt, H.; Berry, W.B.N.; and Brande, S., 1991. Principles of Stratigraphic Analysis. Blackwell Scientific Publications: Boston, p.1-512. ISBN 0-86542-069-6 [Chapter 4 provides an introduction to geologic time. This is a good starting point to get the basic principles.]

Grotzinger, J.P.; Bowring, S.A.; Saylor, B.Z.; and Kaufman, A.J., 1995 (Oct.27). Biostratigraphic and geochronologic constraints on early animal evolution. Science, v.270, p.598-604. [The most recent revision of the age of the Precambrian/Cambrian boundary.]

Harland, W.B.; Armstrong, R.L.; Cox, A.V.; Craig, L.E.; Smith, A.G.; and Smith, D.G., 1990. A geologic time scale, 1989 edition. Cambridge University Press: Cambridge, p.1-263. ISBN 0-521-38765-5 [One of the more recent compilations of the entire geologic time scale.]

Holmes, A., 1937. The Age of the Earth (new edition, revised). Nelson:London, p.1-263. [One of the earlier attempts at an integrated geochronologic time scale.]

Obradovich, J.D., 1993. A Cretaceous time scale. IN: Caldwell, W.G.E. and Kauffman, E.G. (eds.), Evolution of the Western Interior Basin. Geological Association of Canada, Special Paper 39, p.379-396. [Proposes revisions to the Cretaceous time scale at the resolution of stages (finer divisions than shown on diagram above) and sub-stages.]

Authorship

(c) 1996 macrae@geo.ucalgary.ca.

From <http://www.geo.ucalgary.ca/~macrae/timescale/timescale.html>

Appendix D

Glossary

Aseismic: A region without earthquakes (seismic activity).

Asthenosphere: The uppermost layer of the mantle, located below the lithosphere. This zone of soft, easily deformed rock exists at depths of 100 kilometers to as deep as 700 kilometers.

Basin: A depression in the Earth's surface that collects sediment.

Batholith: Very large mass of intrusive (plutonic) igneous rock that forms when magma solidifies at depth. A batholith must have greater than 100 square kilometers (40 square miles) of exposed area.

Cenozoic Era: The time span between 66.4 million years ago to the present

Craton: The relatively stable nucleus of a continent. Cratons are made up of a shield-like core of Precambrian Rock.

Crust: The rocky, relatively low density, outermost layer of the Earth.

Cretaceous: Geologic period that occurred roughly 65 to 144 million years ago. During this period, the first flowering plant species appear and dinosaurs are at their greatest diversity. Dinosaurs die out at the end of this period.

Deformation: General term for folding, faulting, and other processes resulting from shear, compression, and extension of rocks.

Dip: A measure of the angle between the flat horizon and the slope of a sedimentary layer, fault plane, metamorphic foliation, or other geologic structure

Dip-slip fault: A fault that moves rock on one side of the fault up or down relative to the other side. Can be either a normal or thrust fault. The fault plane dips

Earthquake: A sudden ground motion or vibration of the Earth. Produced by a rapid release of stored-up energy along an active fault

Eon: The largest time unit on the geologic time scale.

Fault: A fracture in the Earth along which one side has moved in relative to the other. Sudden movements on faults cause earthquakes

Geotherm: Heat derived from the Earth's interior.

Holocene: An epoch of the Quaternary Period beginning 10,000 years ago and continuing today

Hot spot: An area of concentrated heat in the mantle that produces magma that rises to the Earth's surface to form volcanic islands when penetrating oceanic and extremely large volcanoes 10's of km across when penetrating continental crust. The volcanic activity of the Hawaiian Islands is one example. Hot spots generally persist for millions of years.

Left-lateral: If you were to stand on the fault and look along its length, this is a type of fault where the left block moves toward you and the right block moves away.

Left-stepping: If you were to stand on the fault and look along its length, this is a type of fault where the left portion steps over to the left. Implies that fault is segmented.

Liquefaction: Temporary transformation of a mass of soil or sediment into a fluid mass. Occurs when the cohesion of particles in the soil or sediment is lost. Often triggered by seismic waves from an earthquake. For this condition to take place the pore spaces between soil particles must be at or near saturation.

Lithosphere: A layer of solid, brittle rock making up the outer 100 kilometers of the Earth, encompassing both the crust and the outermost part of the upper *mantle*. See also *asthenosphere*.

Mafic: A term used to describe minerals or igneous rocks that are rich in iron and/or magnesium. Mafic igneous rocks have a high percentage of dark-colored (mafic) minerals. They are relatively heavy.

Mantle: The layer of the Earth below the crust and above the core. The uppermost part of the mantle is rigid and, along with the crust, forms the 'plates' of plate tectonics. The mantle is made up of dense, iron and magnesium rich rock such as dunite and peridotite. It flows at very long time scale.

Moment magnitude: A measure of the total amount of energy released by an earthquake (modulus of rigidity X Area X Slip).

Mesozoic: Geologic era that occurred from 245 to 65 million years ago.

Magmatic: Molten rock. Magma may be completely liquid or a mixture of liquid rock, dissolved gases and crystals. Molten rock that flows out onto the Earth's surface is called lava.

Nonconformity: A type of unconformity in which young sedimentary rocks lie on top of older metamorphic or intrusive igneous rocks.

Normal fault: A fault that drops rock on one side of the fault down relative to the other side. Forms in zones of extension. The fault plane dips.

Precambrian: The 'unofficial' time period that encompasses all time from the Earth's formation, 4.55 billion years ago to 570 million years ago, the beginning of the Paleozoic Era

Paleoseismology: The study of ancient seismic (earthquake) events.

Paleozoic Era: The earliest era of the Phanerozoic Eon, marked by the presence of marine invertebrates, fish, amphibians, insects, and land plants.

Plate: A slab of rigid lithosphere (crust and uppermost mantle) that moves over the asthenosphere

Phanerozoic Eon: The eon beginning about 570 million years ago and continuing to the present. The portion of Earth history with rocks containing abundant fossils

Plutons: An intrusive rock, as distinguished from the preexisting country rock that surrounds it

Quaternary: The most recent Period of the Cenozoic Era. Encompasses the time interval of 1.6 million years ago through today

Reverse/Thrust fault: This dipping fault develops when compressional force causes the displacement of one block of rock over another.

Rift zone: A region of Earth's crust along which divergence is taking place. A linear zone of volcanic activity and faulting usually associated with diverging plates or crustal stretching. When divergence fails to split the two plates, it becomes known as a failed rift zone.

Right-lateral: If you were to stand on the fault and look along its length, this is a type of strike-slip fault where the right block moves toward you and the left block moves away.

Right-stepping: If you were to stand on the fault and look along its length, this is a type of fault where the right portion steps over to the right. Implies that fault is segmented

Sand Blow: A type of liquefaction in which fluidized over-pressured sand fractures its way to the surface creating what looks like a mini-volcano of sand.

Seismicity: The world-wide or local distribution of earthquake in space and time; a general term for the number of earthquakes in a unit of time.

Strike-slip: A left or right-lateral fault. The fault plane is often nearly vertical.

Tertiary Period: The earliest Period of the Cenozoic Era, beginning about 66.4 million years ago and ending 1.6 million years ago

Topography: The shape of the land surface

Unconformity: The contact between older rocks and younger sedimentary rocks in which at least some erosion has removed some of the older rocks before deposition of the younger. An angular unconformity shows that the older rocks have been deformed and eroded before the younger sedimentary rocks were deposited; there is an angle between the beds of the older and the younger

Unconsolidated: Loose sediment; lacking cohesion or cement.

[\[http://www.geos.iitb.ac.in/glossaries.html\]](http://www.geos.iitb.ac.in/glossaries.html)

[\[http://www2.nature.nps.gov/grd/usgsnps/misc/glossaryAtoC.html\]](http://www2.nature.nps.gov/grd/usgsnps/misc/glossaryAtoC.html)

References and Other Influential Papers:

- Atkinson, G. M. and 24 others, Reassessing the New Madrid Seismic Zone, *EOS*, 81, 402-403, 2000.
- Braile, L. W., W. J. Hinze, G. R. Keller, E. G. Lidiak, and J. L. Sexton, Tectonic development of the New Madrid rift complex, Mississippi embayment, North America, *Tectonophysics*, 131, 1-21, 1986.
- Bürgmann, R., P. Segall, M. Lisowski, and J. Svarc, Postseismic strain following the 1989 Loma Prieta earthquake from GPS and leveling measurements, *J. Geophys. Res.*, 102, 4933-4955, 1997.
- Chéry, J., S. Merkel, and S. Bouissou, A physical basis for time clustering of large earthquakes, *Bull. Seis. Soc. Am.*, 91, 1685-1693, 2001.
- Chen W., Molnar P., Focal Depths of Intracontinental and Intraplate Earthquakes and Their Implications for the Thermal and Mechanical Properties of the Lithosphere, *Journal of Geophysical Research*, Volume 88, Issue B5, p. 4183-4214, 1983.
- Chen, W. P., A brief update on the focal depths of intracontinental earthquakes and their correlations with heat flow and tectonic age: *Seismological Research Letters*, v. 59, p. 263-272, 1988
- Chiu, J. M., A. C. Johnston, and Y. T. Yang, Imaging the active faults of the central New Madrid seismic zone using PANDA array data, *Seismol. Res. Lett.*, 63, 375-393, 1992.
- Cohen, S. C., A multilayer model of time dependent deformation following and earthquake on a strike-slip fault, *J. Geophys. Res.*, 87, 5409-5421, 1982.
- Cohen, S. C., and M. J. Kramer, Crustal deformation, the earthquake cycle, and models of viscoelastic flow in the asthenosphere, *Geophys. J. R. Astro. Soc.*, 78, 735-750, 1984.
- Cox, R. T., and R. B. Van Arsdale, Hotspot origin of the Mississippi embayment and its possible impact on contemporary seismicity, *Eng. Geology*, 46, 210-216, 1997.
- Dieterich, J., A constitutive law for rate of earthquake production and its application to earthquake clustering, *J. Geophys. Res.*, 99, 2601-2618, 1994.

- Ellis, W. L., Summary and discussion of crustal stress data in the region of the New Madrid seismic zone, in *Investigations of the New Madrid seismic zone*, edited by K. M. Shedlock and A. C. Johnston, *U. S. Geol. Surv. Prof. Pap.*, 1538-B, B1-B13, 1994.
- Ervin C. P.L. McGinnis D., Reelfoot Rift: Reactivated Precursor to the Mississippi Embayment, *Geological Society of America Bulletin*: Vol. 86, No. 9, pp. 1287–1295, 1975
- Findley W. N., Onaran K., Lai W. J., *Creep and Relaxation of Nonlinear Viscoelastic Materials: With an Introduction to Linear Viscoelasticity* Dover Publications, Mineola, NY, 384 pp, 1990.
- Ginzburg, A., W. D. Mooney, A. W. Walter, W. J. Lutter, and J. H. Healy, Deep structure of the northern Mississippi embayment, *Am. Assoc. Petrol. Geologists Bull.*, 67, 2031-2046, 1983.
- Gomberg, J., Tectonic deformation in the New Madrid seismic zone: Inferences from boundary element models, *Seimol. Res. Lett.*, 63, 407-425, 1992.
- Gomberg, J. S., Tectonic deformation in the New Madrid Seismic Zone: Inferences from Map View and Cross-Sectional Boundary Element Models, *J. Geophys. Res.*, 98, 6639-6664, 1993.
- Gomberg, J., and M. Ellis, Topography and tectonics of the central New Madrid seismic zone: Results of numerical experiments using a three-dimensional boundary element program, *J. Geophys. Res.*, 99, 20,299-20,310, 1994.
- Grana, J. P. and R. M. Richardson, Tectonic stress within the New Madrid seismic zone, *J. Geophys. Res.*, 101, 5445-5458, 1996.
- Grollmund, B., and M. D. Zoback, Did deglaciation trigger intraplate seismicity in the New Madrid seismic zone?, *Geology*, 29, 175-178, 2001.
- Hamilton, R. M., and M. D. Zoback, Tectonic features of the New Madrid seismic zone from seismic-reflection profiles, in *Investigations of the New Madrid, Missouri, earthquake region*, edited by F. A. McKeown and L. C. Pakiser, *U. S. Geol. Surv. Prof. Pap.*, 1236, 55-82, 1982.

- Herrmann R. B., Canas J. A., Focal mechanism studies in the New Madrid seismic zone, *Bulletin of the Seismological Society of America*; v. 68; no. 4; p. 1095-1102, 1978
- Herrmann R. B., Surface wave focal mechanisms for eastern North American earthquakes with tectonic implications, *Journal of Geophysical Research*, Volume 84, Issue B7, p. 3543-3552, 1979
- Hibbit, Karlsson & Sorensen, Inc., *ABAQUS User's Manual*, Volumes 1-3, Version 5.8, 6.3, 6.4 Pawtucket, Rhode Island, 2004.
- Hildenbrand T. G., Rift structure of the northern Mississippi embayment from the analysis of gravity and magnetic data, *Journal of Geophysical Research*, Volume 90, Issue B15, p. 12607-12622, 1985
- Hildenbrand T. G., W. D. Stuart, and P. Talwani, Geologic structures related to the New Madrid earthquakes near Memphis, Tennessee, based on gravity and magnetic interpretations, *Eng. Geol.*, 62, 105-121, 2001
- Hildenbrand, T. G., and J. D. Hendricks, Geophysical setting of the Reelfoot rift and relations between rift structures and the New Madrid seismic zone, in *Investigations of the New Madrid seismic zone*, edited by K. M. Shedlock and A. C. Johnston, *U. S. Geol. Surv. Prof. Pap.*, 1538-E, E1-E30, 1995
- Hinze, W. J., L. W. Braile, G. R. Keller, and E. G. Lidiak, Models for midcontinent tectonism: An update, *Rev. Geophys.*, 26, 699-717, 1988.
- Karato, S. and P. Wu, Rheology of the Upper Mantle: a synthesis, *Science*, 260, 771-778, 1993
- Kenner, S. J., *Mechanical Modeling of Time Dependent Deformation in the Lower Crust and its Effect on Earthquake Recurrence*, Ph.D. Dissertation, Stanford University, July 2000.
- Kenner, S. J. and P. Segall, Time-dependence of the Stress Shadowing Effect and Its Relation to the Structure of the Lower Crust, *Geology*, 27, 119-122, 1999.
- Kenner, S. J. and P. Segall, Postseismic Deformation Following the 1906 San Francisco Earthquake, *J. Geophys. Res.*, 105, 13,195-13,209, 2000.
- Kenner, S. J. and P. Segall, A Mechanical Model for Intraplate Earthquakes: Application to the New Madrid Seismic Zone, *Science*, 289, 2329-2332, 2000.

- Kenner S. J. and P. Segall, Lower Crustal Structure in Northern California: Implications From Strain-rate Variations Following the 1906 San Francisco Earthquake, *J. Geophys. Res.*, 108, 2011, doi:10.1029/2001JB000189, 2003.
- Kenner, S. J., and M. Simons, Temporal clustering of major earthquakes along individual faults due to postseismic reloading, *Geophys. J. Int.*, submitted, September 2003.
- Kerkela, S., M. H. Murray, L. Liu, M. D. Zoback, and P. Segall, Strain accumulation in the New Madrid seismic zone from GPS data, 1993-1997 (abstract), *EOS Trans. AGU*, 79, *Fall Meeting Suppl.*, F210, 1998
- Liu, L., and M. D. Zoback, Lithospheric strength and intraplate seismicity in the New Madrid seismic zone, *Tectonics*, 16, 585-595, 1997.
- Liu, L., M. D. Zoback, and P. Segall, Rapid intraplate strain accumulation in the New Madrid seismic zone, *Science*, 257, 1666-1669, 1992.
- Malvern, L. E., *Introduction to the mechanics of a continuous medium*, 713 pp., Prentice-Hall, Inc., Englewood Cliffs, New Jersey, 1969.
- Mooney, W. D., M. C. Andrews, A. Ginzburg, D. A. Peters, and R. M. Hamilton, Crustal structure of the northern Mississippi embayment and a comparison with other continental rift zones, *Tectonophysics*, 94, 327-348, 1983.
- Newman, A., S. Stein, J. Weber, J. Engeln, A. Mao, and T. Dixon, Slow deformation and lower seismic hazard in the New Madrid seismic zone, *Science*, 284, 619-621, 1999.
- Nur, A., and G. Mavko, Postseismic viscoelastic rebound, *Science*, 183, 204-206, 1974.
- O'Connell D., Bufe C.G., Zoback M., Microearthquakes and faulting in the area of New Madrid, Missouri-Reelfoot Lake, Tennessee, U. S. Geological Survey Professional Paper. Pages 31-38. 1982
- Peltier, W. R., and X. Jiang, Glacial isostatic adjustment and Earth rotation: Refined constraints on the viscosity of the deepest mantle, *J. Geophys. Res.*, 101(B2), 3269-3290, 1996.

- Pollitz, F. F., L. Kellogg, and R. Bürgmann, Sinking Mafic Body in a Reactivated Lower Crust: A Mechanism for Stress Concentration at the New Madrid Seismic Zone, *Bull. Seismol. Soc. Am.*, 91, 1882-1897, 2001.
- Rydelek, P. A, and F. F. Pollitz, Fossil strain from the 1811-1812 New Madrid earthquakes, *Geophys. Res. Lett.*, 21, 2303-2306, 1994.
- Sbar M. L., Sykes L. R., Contemporary Compressive Stress and Seismicity in Eastern North America: An Example of Intra-Plate Tectonics *Geological Society of America Bulletin*: Vol. 84, No. 6, pp. 1861–1882, 1973
- Schweig E. S., Ellis M. A, Reconciling Short Recurrence Intervals With Minor Deformation in the New Madrid Seismic Zone, *Science*, Volume 264, Issue 5163, pp. 1308-1311, 1994.
- Stauder, W.; et al., Central Mississippi Valley Earthquake Bulletin: *first quarter 1982, 1 January-31 March 1982*
- Stuart, W. D., T. G. Hildenbrand, and R. W. Simpson, Stressing of the New Madrid seismic zone by a lower crust detachment fault, *J. Geophys. Res.*, 102, 27, 623-27, 633, 1997.
- Swanberg, C. A., B. J. Mitchell, R. L. Lohse, and D. D. Blackwell, Heat flow in the upper Mississippi Embayment, in *Investigations of the New Madrid, Missouri, earthquake region*, edited by F. A. McKeown and L. C. Pakiser, *U. S. Geol. Surv. Prof. Pap.*, 1236, 185-189, 1982.
- Tuttle, M. P., E. S. Schweig, J. D. Sims, R. H. Lafferty, L. W. Wolf, and M. L. Haynes, The earthquake potential of the New Madrid Seismic Zone, *Bull. Seismol. Soc. Am.*, 92, 2080-2089, 2002.
- Tuttle, M. P., E. S. Schweig, Earthquake potential of the New Madrid seismic zone (abstract), *EOS Trans. AGU*, 79, *Spring Meeting Suppl.*, S308-S309, 2000.
- Van Arsdale, R., Displacement history and slip rate on the Reelfoot fault of the New Madrid seismic zone, *Engineering Geology*, 55, 219-226, 2000.

Van Arsdale, TenBrink, Late Cretaceous and Cenozoic Geology of the New Madrid Seismic Zone, *Bulletin of the Seismological Society of America*.2000; 90: 345-356.

Zoback, M.L.; Zoback, M.D. Global patterns of tectonic stress, *Nature*, 9/28/89, Vol. 341 Issue 6240, p291, 8p, 3 charts, 2 diagrams, 10 graphs; (AN 8910231313)

Zoback, M. D., R. M. Hamilton, A. J. Crone, D. P. Russ, F. A. McKeown, and S. R. Brockman, Recurrent intraplate tectonism in the New Madrid seismic zone, *Science*, 209, 971-975, 1980.

Vita

Date and place of birth: Ajmer, India, November 22, 1981

Education: Bachelor of Engineering in Mechanical Engineering
Rajiv Gandhi Technical University, Bhopal, India, 2002

Professional Positions: Graduate Research Assistant, 2002-2004
Department of Geological Sciences
University of Kentucky, Lexington, USA

Honors: Kentucky Graduate Scholarship
University of Kentucky, 2002

Abhishek Joshi